



This is to certify that the
thesis entitled

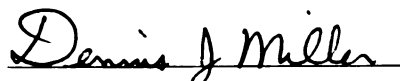
Reactive Properties of Hydrogen Adsorbed
on Carbon Surfaces

presented by

Zhigang Zhang

has been accepted towards fulfillment
of the requirements for

M.S. degree in Chemical Engineering


Major professor

Date Sept. 11, 1997

LIBRARY
Michigan State
University

PLACE IN RETURN BOX
to remove this checkout from your record.
TO AVOID FINES return on or before date due.

DATE DUE	DATE DUE	DATE DUE
JUN 28 2001		

Reactive Properties of Hydrogen Adsorbed on Carbon Surfaces

By

Zhigang Zhang

A THESIS

Submitted to
Michigan State University
in partial fulfillment of the requirements for the degree of

MASTER OF SCIENCE

Department of Chemical Engineering

1997

Reactive Properties of Hydrogen Adsorbed on Carbon Surfaces

Abstract

During carbon gasification (H_2 /steam/Argon), hydrogen quickly adsorbs on and covers most of the surface active sites of carbon. It is well known that hydrogen seriously inhibits further steam gasification. In this thesis, adsorbed hydrogen is investigated extensively, including its desorption properties (temperature program desorption profile), stability, and reactivity.

The adsorbed hydrogen is quite stable on the char surface. To desorb all hydrogen, it is necessary to heat carbon to 1500°C . Molecular oxidation has no preference to remove hydrogen. From D-H exchange, we have confirmed that adsorbed hydrogen is in a dynamic state during gasification and continuously exchanges with hydrogen in the gas phase.

From a kinetic model of the steam/ H_2 gasification data, we conclude that hydrogen inhibits steam gasification of carbons by reverse oxygen exchange that depends on hydrogen partial pressure.

Gasification rate can be enhanced by molecular oxidation, but mechanism is very complicated. Removal of adsorbed hydrogen, surface area change, and change in the carbon surface structure all contribute to the rate enhancement; further, the gasification temperature and reactant composition both affect the mechanism of rate enhancement.

ACKNOWLEDGMENTS

The author wishes to thank Dr. Dennis J. Miller for his guidance, understanding and financial support throughout this project.

I would like to thank Michael Lussier for his cooperation and help during this project.

I would like to thank professor Pinnavaia and professor Drazl for their severing my committee members.

Finally the author owes a great debt to his wife for her unselfish patience and understanding during his studies and the preparation of this thesis.

TABLE OF CONTENTS

LIST OF TABLES	vi
LIST OF FIGURES	vii
CHAPTER 1. INTRODUCTION	1
1-1. Background.....	2
1-2. Literature Review	3
1-2-1. Hydrogen Adsorbed on the Carbon Surfaces.....	3
1-2-2. Oxygen Complexes on the Carbon Surfaces	6
1-2-3. Methane Formation in Gasification	7
1-2-4. CO Formation in Steam Gasification.....	10
1-2-5. Hydrogen Inhibition	11
1-2-6. Isotopic Effect	12
1-3. Research Objectives.....	13
1-3-1. Characterization of Adsorbed Hydrogen	13
1-3-2. Isotope Effects	13
1-3-3. Rate Enhancement by Molecular Oxygen	13
1-3-4. Hydrogen Stability on Carbon Surfaces	14
1-3-5. Surface Oxygen Group Desorption.....	14
CHAPTER 2. EXPERIMENTAL	15
2-1. Reactants.....	16
2-1-1. Carbon Sample	16
2-1-2. Reactant Gases.....	17
2-2. Equipment and Analytical Instruments.....	18
2-2-1. High Pressure Reactor	18
2-2-2. Flow Control System	19
2-2-3. Ceramic Reactor	20
2-2-4. Mellen Split Tube Furnace System.....	21
2-2-5. Mass Spectrometer	22
2-3. Reactor Characterization.....	23
2-3-1. High Pressure Reactor Internal Bypass Detection	23
A. <i>Structure Analysis and Experiment Design</i>	23
B. <i>Experiments and Results</i>	24
2-3-2. Ceramic Reactor Response	28
2-3-3. Fluid Dynamics Calculation	28
2-4. Reaction Conditions and Experimental Procedures	29
2-4-1. Reaction Conditions	29
2-4-2. Experimental Procedures.....	30
A. <i>Preparation of Mass Spectrometer</i>	30
B. <i>Gasification</i>	30
C. <i>Temperature Programmed Desorption(TPD)</i>	31
D. <i>Surface Structure Characterization</i>	32

2-5. Data Analysis.....	33
2-5-1. Mass Spectrometer Calibration.....	33
2-5-2. General Data Deconvolution	33
A. <i>Time Shift in MASS Data</i>	35
B. <i>Species Deconvolution</i>	37
2-5-3. CD ₄ and D ₂ O Deconvolution	38
2-6. Carbon Sample Characterization	40
2-6-1. Outgas of As-prepared Saran and Coal Char	40
A. <i>Outgas of Saran Char</i>	40
B. <i>Coal Char TPD Profiles</i>	43
2-6-2. Saran Char Annealing.....	43
A. <i>The Effects of Heating Rate and Annealing Temperature on BET</i>	44
B. <i>The Effect of Annealing Time</i>	46
C. <i>Conclusions</i>	48
2-6-3. Annealed Saran Char Exposure in Air.....	49
 CHAPTER 3. THEORETICAL CALCULATIONS.....	 50
3-1. Shift Reaction Equilibrium	51
3-1-1. Equilibrium Constant Changes with Temperature.....	55
3-1-2. Simulation of Steam Gasification (with Shift Reaction)	56
3-1-3. Comparing with Experiment Data	59
3-2. Desorption Activation Energy of Hydrogen	60
3-2-1. Average Desorption Activation Energy.....	60
3-2-2. Peak Shape Simulation	63
3-2-3. Estimating the Desorption Activation Energy	65
3-2-4. Distribution of Desorption Activation Energies	66
3-3. Active Site Density Estimation	69
3-3-1. BET Surface Area and Adsorbed H ₂	69
3-3-2. Comparing with Hermann (1986)'s Data	70
3-4. Reaction Activation Energy	71
 CHAPTER 4. CHAR GASIFICATION	 73
4-1. Saran Char Gasification	74
4-1-1. As-prepared Saran Char Steam and Steam/H ₂ Gasification	74
4-1-2. Annealed Saran Char H ₂ /Steam Gasification	76
4-1-3. Hydrogen TPD Profiles of Annealed Saran Char Following Gasification	78
A. <i>H₂ gasification</i>	78
B. <i>H₂/Ar Gasification</i>	80
C. <i>Steam Gasification</i>	80
D. <i>Adsorbed Hydrogen (Deuterium) Change with Conversion</i>	80
E. <i>BET Area Changes with Conversion</i>	82
4-1-4. The Desorption Profiles of CO and CO ₂ after Gasification	82
4-1-5. Weakly Bound Hydrogen Detection	84
4-1-6. Discussion of Saran Char Gasification	84

4-2. Coal Char Gasification.....	87
4-2-1. As-received Coal Char Steam/H ₂ Gasification	87
4-2-2. Annealed Coal Char Steam Gasification	89
4-2-3. Hydrogen TPD Profiles of Annealed Coal Char Following Gasification	91
4-2-4. The TPD Profiles of CO and CO ₂ after Coal Gasification.....	92
4-2-5. Discussion of Coal Gasification	92
4-3. Isotopic Effects	93
4-3-1. Annealed Saran Char Gasification by D ₂	93
4-3-2. Annealed Saran Char Gasification by D ₂ O.....	95
4-4. Mechanism Derivation and Identification.....	96
4-4-1. Mechanism	96
A. <i>Reverse Oxygen Exchange Inhibition</i>	96
B. <i>Hydrogen Inhibition by Formation of a C(H)₂ Complex</i>	96
C. <i>Hydrogen Inhibition by Formation of a C(H) Complex</i>	96
4-4-2. Kinetic Model.....	97
4-5. Conclusion	99
 CHAPTER 5. HYDROGEN STABILITY ON CARBON SURFACES	100
5-1. Stability of Adsorbed Hydrogen to Oxidation by O ₂	101
5-2. D-H Exchange During Gasification	106
5-3. H-D Exchange During Gasification	110
5-4. Conclusions.....	113
 CHAPTER 6. RATE ENHANCEMENT.....	114
6-1. Oxidation Effects	116
6-2. H ₂ gasification Rate Enhancement.....	118
6-3. Steam Gasification Rate Enhancement	121
6-4. H ₂ /Steam Gasification Rate Enhancement	125
6-5. Conclusions.....	126
 CHAPTER 7. CONCLUSIONS AND RECOMMENDATIONS.....	127
7-1. Conclusions.....	128
7-1-1. The Stability of deposited Hydrogen during Gasification	128
7-1-2. Gasification and Hydrogen Inhibition	128
7-1-3. Rate Enhancement by Molecular Oxygen Oxidation	129
7-1-4. Isotopic Effects	129
7-2. Recommendations.....	130
 LIST OF REFERENCES	131

LIST OF TABLES

CHAPTER 2

Table 2-1 Analysis of Carbon Sample	16
Table 2-2 Dynamics Calculation	28
Table 2-3 Possible Fragmentation	34
Table 2-4 Fragmentation Patterns in Argon Carrier	34
Table 2-5 The K_2 Change with Carrier Gas	39
Table 2-6 Comparison of Element Analysis and TPD	41
Table 2-7 Impurities from Exposure	49
Table 2-8 The Peak Position changes with Exposure Time	49

CHAPTER 3

Table 3-1 Thermodynamic Data	55
Table 3-2 Heat Capacity Coefficients	55
Table 3-3 Active Sites Occupied by Oxygen	70
Table 3-4 Active Sites Occupied by Hydrogen	70
Table 3-5 Experimental Data	71
Table 3-6 Apparent Active Energy for H_2/Ar Gasification	71
Table 3-7 Apparent Active Energy for $H_2O/H_2/Ar$ Gasification	72

CHAPTER 4

Table 4-1 Rate Constants from Experimental Data at 850 °C	89
--	----

CHAPTER 5

Table 5-1 Experimental Data Summary	101
Table 5-2 Material Balance	103
Table 5-3 Oxidation Effects	104
Table 5-4 D-H Exchange Effects	109
Table 5-5 H-D Exchange Effects	112

CHAPTER 6

Table 6-1 Estimation of the Surface Site Density	116
---	-----

LIST OF FIGURES

CHAPTER 1

Figure 1-1 Zig-zag and arm-chair configuration	5
Figure 1-2 Hexagonal etch pit on the basal plane formed by steam	5
Figure 1-3 Mechanism for methane formation	7
Figure 1-4 Methane formation mechanism of Hutter	9

CHAPTER 2

Figure 2-1 Overall system sketch	18
Figure 2-2 High pressure reactor sketch	19
Figure 2-3 Flow control system	19
Figure 2-4 Ceramic reactor (not to scale)	20
Figure 2-5 Mellen split tube furnace	21
Figure 2-6 Temperature profile of Mellen furnace	21
Figure 2-7 MASS spectrometer	22
Figure 2-8 High pressure reactor cell (not to scale)	23
Figure 2-9 Charred cherry pits oxidation (ceramic reactor)	25
Figure 2-10 Charred cherry pits oxidation (high pressure reactor)	25
Figure 2-11 Oxygen by-pass in high pressure reactor (-60~+100 cherry pits)	26
Figure 2-12 Oxygen by-pass in high pressure reactor(-30~+60 cherry pits)	27
Figure 2-13 TPD system response (30 cc H ₂ pulse)	27
Figure 2-14 Experimental scheme	30
Figure 2-15 Before time shift	35
Figure 2-16 After time shift correction	36
Figure 2-17 After the time shift, artificial peak no longer exists	37
Figure 2-18 Outgas of as-prepared Saran Char (H ₂ profile)	41
Figure 2-19 Outgas of as-prepared Saran Char(CO profile)	41
Figure 2-20 Outgas of as-prepared Saran Char(CO ₂ profile)	42
Figure 2-21 Low heat rate profile	42
Figure 2-22 Coal char TPD profile, heating rate 10 °C /min	43
Figure 2-23 BET with pretreatment temperature (Heating rate 3°C/min)	44
Figure 2-24 BET with pretreatment temperature (5°C/min heating rate)	45
Figure 2-25 BET area changes with high temperature annealing time	46
Figure 2-26 N ₂ profile in BET for Saran char	47
Figure 2-27 N ₂ profile in BET for annealed Saran char	47
Figure 2-28 TPD profile following 2 min. hour exposure	49
Figure 2-29 TPD profile following 0.5 hour exposure	50
Figure 2-30 TPD profile following 2 days exposure	50
Figure 2-31 Uptakes of hydrogen changes with exposure time in air	51
Figure 2-32 Uptakes of CO and N ₂ changes with exposure time char in air	51
Figure 2-33 Uptakes of CO ₂ changes with exposure time in air	52
Figure 2-34 Uptakes of H ₂ O changes with exposure time	52

CHAPTER 3

Figure 3-1 Equilibrium changes with temperature	56
Figure 3-2 Simulation of shift reaction($T=850^{\circ}\text{C}$, $\text{H}_2=120$, $\text{H}_2\text{O}=120\text{ml/min}$)	58
Figure 3-3 Simulation of shift reaction($T=850^{\circ}\text{C}$, $\text{H}_2=120$, $\text{H}_2\text{O}=120\text{ml/min}$)	58
Figure 3-4 Simulation of shift reaction ($T=850^{\circ}\text{C}$, $\text{H}_2=5$, $\text{H}_2\text{O}=120\text{ml/min}$)	58
Figure 3-5 Simulation of shift reaction($T=850^{\circ}\text{C}$, $\text{H}_2=0$, $\text{H}_2\text{O}=120\text{ml/min}$)	58
Figure 3-6 Simulation of shift reaction($T=725^{\circ}\text{C}$, $\text{H}_2=120$, $\text{H}_2\text{O}=120\text{ml/min}$)	58
Figure 3-7 Simulation of shift reaction($T=725^{\circ}\text{C}$, $\text{H}_2=120$, $\text{H}_2\text{O}=120\text{ml/min}$)	58
Figure 3-8 Simulation of shift reaction($T=725^{\circ}\text{C}$, $\text{H}_2=5$, $\text{H}_2\text{O}=120\text{ml/min}$)	59
Figure 3-9 Simulation of shift reaction($T=725^{\circ}\text{C}$, $\text{H}_2=0$, $\text{H}_2\text{O}=120\text{ml/min}$)	59
Figure 3-10 Comparison of experiment data with the equilibrium CO & CO_2	59
Figure 3-11 Desorption activation energies change with peak temperature	61
Figure 3-12 Simulation of desorption($T_m=1000^{\circ}\text{C}$ and $E=237.8\text{KJ/mol}$)	65
Figure 3-13 Activation energy depends on peak temperature T_m	66
Figure 3-14 Distributions of desorption activation energies for D_2 TPD	68
Figure 3-15 Distributions of desorption activation energies for H_2 TPD	68
Figure 3-16 Adsorbed Hydrogen vs. Conversion	69

CHAPTER 4

Figure 4-1 Gasification of Saran char in 3.1 MPa $\text{H}_2\text{O}(40\%)/\text{Ar}(60\%)$ at 725°C	74
Figure 4-2 Saran char gasification in 3.1 MPa $\text{H}_2\text{O}(40\%)/\text{H}_2(60\%)$ at 725°C	75
Figure 4-3 4 hr. Annealed Saran char H_2 Gasification at 850°C and 3.1 MPa	75
Figure 4-4 Annealed Saran char gasification.....	77
Figure 4-5 Annealed Saran char 40% $\text{H}_2\text{O}/60\%\text{H}_2$ gasification.....	77
Figure 4-6 H_2 TPD profile following 6 hr pure H_2 gasification of Saran char	78
Figure 4-7 Comparison of H_2 TPD profiles.....	79
Figure 4-8 H_2 TPD profile following 6 hr 60% $\text{H}_2/40\%\text{Ar}$ gasification.....	79
Figure 4-9 H_2 TPD profile following Steam 40%/ Ar gasification.....	80
Figure 4-10 Adsorbed hydrogen change with conversion	81
Figure 4-11 BET changes with conversion.....	81
Figure 4-12 CO TPD profiles following 40% steam/60% argon gasification	83
Figure 4-13 H_2 TPD profiles of annealed Saran char after gasification.....	83
Figure 4-14 Coal char gasification in 40% $\text{H}_2\text{O}/60\%\text{Ar}$	87
Figure 4-15 Coal char gasification at 725°C	88
Figure 4-16 Annealed coal char Gasification at 850°C	88
Figure 4-17 N_2 BET surface area with conversion	89
Figure 4-18 40% $\text{H}_2\text{O}+60\%\text{Ar}$ Gasification at 850°C and 1MPa.....	90
Figure 4-19 40% $\text{H}_2\text{O}+60\%\text{Ar}$ Gasification at 850°C and 1Mpa.....	90
Figure 4-20 Desorbed H_2 changes with conversion.....	91
Figure 4-21 CO TPD profiles following steam gasification	92
Figure 4-22 Annealed Saran char $\text{D}_2(60\%)/\text{Ar}$ gasification	94
Figure 4-23 Deposited D during D_2 gasification	94
Figure 4-24 D_2O gasification of annealed Saran char at 3.1 MPa and 850°C	95

CHAPTER 5

Figure 5-1	CO and CO ₂ profile during the oxidation	102
Figure 5-2	H ₂ TPD profiles change with oxidation time	102
Figure 5-3	D ₂ TPD profiles change with different oxidation time.....	103
Figure 5-4	D ₂ O profile during the oxidation	105
Figure 5-5	H ₂ O profile during the oxidation	105
Figure 5-6	TPD of 6 hours D ₂ +Ar and 0.8 hr H ₂ +Ar gasification	106
Figure 5-7	TPD of 6 hr. D ₂ +Ar and 2.5 hours H ₂ +Ar gasification	107
Figure 5-8	CD ₄ and CH ₄ evolution during switch	107
Figure 5-9	D ₂ TPD profiles with H ₂ gasification time.....	109
Figure 5-10	TPD of 4 hours H ₂ +Ar and 0.7 hr. D ₂ +Ar gasification	110
Figure 5-11	TPD of 4 hours H ₂ +Ar and 1.3 hr. D ₂ +Ar gasification	111
Figure 5-12	TPD of 4 hours H ₂ +Ar and 2.5 hr. D ₂ +Ar gasification	111
Figure 5-13	H ₂ TPD profiles with D ₂ gasification times	112

CHAPTER 6

Figure 6-1	Experimental scheme	115
Figure 6-2	CO and CO ₂ desorption profiles	116
Figure 6-3	TPD profiles after D ₂ gasification and oxidation	117
Figure 6-4	Rate enhancement by oxidation (H ₂ gasification	118
Figure 6-5	Armchair carbon maintain its structure during gasification	119
Figure 6-6	Rate enhancement by oxidation (725 °C)	121
Figure 6-7	Rate enhancement by oxidation.(850 °C)	123
Figure 6-8	Rate enhancement by oxidation (725 °C)	125

CHAPTER 1

INTRODUCTION

1-1. Background

The production of gaseous fuel from coal has been practiced for hundreds of years. In 1947, production reached a peak in the US, and then was gradually replaced by natural gas and petroleum. During the 1970's, it came to be realized that the world's supplies of inexpensive petroleum and natural gas are limited. The eventual depletion of petroleum and natural gas reserves necessitates the development of alternative sources to replace these inexpensive and clean fuels.

In US and most other countries in the world, one potentially alternative fuel source is substitute(synthetic) natural gas (SNG) produced by gasification of coal, of which the world has abundant reserves. SNG is superior to coal as an energy source because it is an easily transported fuel, burns much cleaner and more efficiency than coal, and can be converted to oil and other chemicals without technical and economic difficulty. For all possible gasification processes, steam gasification is a top choice, because water is cheap and the gasification process is simple to carry out. Coal gasification is not currently used on a wide scale because extreme conditions are needed to achieve reasonable reaction rates. The extreme conditions lead to high production cost. Another economic reason is the cheap petroleum and natural gas still are available, so we do not have to use the troublesome coal resource.

The presence of hydrogen at carbon (or coal) surfaces strongly influences steam gasification rate. The process by which hydrogen inhibits gasification is not yet well characterized. If the inhibition were there, understanding its mechanism would have potential to minimize this retardation.

1-2. Literature Review

1-2-1. Hydrogen Adsorbed on the Carbon Surfaces

Hydrogen chemisorbed on a carbon surface is very stable, and is generally accepted as dissociative in nature. Numerous studies (for example Steinberg^[1]) have shown that prolonged outgassing at 1000 °C will not remove all dissociatively adsorbed hydrogen; temperatures approaching 1500 °C are required (Redmond^[2]). Also, the hydrogen adsorption rate is very rapid. Biederman et al^[3] found that dissociatively adsorbed hydrogen could saturate a graphite surface at 1100 °C and 3 millitorr H₂. The hydrogen adsorption equilibrium constant is high, up to 253 atm^{-0.5} at 700°C (Yang and Yang^[4]). Furthermore, this constant can be strongly affected by impurities in the carbon surface which may act as hydrogen dissociation sites.

Adsorbed hydrogen can be characterized by temperature programmed desorption (TPD). In addition to a peak in starting around 900 °C in TPD profile, which is indicative of dissociatively bound hydrogen (C(H)), several investigators (Huttinger et al^[5]) reported a second peak around 600~800 °C following exposure to gases containing molecular hydrogen. This peak is suggested to represent associatively bound hydrogen (C(H)₂) on the carbon surfaces.

¹ Steinberg, M., 1987 Int. Conf. on Coal Sci. 11, J.A. Moulijn, ed., 953 (1987).

² Redmond, J.P. and Walker, P.L. Jr., J. Phys. Chem. 64, 1093 (1960).

³ Biederman, D.L. et al., Carbon 14, 351 (1976).

⁴ Yang, R.T. and Yang, K.L., Carbon 23(5), 537 (1985).

⁵ Huttinger, K.J. and Merdes, W.F., Carbon 30(6), 883 (1992).

Uncatalyzed carbon gasification rate decreases dramatically with conversion. At the beginning of the gasification, the ratio of carbon edge atoms in zigzag and arm chair configuration may be undefined (**Figure 1-1a**). Because of the irreversible hydrogen inhibition, the reaction rate is reduced to near zero when the edges of the carbon layers are formed exclusively by carbon atoms in zigzag form (**Figure 1-1b**) (Huttinger^[5]).

Experiments and molecular orbital simulation showed that the hydrogen only could chemisorb on edge sites of graphite, not on the basal plane. The gasification of "armchair" edge carbons is much easier in hydrogasification and steam gasification (Pan and Yang^[12]), while the gasification of oxygen and carbon dioxide shows no edge preference (Yang and Duan^[6], Yang and Yang^[4]). Therefore, as hydrogasification and steam gasification proceed, the more highly reactive armchair carbons will be consumed. As shown in **Figure 1-2**, the edges of hexagons are formed by carbon edge atoms in zigzag configuration. The reason is that these carbon edge atoms are blocked by formation of C(H) complexes, because their further reactivity with hydrogen is lower than that of the carbon atoms in armchair configuration (Pan and Yang^[12]). This interpretation is strongly supported by the observation that gasification inhibitors based on halogen, boron, or phosphorus compounds block only carbon edge atoms in zigzag configuration (Hippo^[7]).

Although an enormous number of studies have been done on hydrogen adsorption and its role in gasification, the exact structure or pathway of formation of this associatively bound hydrogen is not fully understood.

⁶ Yang, R.T. and Duan, R.Z., Carbon 23(3), 325 (1985).

⁷ E.J Hippo, N murdie and A. Hyjiazie, Carbon 27, 689 (1989)

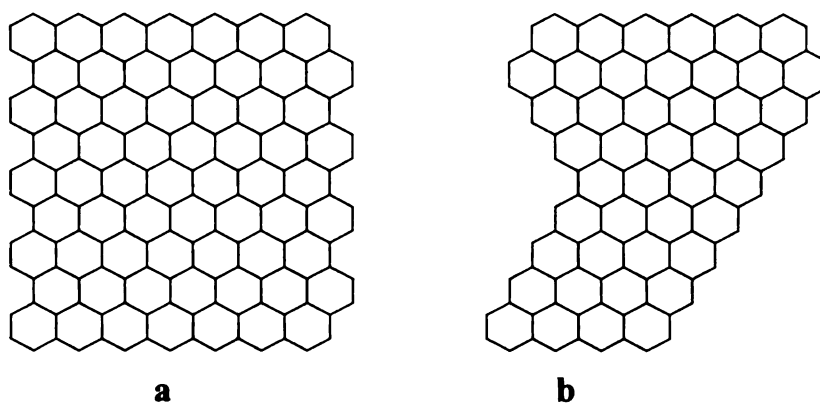


Figure 1-1 (a) Before reaction: undefined ratio of carbon edge atoms in zig-zag and arm-chair configuration **(b)** After reaction: prevailing carbon edge atoms in zig-zag configuration

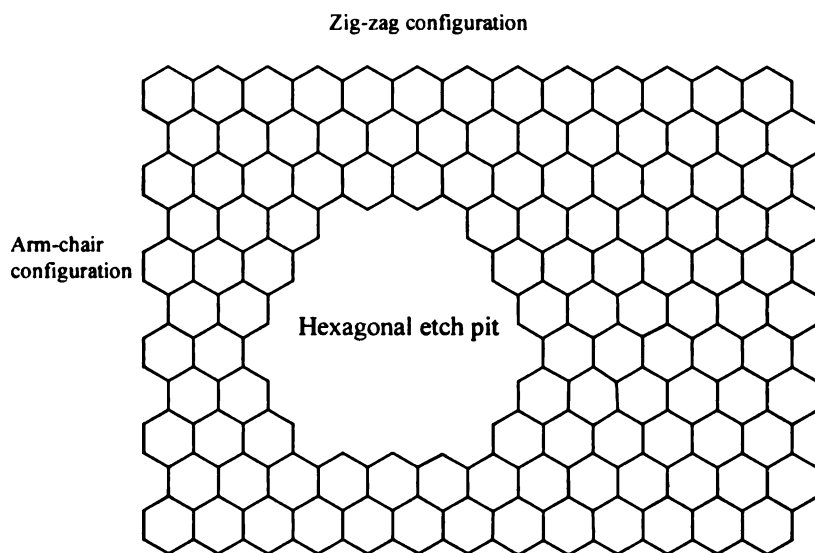


Figure 1-2 Hexagonal etch pit on the basal plane formed by steam

1-2-2. Oxygen Complexes on the Carbon Surfaces

It is generally believed that the major source of active sites in all gasification reactions comes from the desorption of oxygen functional groups from the carbon surface. These groups desorb in the form of carbon monoxide and carbon dioxide when samples are heated to reaction temperatures (Treptau and Miller^[8]), and in the form of water during hydrogasification (Blackwood^[9]). Hydrogasification rate has been shown to be a strong function of the oxygen content of various chars (Blackwood^[9]), and initial rate is a strong function of oxygen surface concentration (Treptau and Miller^[8]). Hydrogasification rate can be increased by an order of magnitude by addition of 0.1% oxygen to the reactant gas (Cao and Back^[10]). However, the temperature of C-H₂O reaction is higher than 700°C, so only surface oxygen groups with intermediate stability at these temperature will contribute to the reaction. Highly stable groups may actually be considered as poisons (Walker^[11]).

Recently, Pan and Yang^[12] had detected a significant amount of oxygen complex on graphitic carbon (but not on nongraphite carbon) which desorbed as CO at temperature higher than 1200°C. On the basis of this result and molecular orbital calculations, they proposed an oxygen complex which was formed by bonding oxygen atoms on the lattice carbon atoms that were saturated. It was shown that the caved in carbon atoms on the zigzag edge of the graphite could form bonds with oxygen atoms and that such bonding would significantly weaken the carbon- carbon bonds, hence

⁸ Treptau, M.H. and Miller, D.J., Carbon 29, 531 (1991).

⁹ Blackwood, J. D. Aust. J. Chem. 12, 14 (1959).

¹⁰ Cao, J.R., and Back M.H., Carbon 23, 141 (1985).

¹¹ Walker, Carbon, Vol. 29, P41, 1991

¹² Pan, Z., J and Yang, R. T. Ind Eng. Chem Res 1992, 31, 2675

leading to gasification. So, the understanding of active surface oxygen complexes is a key to understanding the carbon gasification reaction. Surface oxygen groups play a dominant role in the steam gasification reaction. Mostly recently, the molecular orbital calculations (Chen and Yang^[13]) showed that C-C bond energies (for desorption from graphite) are lowered by approximately 30% by bonding of oxygen on the saturated carbon atoms. The bonding of an oxygen atom to a saturated carbon atom (in caved-in position) adjacent to the unsaturated edge carbon atoms that already bonded to an oxygen atom forms a new type of complex. The molecular orbital calculation results also showed that this type of complex is substantially more active than known complexes (semiquinones and carbonyl). This more active complex may be a main contributor to the carbon gasification.

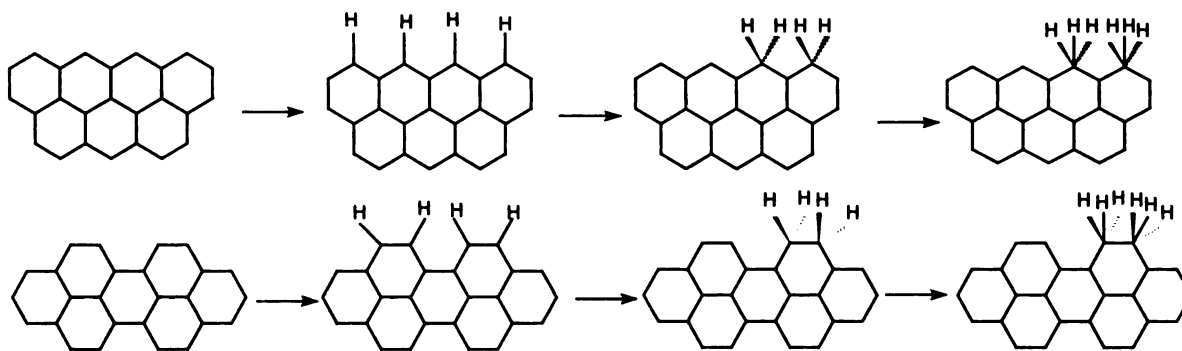


Figure 1-3 Mechanism for methane formation on zigzag and armchair faces by successive H addition. C-C bond breakage upon the third H addition. (Redrawn from Pan and Yang, 1990^[12])

1-2-3. Methane Formation in Gasification

There are two relatively new theories to account for methane formation. The first one attributes methane formation to direct attack of carbon by molecular hydrogen, which

¹³ Chen and Yang, Ind. Eng. Chem. Res., 32, 2835, 1993

is given by Pan and Yang (1990^[12]). The second one proposes methane formation only occurs on dangling carbon atoms (Huttinger,1992^[5]).

Pan and Yang's mechanism is shown in **Figure 1-3**. Methane formation may come from both zigzag and armchair edge faces. In both case, the surface C-C bond cleavage is required for the third H addition. After that, dangling bonds remain and methane formation is energetically very favorable. The simulation results of extended Hucke molecular orbital (EHMO) showed that the first H addition is relatively easier than the second H addition on both edge faces of graphite. The simulation also indicates the edge surface carbon atoms become saturated (hence free valence reaches a minimum) and inactive for the chemisorption after two H addition. Consequently, the third H addition or the C-C bond breakage step is the rate limiting step for methane formation. The zigzag edge atoms are more reactive for hydrogen chemisorption for both first and second H addition. A most significant result from this simulation is that there is a reversal in the relative reactivity between the two edge planes upon the second H addition. After second H addition, the cleavage of C-C bond is easier for armchair face. These results are consistent with the experimental observations. It seem the formation of two CH₃ groups on the armchair face appears to be sterically unfavorable due to possible H-H interactions from neighboring -CH₃ groups. However, their EHMO calculation showed that the formation of such a structure is entirely feasible with no H-H interactions.

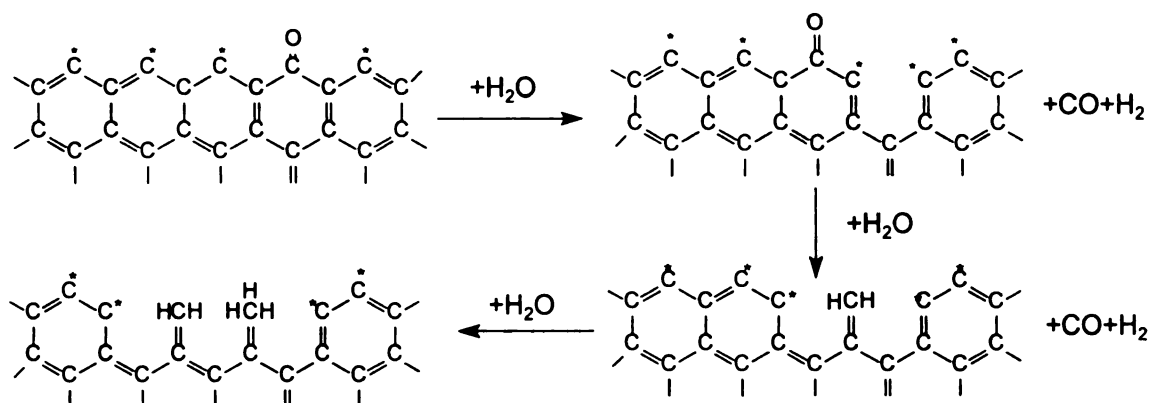


Figure 1-4 Methane formation mechanism of Huttinger^[5]

The second mechanism^[5] is totally derived from the gasification of PVC coke. After proving the homogeneous formation of methane is impossible (1000 °C and 10 bar) by experiments, they claimed the methane must come from the carbon surface. But the $-\text{CH}_2$ complex is definitely not involved in the formation of methane and is a inhibitor to methane formation. The present of steam is an absolute prerequisite. They used a old model (Blackwood, 1958^[19]) (**Figure 1-4**) to rationalize their mechanism. The decisive intermediates of methane formation are dangling carbon atoms which form methylene or methyl groups, but no surface complexes. A pre-condition of the formation of dangling carbon atoms, and thus methylene or methyl groups, is ring opening reactions, which are only possible by the attack of steam.

Another possibility would be that methylene groups are directly formed as intermediates. Finally, methane is formed by the reaction of methylene or methyl groups with hydrogen. From this mechanism^[14], the hydrogen inhibition of methane formation and hydrogen is also necessary to form methane.

It seems that these two theories are contrary at first glance. But when we look into the materials they used, it is not difficult to understand the consistency of the two

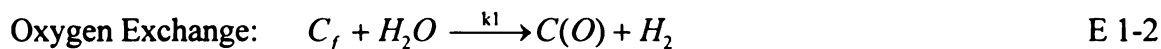
mechanisms. Pan and Yang's mechanism is mainly from graphite (gasification and pits etching) and Huttinger's mechanism is from the gasification of disordered (turbostratic) carbon (PVC coke). The first mechanism may be always correct, but the rate is very slow (etch decoration experiments need 10 hours to get a pit of 0.1 μm). Huttinger even could not detect the methane formation using their coke (low surface area 1 m^2/g) in pure hydrogen. The second mechanism is relative fast for amorphous carbon. For the really possible gasification processes (low to middle rank coal), the carbon is most like Huttinger's coke and not graphite. So, relatively, the second mechanism is more important.

1-2-4. CO Formation in Steam Gasification

Gasification of carbon (coal, coke) with steam leads to carbon monoxide and hydrogen as main products. The overall reaction is:



This reaction has been the basis for production of synthesis, reduction, town and fuel gases for many decades before petroleum. In view of the great importance of this reaction, it is surprising that the ideas about the mechanism and also the rate limiting step are still speculative. Three models are proposed for this reaction, namely the oxygen exchange model (Ergun^[15]) and two hydrogen inhibition models (Long^[16] and Gadsby et al^[17]). Huttinger^[18] gave a summary of all three models:



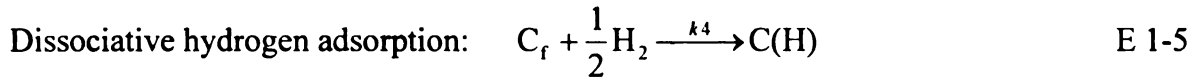
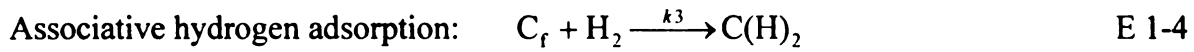
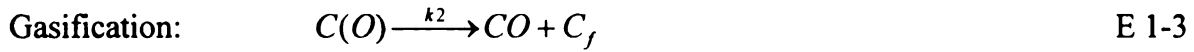
¹⁴ Zielke, C.W. and Gorin, E., *Ind. and Eng. Chem.* 47(4), 820 (1955).

¹⁵ Ergun, S and Mentser, M In Chemistry and Physics of Carbon (by P.L.Walker, Jr) Vol. 2 P203. 1966

¹⁶ Long, F.J., and Sykes, K.W., Proc. Royal Soc. London A193, 377 (1948).

¹⁷ Gadsby, J., Hinshelwood, C.N., and Sykes, K.W., Proc. Royal Soc. London A187, 129 (1946).

¹⁸ Huttinger, K.J., ACS Div. Fuel Chem. Prepr. 34(1), 56 (1989).



where C_f represent a free carbon site.

All models yield formally identical surface CO formation rate equation:

$$\text{CO formation rate } r_s = \frac{k_1 P_w}{1 + k_2 P_w + k_3 P_{H_2}''} \quad \text{E1-6}$$

Of these model , dissociative hydrogen adsorption gives a value of 0.5 for n in Equation E 1-6, which has been found to be correct for low hydrogen pressures and subatmospheric steam pressures (Yang and Yang ^[4]). Reverse oxygen exchange and associative hydrogen adsorption both give values of n=1.0 in this rate expression, which was reported in early studies (Blackwood^[19])

1-2-5. Hydrogen Inhibition

All researcher agrees that the presence of hydrogen greatly reduces steam gasification rate. Steam gasification rate drops by an order of magnitude with the addition of only 1 PPM hydrogen (Montet^[20]). Carbon dioxide gasification is also inhibited to this degree by hydrogen at low pressures (Yang et al ^[4,6]). During steam gasification, carbon dioxide and methane formation rates are decreased as well as carbon monoxide and hydrogen formation rates due to hydrogen inhibition [Huttinger ⁵]. Associative hydrogen adsorption has been found to contribute to inhibition in steam gasification at higher pressures (Huttinger^[18]). TPD studies show a hydrogen desorption peak following gasification at 600 °C, indicative of $C(H)_2$ surface groups. Much larger peaks were found

above 1000 °C , proving that dissociative hydrogen inhibition still dominates the carbon surface. These investigators have reported reaction rates approaching zero at carbon conversions as low as 40% in steam/hydrogen mixtures. Gasification rate is also greatly reduced after exposure of carbon to hydrogen in sequential steam/hydrogen/steam reactions (Hutinger^[5]). The rate does not return to its previous value after the second steam gasification is initiated, suggesting irreversible blockage of active sites.

1-2-6. Isotopic Effect

Relatively few gasification studies have been performed using isotopes, even though isotope effects in chemical reactions is very important (Yates^[21]). Gasification rates of graphite in H₂O are reported to be twice as high as graphite in D₂O. Some investigators concluded that breakage of the C-H bond is involved in the rate limiting transition state complex (Yates^[21]), while investigators of later studies concluded that the difference in rate is due to a shift in the oxygen exchange equilibrium constant (Mins^[22]). Very small isotopic effects were found in the H₂ and D₂ gasification of graphite at 1200 °C and 20 torr hydrogen pressure (Gulbransen^[23]). H/D exchange has been shown to take place readily over carbon at 300 °C (Ishikawa, Y. et al^[24]).

¹⁹ Blackwood, D.J. and McGrory, F., Aust. J. Chem. 11, 16 (1958).

²⁰ Montet, G.L., and Myers, G.E., Carbon 9, 673 (1971).

²¹ Yates, J. T. Jr. and McKee, D.W., J. Chem. Phys. 75, 2211, (1981).

²² Mims, C.A. and Pabst, J.K., ACS Div. Fuel Chem. Prepr. 25(3), 263 (1980).

²³ Gulbransen, E.A., Nature 212, 1420 (1966).

²⁴ Ishikawa, Y. et al., Chem. and Phys. of Carbon 12, Walker, P.L.Jr. and Thrower, P.A., ed., 40 (1975).

1-3. Research Objectives

The main objective of this thesis is to characterize the concentration, stability, and reactivity of hydrogen adsorbed on carbon surfaces after gasification.

We use annealed Saran char as main carbon sample. Saran char is generally considered to be amorphous, but it does contain small regions of ordered, graphitic structure. From the book of Blackman^[31], we know the coke would consist of small crystals when the pitch is charred above 1000°C. Our X-ray experiments^[27] confirm that the Saran char contains graphitic structure over small domains and also contains disordered structure over larger domains. The small graphitic crystals in Saran char make the sample have structures similar to graphite; the small size of these ordered structures increases the gasification rate to measurable levels.

1-3-1. Characterization of Adsorbed Hydrogen

We use high temperature TPD (temperature program desorption) to measure the desorption of hydrogen following H₂/steam gasification. Using this information to understand the nature of adsorbed hydrogen, attempt to characterize the hydrogen inhibition mechanism.

1-3-2. Isotope Effects

Prior research has shown that char gasification rate in H₂O/H₂ and D₂O/D₂ was different. This phenomena probably is from different adsorption energies (Ozaki^[25]). If oxygen exchange is reversible and rapid, there will be an isotope effect on the equilibrium

²⁵ Ozaki, A., Isotopic Studies of Heterogeneous Catalysis, New York, Academic Press, Inc. (1977).

gasification experiments and evaluation D_2 stability on the carbon surface to verify the isotopic effect and try to get some details about this issue.

1-3-3. Rate Enhancement by Molecular Oxygen

If adsorbed hydrogen does inhibit the steam/ H_2 gasification, it is reasonable to believe removing the adsorbed hydrogen to recover the activity of carbon. Of course, we already know that the reaction rate will decrease rapidly in the initial phase of gasification. So, we cannot expect the rate recovery to last very long. Also, oxidation by molecular O_2 will not only react with surface hydrogen, it also will react with surface carbon. This may change the surface structure. The formation of new arm-chair edges will increase the reaction rate too.

1-3-4. Hydrogen Stability on Carbon Surfaces

Understanding the stability of adsorbed hydrogen is also important for figuring out the hydrogen inhibition mechanism. H-D, D-H exchange and oxidation by O_2 will be used to exam the stability of adsorbed H_2/D_2 .

1-3-5. Surface Oxygen Group Desorption

The oxygen group on carbon surface is already investigated by many researchers. Huttinger^[5] also attributed to methane formation to the existence of surface oxygen. Determining the relative amount of oxygen and hydrogen on the carbon surface will help to further understand the inhibition mechanism.

CHAPTER 2

EXPERIMENTAL

2-1. Reactants

2-1-1. Carbon Sample

In this study, samples used for gasification are Saran char, coal char and charred cherry pits. Saran char was prepared from Dow Saran resin by heating at 10°C/min to 900°C and holding 30 minutes in a nitrogen flow of 400 cc/min. The average char yield is 25.50%. The foam-like char is crushed and sieved into -60~+100 mesh powder by a ceramic pestle and mortar. Saran chars are further pretreated by heating at 5 °C /min. to 1500 °C in argon for 6 hours in order to anneal and clean the sample surface. Coal char is from the previous research (PSOC 1493), and is also further heated at 5°C /min. to 1500°C in argon for 6 hours. Charred cherry pits are only used for by-pass detection in the high pressure reactor, and were prepared in previous research^[26]. The properties of two chars are given in **Table 2-1**.

Table 2-1 Analysis of Carbon Sample

Component	Saran Char	Coal Char	Annealed Saran	Annealed Coal
Carbon (wt.)	96.4	75.3	97.76	87.19
Hydrogen (wt.)	0.5	0.5	0.019	< 0.001
Nitrogen (wt.)	1.0	1.3	< 0.5	< 0.5
Sulfur (wt.)	0.4	3.6	0.0023	1.36
Chlorine (wt.)	NA	NA	< 0.0010	0.0062
Ash (wt.)	0.1	17.3	0.46	15.00
Oxygen (by diff.)	1.3	2.0	1.78	< 0.1
TSA (BET) m ² /g	850	280	800 N ₂ BET	13.5 N ₂ BET
TSA (CO ₂) m ² /g	1330	440		

2-1-2. Reactant Gases

All gases (Argon, Argon with 1% Krypton and Hydrogen) used are ultra high purity grade (99.999%) except for D₂, which contains 99.4% D₂ and 0.6% HD. Two kinds of argon gases are used. One is mixed with 1% krypton for characterization of

system transients during gasification and is also used as the dilute (product carrier for mass analysis) along with hydrogen and steam. The other one is pure argon and is used as an inert only. All gases are further purified by flowing through R&D Separations Model OT500-2 Oxygen/Moisture Traps to remove water and reduce oxygen to less than 10 PPM. HPLC grade H₂O is outgassed at 100 °C (boiling) for 30 min to remove the dissolved air and stored under argon or nitrogen to minimize dissolved oxygen contain in the steam.

²⁶ **Michael G. Lussier** etc. Carbon Vol. 32 No8, Pp1493-1598,1994

2-2. Equipment and Analytical Instruments

A high pressure reactor, gas flow controllers and a mass spectrometer are the main experimental apparatus. A high temperature reactor (1500 °C) is used for TPD (temperature program desorption) and char annealing. A sketch of the overall system is in **Figure 2-1**. All equipment is designed and installed by Lussier^[27], the more descriptions are given in his dissertation.

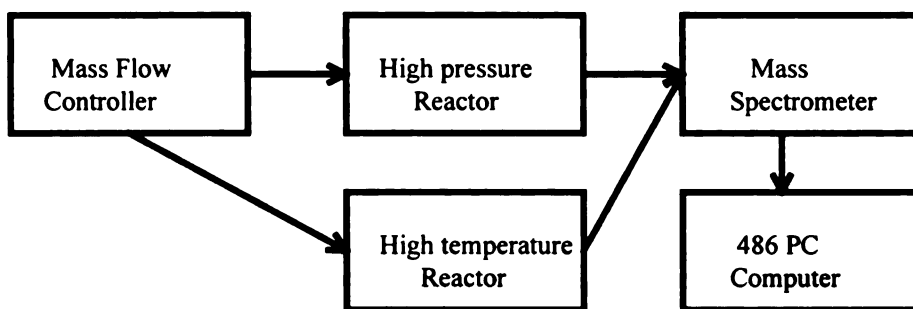


Figure 2-1 Overall system sketch

2-2-1.High Pressure Reactor

The high pressure reactor (**Figure 2-2**) consists of a horizontally mounted 5.1 cm OD x 1.9 cm ID Haynes Superalloy pressure vessel capable of operation at 1000 °C and 6.6 MPa, with a flange closure on one end. It is externally heated with a Lindberg electric furnace. The main pressure vessel houses a 19 mm OD x 11 mm ID x 57 mm length Inconel 625 packed bed microreactor, which is capped at both ends. The microreactor, shown in **Figure 2-8**, is quartz lined, has quartz frits on both ends, and has ceramic fiber gaskets to prevent any sample contact with metal surfaces. This provides a 9 mm diameter x 31mm length internal sample chamber.

²⁷ **Michael G. Lussier**, Ph.D. dissertation Michigan State University (1997)

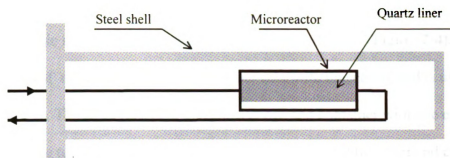
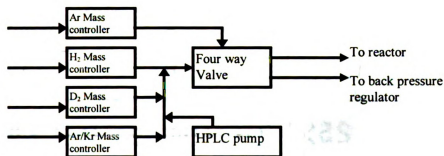


Figure 2-2 High pressure reactor sketch

2-2-2. Flow Control System

Four mass flow controllers and a four way valve allow rapid switching and mixing of up to four gas streams at flow rates of 0-300 cm³ (STP)/min per stream as shown in **Figure 2-3**. For introduction of steam into the manifold system, a Series 1350 Bio-Rad Laboratories HPLC pump is used to inject water into the reactant gas stream at flow rates as low as 10 cm³ (STP)steam/min. Heating tapes are used to prevent steam



condensation.

Figure 2-3 Flow control system

2-2-3. Ceramic reactor

The ceramic reactor is an externally heated fixed bed reactor (**Figure 2-4**). Its main structure consists of three ceramic tubes. The inner tube with one end sealed is used to put in a thermocouple. The outer tube acts as a gas passage and container with one end sealed. The middle tube is the sample bed with one end open and the other end capped by a porous ceramic frit that can allow the gas to enter the reactor and seal the char sample at the same time. Special stainless steel valves and polyfluorotetraethylene and rubber rings are used to seal the gaps between tubes. The reactor can be heated to 1500 °C by a **Mellen** split tube furnace (see next section), which is equipped with a programmable temperature controller to facilitate a linear temperature ramping. This reactor is designed for TPD. Blowing air is used to cool down the part of the reactor outside the furnace to protect the rubber seals.

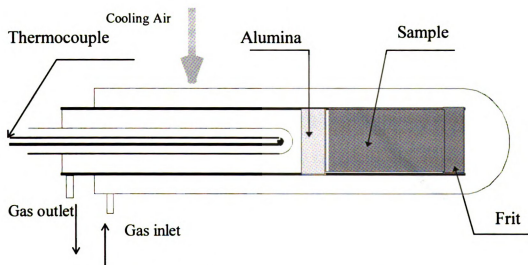


Figure 2-4 Ceramic reactor (not to scale)

2-2-4. Mellen Split Tube Furnace System

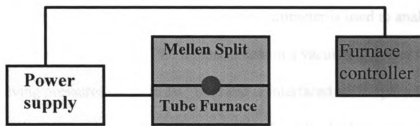


Figure 2-5 Mellen split tube furnace

This system (**Figure 2-5**) contains a tubular furnace and programmable controller. The designed temperature of the furnace is 1500°C. The fastest heating rate is about 5°C/min (between 20°C to 1500°C). At the lower temperature, the heating rate may be over 5°C/min, but above 1350°C, it is difficult to achieve a rate over 5°C/min. Only when the furnace is well preheated (for example, the furnace is over about 700°C), can the heating rate exceed 5°C/min at temperatures over 1350°C. The temperature profile of this furnace is quite flat (**Figure 2-6** is the temperature profile at 1500°C).

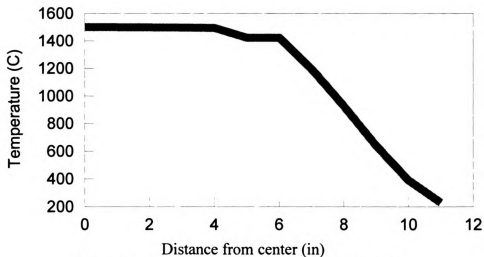


Figure 2-6 Temperature profile of Mellen furnace

2-2-5. Mass Spectrometer

An Ametek Dycor M100 Quadrupole Mass Spectrometer is used to analyze product gases from gasification and TPD. It is mounted on a vacuum chamber that is capable of achieving pressures down to 10^{-8} torr, and is interfaced with a personal computer for data collection and storage. Product gases from the high pressure reactor pass through a back pressure regulator to reduce pressure to atmosphere. A condensation trap is used to separate steam from other gases, to avoid flooding the vacuum chamber. By a fine quartz capillary tube, sample gases are continuously drawn to the vacuum chamber. System sketch is given in **Figure 2-7**.

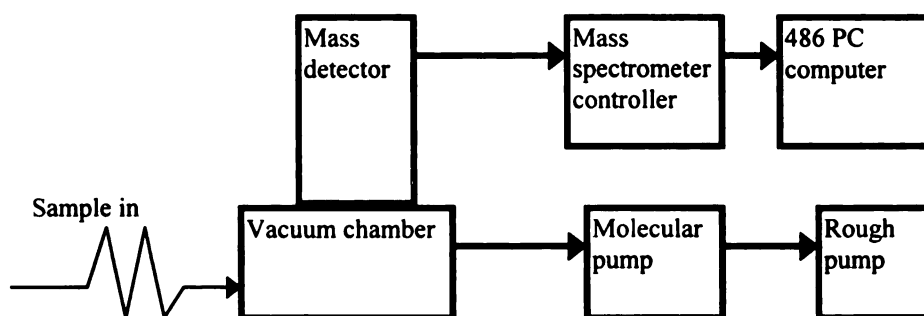


Figure 2-7 MASS spectrometer

2-3. Reactor Characterization

2-3-1. High Pressure Reactor Internal Bypass Detection

A. Structure Analysis and Experiment Design

Because of the structure of the high pressure reactor (Figure 2-8), by-pass is unavoidable.

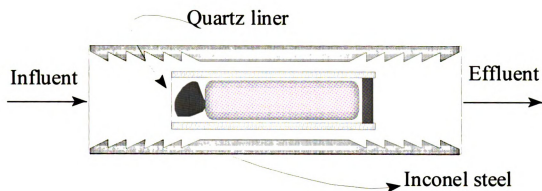


Figure 2-8 High pressure reactor cell (not to scale)

The reactant gases have two possible ways to go:

1. Flow through the packed char bed
2. By-pass through the gap between the quartz liner and Inconel steel reactor.

The quartz is very fragile, so it is impossible to use force to avoid by-pass.

To detect the extent of by-pass, three experiments were designed. The ideas are

- Use high activity carbon (charred cherry pits) to make sure O_2 converts to CO_2 quickly and completely.
- Using low temperature (about 600°C) to limit the $\text{CO}_2 + \text{C} \leftrightarrow \text{CO}$ reaction (at that temperature, the equilibrium constant is 0.27).

- In ceramic reactor, the internal by-pass is impossible. By comparing the experimental results of extent of gasification in the two reactors, we can calculate the extent of by-pass.

Two different particle sizes (-60~+100 and -30~+60) are used to detect the relative amount of bypass, which should change with particle size. The actual experimental conditions are

- ◆ 606 °C
- ◆ 60 cc/min. 5% O₂ (or 2.5%) in argon
- ◆ 1~2 hours gasification.
- ◆ -60~+100 and -30~+60 charred cherry pits
- ◆ atmospheric pressure in ceramic reactor and high pressure reactor

B. Experiments and Results

Figure 2-9 gives the product gas profiles for -60~+100 charred cherry pit oxidation in the ceramic reactor. From this figure, we can clearly see that the dominant product is CO₂ and no O₂ can be found in the outlet. That means all reactant O₂ is converted to CO₂ and CO in these reaction conditions.

Using the same sample and conditions, the product profile from the high pressure reactor is much different (**Figure 2-10**). Quite a lot of molecular O₂ still exists in products. That means that by-pass happens.

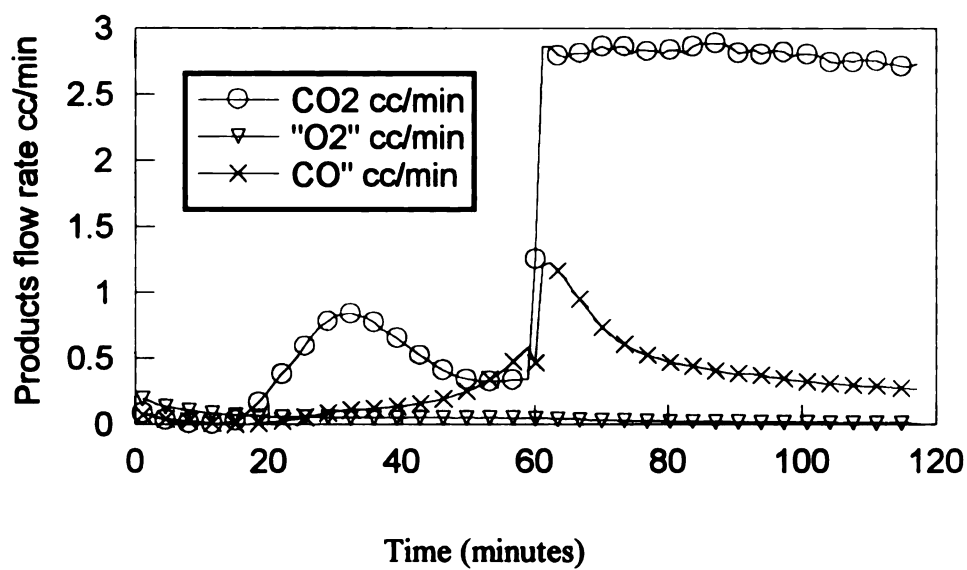


Figure 2-9 Charred cherry pits oxidation (ceramic reactor)

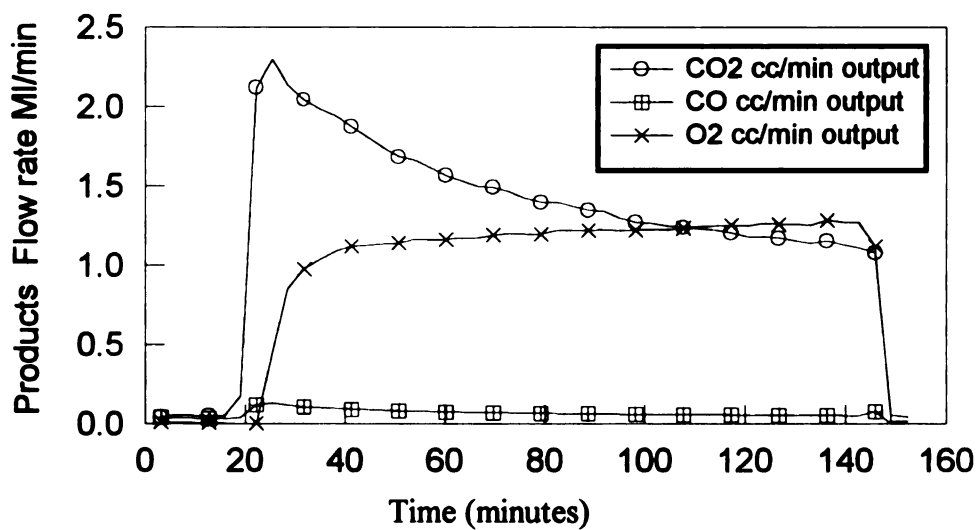


Figure 2-10 Charred cherry pits oxidation (high pressure reactor)

At this low temperature, the catalytic effect of the ceramic reactor wall is negligible. The second reaction ($\text{CO}_2 + \text{C} \leftrightarrow \text{CO}$) is limited. So, we can estimate the bypass fraction by the ratio of $\left(\frac{\text{Outlet O}_2}{\text{Inlet O}_2}\right)$.

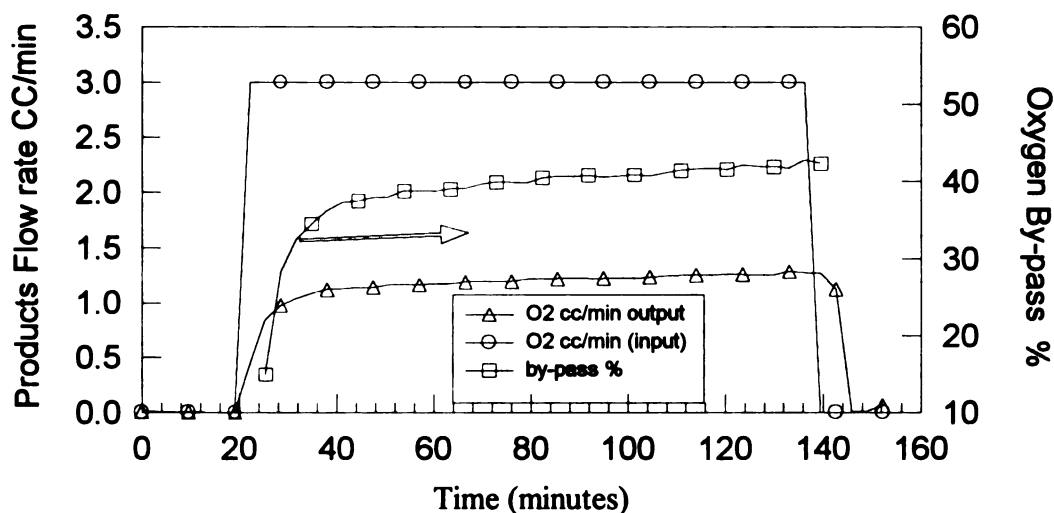


Figure 2-11 Oxygen by-pass in high pressure reactor (-60~+100 cherry pits)

For -60~+100 charred cherry pits (**Figure 2-11**), from the amount of exiting O_2 we can calculate the bypass fraction, which is about 40%. Little increase with conversion can be found. This phenomenon is caused by the ash particles collapsing, which increases the char bed resistance. After the experiment, a layer of ash was found on the inlet side of the sample.

For -30~+60 charred cherry pits (**Figure 2-12**), the bypass is about 30 %. It is reasonable, because the flow resistance in the char bed is smaller than for the -60~+100 char.

From the above experiments, we can conclude that the extent of gas by-pass in the high pressure reactor is about 40% for -60~+100 char.

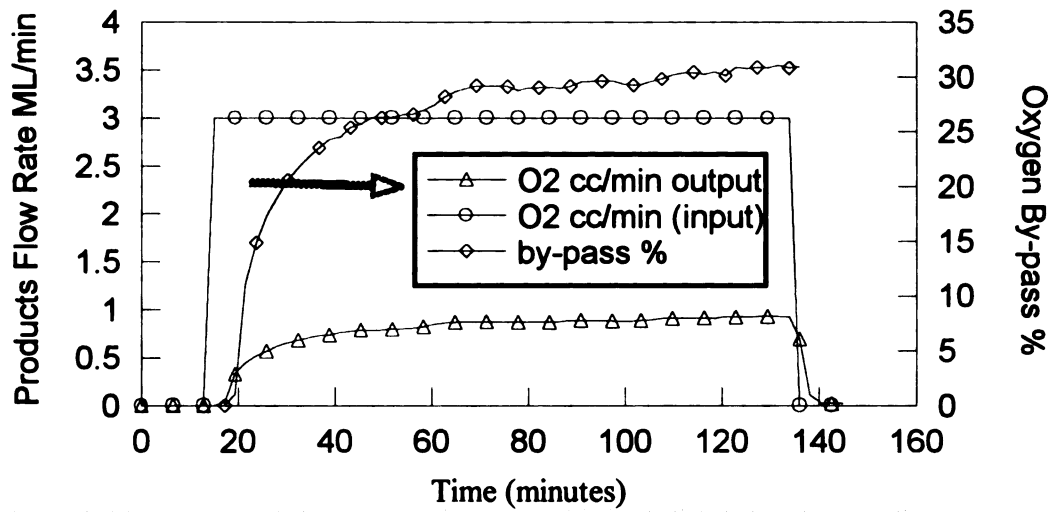


Figure 2-12 Oxygen by-pass in high pressure reactor(-30~+60 cherry pits)

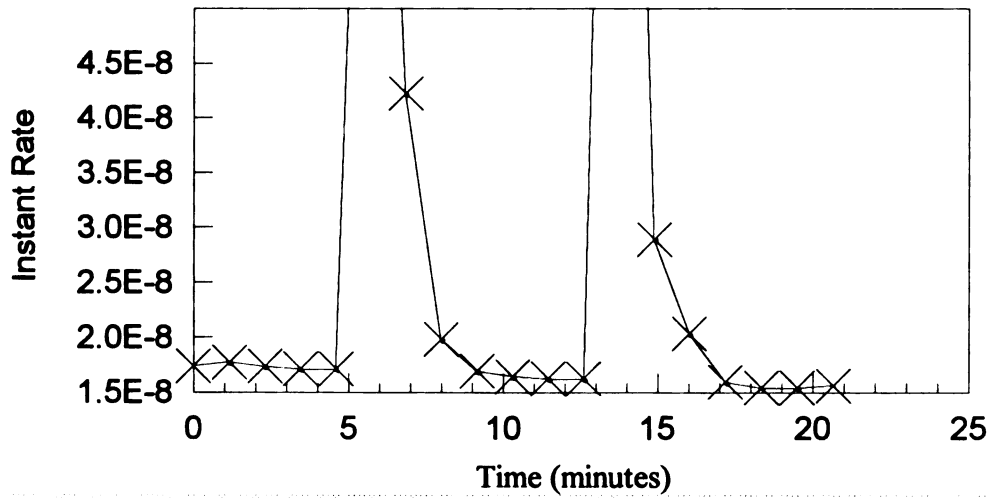


Figure 2-13 System response to pulse

2-3-2. Ceramic Reactor Response

The dead volume in the TPD reactor will broaden the TPD peak. To eliminate this problem, the ceramic reactor was designed to achieve as small as possible a dead volume.

Figure 2-13 is a specially designed pulse experiment to check the effect of back mixing on the TPD profile, in which a H_2 pulse was injected into the purge line. The two injections produced two sharp step responses. The tail of the peak exists for less than 3 minutes. For a typical TPD experiment, the desorption time is more than 300 minutes. So, we have confirmed that back mixing can be neglected in our TPD experiments.

2-3-3. Fluid Dynamics Calculation

Because of the by-pass, it is necessary to check diffusion resistance. The internal diameter of quartz liner is 9 mm. Char particle size is $-60 \sim +100$ (0.149~0.250 mm). The sample average particle diameter is 0.2 mm. The ratio of particle diameter to quartz liner is about 0.02. From Perry's handbook, we can get bed porosity $\varepsilon=0.32$. The parameters calculated are given in **Table 2-2**.

Table 2-2 Dynamics Calculation

Pressure (MPa)	Gas flow rate $cm^3/min.$	Cross area cm^2	U cm/sec. (apparent)	U_T cm/sec. true velocity	U_T cm/sec. after by-pass
0.1	300	0.63585	7.863	24.57	14.74
1	300	0.63585	0.7863	2.45	1.47
2	300	0.63585	0.3931	1.23	0.74
3	300	0.63585	0.2621	0.82	0.49

In most case we operate the reactor at 3.1 MPa. After 40% by-pass, the true gas velocity of 0.49 cm/s is large enough compared with the very low gasification rate. So, we can conclude that the mass transfer resistance will not affect the gasification reaction.

2-4. Reaction Conditions and Experimental Procedures

2-4-1. Reaction Conditions

For our gasification process, temperature, pressure, H_2 (D_2)/steam/argon ratio, and the reaction times are the changeable parameters.

- ◆ For most experiments, the temperature was fixed at 850 °C. At this temperature, the effluent species concentrations are well within the detectable range, and mass transport resistances are not significant (see Section 2-3). For some highly active samples (coal char, cherry pits char), a temperature of 725 °C also was used to slow down the reaction rate.
- ◆ The pressure is limited by the reactor pressure chamber, which can withstand up to 6MPa. Most experiments were conducted at 0, 0.3, 1.0, or 3.1 MPa.
- ◆ The reactant flow rates are up to 300 cc(STP)/min, which is limited by the mass flow controller. This flow rate is also required to eliminate the transport resistance to get true kinetics.
- ◆ The sample sizes are limited by the size of the quartz liner. For Saran char, maximum sample size is 0.35 to 0.45 g; for coal char and cherry pit char, it is about 0.7 to 0.9g, depending on the sample density.
- ◆ Steam flow rate was fixed at 120 cc/min(40 mole %) for most experiments.

2-4-2. Experimental Procedures

The experimental scheme is given in **Figure 2-14**.

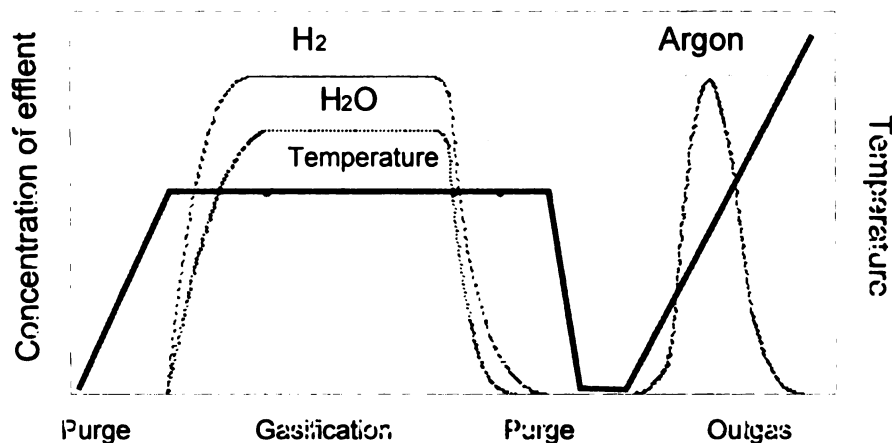


Figure 2-14 Experimental scheme

A. Preparation of Mass Spectrometer

Before gasification and TPD, we need to prepare the mass spectrometer. After opening the capillary inlet valve, the vacuum chamber was pressurized with purge argon (from the bypass line). When the background of the mass spectrometer was stabilized, we collected the background data (usually 5 scans), and then conducted the calibration for H₂(D₂), CO, CO₂, and CH₄ (or CD₄) to get the real time responses.

B. Gasification ^[*]

After the high pressure reactor was purged 20~30 minutes to expel residual air, the heating tape and furnace power was turned on. At same time, the reactor was pressurized with argon. The bypass line was pressurized with reactant gas a little later, and the steam trap was filled with crushed ice (if the reactant including steam). Once the pressure and temperature of the entire system were stabilized, mass spectrometer data

* Most 7000 series gasification experiments were done by Lussier

collection was begun. After five or more scans, a step change in reactor feed from purge argon to reactant gas was made to begin the gasification by switching a 4-way valve that interchanges the flow paths of these two streams. Pressure and temperature were monitored and required small periodic adjustments of regulator and temperature controller during the course of experiments. After a planned length of time, the 4-way valve position was switched back to create a step change in reactor feed composition from reactant gas to purge argon. After the reactor effluent composition (monitored by mass spectrometer) had stabilized, the data collection was stopped and the vacuum chamber was closed. The reactor and bypass lines were then depressurized and furnace and heating tapes power was turned off. The reacted sample was allowed to cool down for about 10 hours (usually overnight), and maintained in an argon purge of 2~5 cc/min for the purpose of protection.

C. Temperature Programmed Desorption(TPD)

After samples were removed from the gasification reactor and weighed, they were loaded into the high temperature ceramic reactor quickly to limit the exposure time in air. Short exposure of samples did not affect the accuracy of hydrogen measurement, as shown in Section 2-6-3.

After samples were loaded into the ceramic reactor, we added a small amount of tabular alumina (-14~ +28 mesh) on the top of the sample to prevent sample spillage into the annular portion of the reactor. The alumina particle size was chosen to ensure that the alumina was too big to enter the annular area, but small enough so as not to allow char to pass through it. The reactor was then assembled and sealed by tightening fittings. After

loading the whole reactor into the high temperature furnace, the reactor was purged with argon for 30 minutes. When the calibration (H_2 or CO , CO_2 , CH_4) was finished, the furnace was turned on and the mass data collection begun. A linearly heating rate of 5 and $10\text{ }^\circ\text{C}/\text{min}$ were used in most TPD experiments. The highest temperature the furnace can reach is $1500\text{ }^\circ\text{C}$. This temperature is necessary for hydrogen desorption. Lower flow rates broaden the TPD profile, while higher flow rates dilute H_2 (CO and CO_2) concentrations in the effluent gas. A flow rate of $30\text{ cm}^3\text{ (STP)}/\text{min}$ was used to balance the two factors. The desorbing species were continuously monitored for the entire TPD process. After the temperature reached $1500\text{ }^\circ\text{C}$, a one hour holding time was used for further possible desorption. After that, the furnace power was shut off automatically by the temperature program controller.

D. Surface Structure Characterization

A Micromeritics Pulse Chemisorb 2700 was used to measure the BET surface area. The total surface areas of char were measured by nitrogen adsorption. Twenty to fifty mg of char were loaded into a quartz sample tube, which was then sealed to the Chemisorb and heated to $150\text{ }^\circ\text{C}$ for more than 30 min to drive off possible weakly adsorbed species (mostly water, which makes the instrument unstable). After finishing the calibration, a mixed gas, which contained 5%, 10% and 18.75% N_2 in helium at a total flow rate of $16\text{ cc}/\text{min}$, was passed over the sample. The effluent gas composition was measured for nitrogen concentration by detector, and the desorption and adsorption profiles and peak area were recorded.

2-5. Data Analysis

2-5-1. Mass Spectrometer Calibration

Calibration of the mass spectrometer was performed by scanning two AGA certified standard multi component gas mixtures. The first contains 2.00% CO, 2.03% CO₂, 2.00% CH₄, and balance argon, while the second contains 2.05% CO, 2.03% CO₂, 2.01% CH₄, and balance hydrogen. Five scans of carrier gas containing no key species of interest were taken to obtain background levels, averaged, and then subtracted from the average of five scans of calibration gas to obtain actual peak values. The mole fractions of key species in the calibration gas were then divided by the corrected mass spectrometer peak values to obtain actual responses. Purge gas composition and calibration carrier gas composition must both be identical and must match the reactant gas composition to be used for gasification because the response of key species is a function of carrier gas composition and is about three times higher in hydrogen than in argon.

2-5-2. General Data Deconvolution

The most difficult work in mass spectrometer use lies in data deconvolution. Fragmentation, double ionization, and natural isotopes all may cause peak overlap in the mass spectrum. In our system, only M84 (krypton), M44(CO₂) and M40 (argon) are simple peaks with no overlapping. The main purpose of our analysis is to detect the CO, H₂, CH₄ and CO₂. That mean only CO₂ does not involve peak overlap. **Table 2-3** gives the possible fragmentation of these species.

Table 2-3 Possible Fragmentation

Channel						
M2	H ₂					
M3	HD					
M4	D ₂					
M14	N(N ₂)	CH ₂ (CH ₄)	CD(CD ₄)			
M15	CH ₃					
M16	CH ₄	O	O(H ₂ O)	O(CO ₂)	O(CO)	O(O ₂)
M17	CH ₃ D	CD ₂ H	OH	O ¹⁷		
M18	H ₂ O	CD ₃				
M19	CD ₂ H	DHO				
M20	CD ₄	D ₂ O				
M28	CO	N ₂	CO*			
M32	O ₂					
M44	CO ₂					

Table 2-4 Fragmentation Patterns in Argon Carrier^[*]

Channel	CO ₂	CO	CD ₄	CH ₄	D ₂ O	H ₂ O	D ₂
M2							0.031
M3							
M4							1.00
M14				0.06			
M15				0.85			
M16			0.04	1.00		0.01	
M17						0.14	
M18			0.80			1.00	
M19							
M20			1.00				
M28	0.11	1.00					
M32							
M44	1.00						

* These experiments were done by Lussier.

A. Time Shift in MASS Data

All 12 channels of the mass spectrometer were scanned sequentially. That causes another problem, time shift.

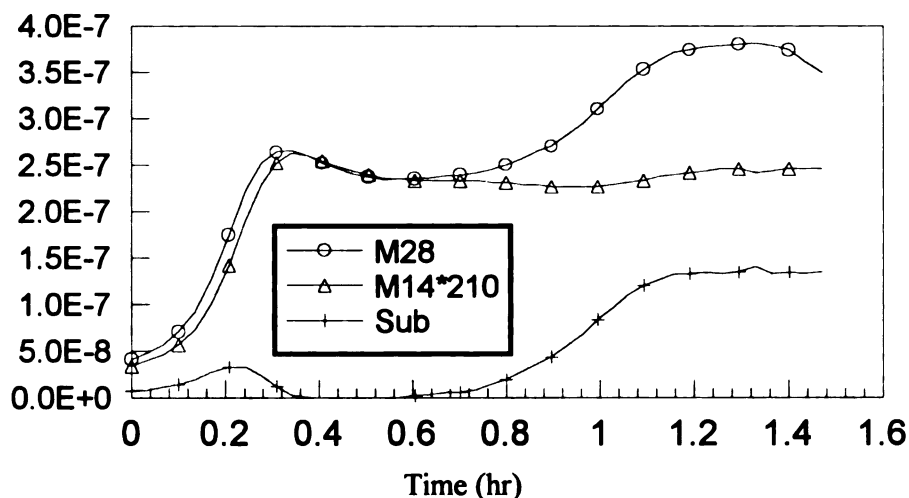


Figure 2-15 Before time shift

For a one second dwell time, it takes 2 minutes to scan all 12 channels. That means the time difference between channel 1 and channel 12 is up to 2 minutes. But in the data file, we have to put all 12 channels into the same time array. If we set channel 1 and 12 to same mass, the curve will shift about 2 minute. If we only use one channel to deconvolute the data, it does not matter. But when we need to deconvolute the overlapped peak (CO and N₂ of M28), we have to subtract one channel from another. This problem appears and will produce an artificial peak due to the time shift (**Figure 2-15**). To eliminate the time shift effect, we need to shift the time axis for a special time for each channel. In that way, we can get the exact overlapped curves (**Figure 2-16**).

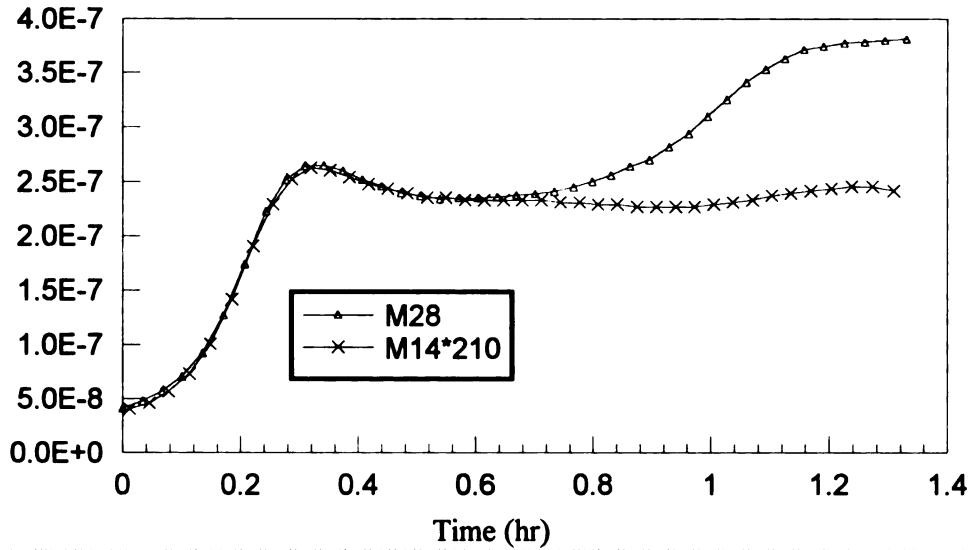


Figure 2-16 After time shift correction

But the subtraction still is impossible, because we do not have corresponding points after the time shift (**Figure 2-16**). Before we can subtract spectra, we have to fit the data by a function.

First order fitting seem does not work around the peaks (the data values change rapidly). The second order fitting ($Y=a+bX+cX^2$) works much better.

From continuous three points, we can get the fitting parameters:

$$b = \frac{(y_2 - y_3)(x_1^2 - x_2^2) - (y_1 - y_2)(x_2^2 - x_3^2)}{(x_2 - x_3)(x_1^2 - x_2^2) - (x_1 - x_2)(x_2^2 - x_3^2)}$$

$$c = \frac{(y_1 - y_2) - b(x_1 - x_2)}{x_1^2 - x_2^2}$$

$$a = y_1 - bx_1 - cx_1^2$$

The fitted results are given in **Figure 2-17**. We can see the second order fit is good enough. From $Y=a+bX+cX^2$, we can get corresponding points using the shifted time. Now, we can subtract any channel. **Figure 2-17** gives the results. We can see that the artificial peak almost disappears.

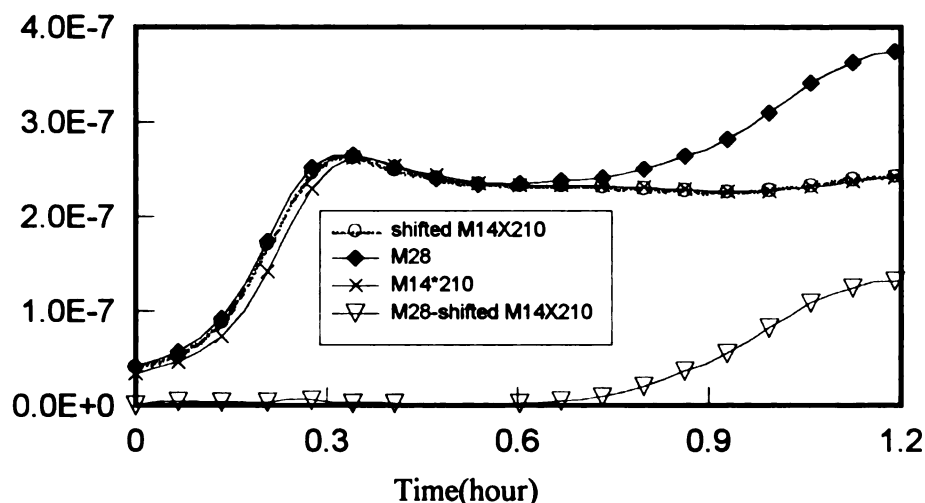


Figure 2-17 After the time shift, artificial peak no longer exists

B. Species Deconvolution

- Methane: M=15 for CH₄ (to avoid confusion with fragmentation of species containing oxygen).

$$CH_4 = \frac{(M15 - M15_{background}) \times \text{Flowrate} \times \text{Reponse}}{\text{Sample weight}} \quad \left(\frac{\text{ml}}{\text{min. gram}} \right)$$

- H₂/D₂: M=4 for D₂, M=3 for HD, and M=2 for H₂ (after subtraction of contribution from D₂ fragmentation).

$$H_2 = \frac{(M1 - M2_{background}) \times \text{Flowrate} \times \text{Reponse}}{\text{Sample weight}} \quad \left(\frac{\text{ml}}{\text{min. gram}} \right)$$

- CO₂: CO₂ is the easiest among all deconvolutions. After subtract the background, we simply multiple the mass data by the response factor and carrier gas flow rate.

$$CO_2 = \frac{(M44 - M44_{background}) \times \text{Flowrate} \times \text{Reponse}}{\text{Sample weight}} \quad \left(\frac{\text{ml}}{\text{min. gram}} \right)$$

- CO: The M28 peak includes CO, fragmentation of CO₂ and N₂. After time shift of CO₂ and M14, we can subtract contribution from CO₂ and N₂ fragmentation, and then subtract the background. At last we can get the real CO flow rate:

$$CO = \frac{(M28 - 0.15 \times M44^* - 210 \times M14^*) \times \text{Flowrate} \times \text{Reponse}}{\text{Sample weight}} \left(\frac{\text{ml}}{\text{min.gram}} \right)$$

Note: M44* and M14* are the data which are processed using the time shift technique to avoid artificial peak.

2-5-3. CD₄ and D₂O Deconvolution

CD₄ and D₂O deconvolution is the most complex of all deconvolutions. The principle is

- ⇒ P18 from H₂O, CD₃, DO
- ⇒ P20 from D₂O, CD₃
- ⇒ P17 from OH, CD₂H, CDH₃

From the fragmentation experiments, we know most P17 comes from OH. After using the H₂O fragmentation data, we can subtract the H₂O part from P18, so that only CD₄ and D₂O contributes to P18 and P20. We try to use the two dimensional matrix to deconvolve the CD₄. First we need to find background for P17, P18, P20.

- ◆ P20_{back}: If there no D₂ and D₂O present, the P20 chamber pressure should be at the background, it is 4.5×10^{-11} torr.
- ◆ P17_{back}: In D₂ fragmentation experiments, after a long time purging the chamber, we believe that no more OH exists in the chamber. The P17 can thus be used as background, again 4.5×10^{-10} torr.
- ◆ P18_{back}: In D₂O fragmentation experiments, P18 is only from DO (not from H₂O). So

$$(P20 - P20_{\text{back}}) * K_{D2O} = (P18 - P18_{\text{back}}) \Rightarrow P20 = P18 / K_{D2O} - P18_{\text{back}} / K_{D2O} + P20_{\text{back}}$$

This is a linear equation and after fitting the experiment data, we can get P18_{back}, 1.8×10^{-11} torr.

Because of the slow displacement of H_2O by D_2O in the vacuum chamber, we need to take into account the H_2O fraction in P18. We have to subtract the H_2O from P18 before deconvolution. From H_2O fragmentation experiments, we can get $K_{\text{H}_2\text{O}}$ (fragmentation factor) by

$$(P18 - P18_{\text{back}}) * K_{\text{H}_2\text{O}} = (P17 - P17_{\text{back}}).$$

The value of $K_{\text{H}_2\text{O}}$ is 0.163. At last, we can get the “real” P20 and P18 (only from D_2O and CH_4) from

$$P20_r = P20 - P20_{\text{back}} ; \quad P18_r = P18 - (P17 - P17_{\text{back}}) / K_{\text{H}_2\text{O}}$$

Now, we can deconvolute the CD_4 and D_2O . If we set

X is fraction of M20 from D_2O , K_1 is the M18 fragment of D_2O

Y is fraction of M20 from CD_4 , K_2 is the M18 fragment of CD_4

We have : $X + Y = P20_r$ and $X * K_1 + Y * K_2 = P18_r$. From these two equation we can get:

$$X = [P20_r - P18_r / K_2] / [1 - K_1 / K_2] \text{ and } Y = [P20_r - P18_r / K_1] / [1 - K_2 / K_1]$$

The procedure of getting K_1 and K_2 is given as follows. In CD_4 fragmentation

experiment, $X=0$, So $K_2 = [P18 - P18_{\text{back}}] / [P20 - P20_{\text{back}}]$.

The value is given in **Table 2-5**.

Table 2-5 The K_2 Change with Carrier Gas

K_2	0.71	0.53	0.38
Carrier gas($\text{Ar} + \text{D}_2$)	100%Ar	66%Ar	33%Ar

In D_2O fragmentation experiment, $Y=0$, So

$$K_1 = [P18 - P18_{\text{back}}] / [P20 - P20_{\text{back}}]$$

K_1 is 0.17 in argon carrier gas. Thus we can deconvolute CD_4 and D_2O in $\text{D}_2\text{O}/\text{D}_2$ gasification.

2-6. Carbon Sample Characterization

2-6-1. Outgas of As-prepared Saran and Coal Char

A. Outgas of Saran Char

The results of outgassing as-prepared Saran char are given in **Figure 2-18 to 2-21**.

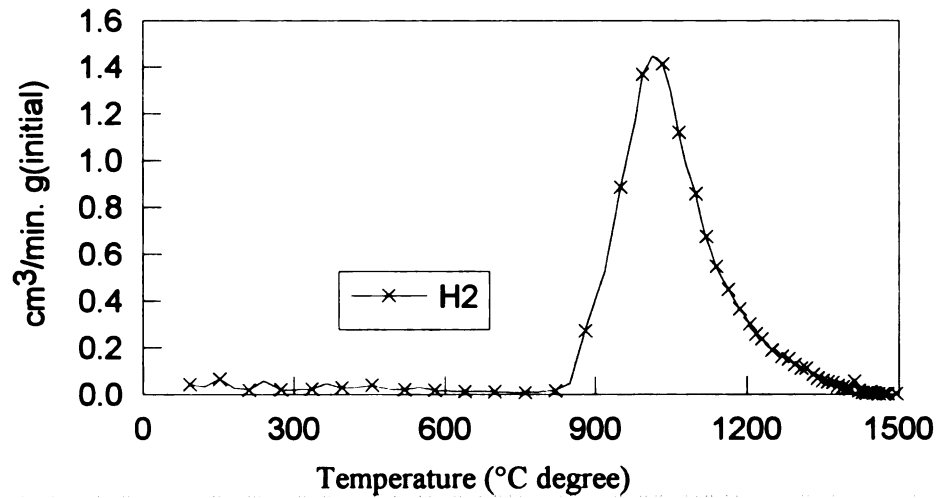
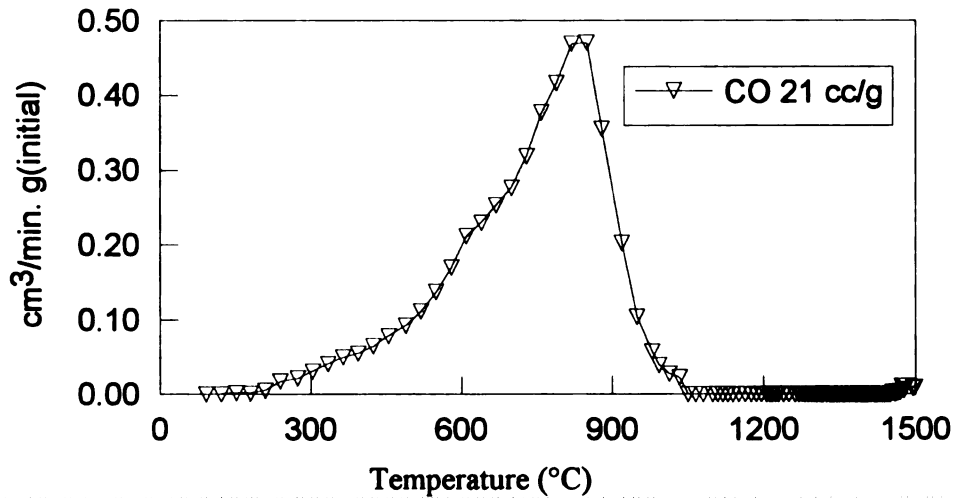
Peaks for CO₂ desorption in the range of 250°C ~1000°C, for CO in the range of 500~900 °C, and for H₂ from 700°C up to 1500 °C were observed.

We can find from these figures that a temperature of 1500 °C is enough to removes essentially all adsorbed species from the surface. If only removing surface oxygen groups, 1050°C is enough. Above this temperature, all CO and CO₂ peaks disappear. For H₂, a higher temperature, over 1400 °C, has to be used to get a flat peak tail.

To verify the above finding ,we determined the total amount of H₂, CO, and CO₂ desorbed from as prepared Saran char by integrating the desorption curves over the course of outgassing. A comparison of the quantity desorbed with that calculated from the char hydrogen and oxygen contents as determined by ultimate analysis is given in **Table 2-6**. The agreement is surprisingly good, and indicates that heating to 1500°C effectively removes essentially all hydrogen and oxygen from the Saran char. Only the sum of CO and CO₂ can be compared, as both contain oxygen. This result is important in light of our goal of measuring the quantity of hydrogen on char surface following gasification and correlating the quantity to gasification rate.

Table 2-6 Comparison of Element Analysis and TPD

	Hydrogen	Oxygen from CO	Oxygen from CO ₂	Total Oxygen
H ₂ from Outgas	62 cc/g	0.5×21 cc/g	6.5 cc/g	15 cc/g
Weight % from outgas	0.55%	0.75%	0.46%	1.21%
Ultimate analysis	0.5%		1.3%	

**Figure 2-18 Outgas of as-prepared Saran char****Figure 2-19 Outgas of as-prepared Saran char**

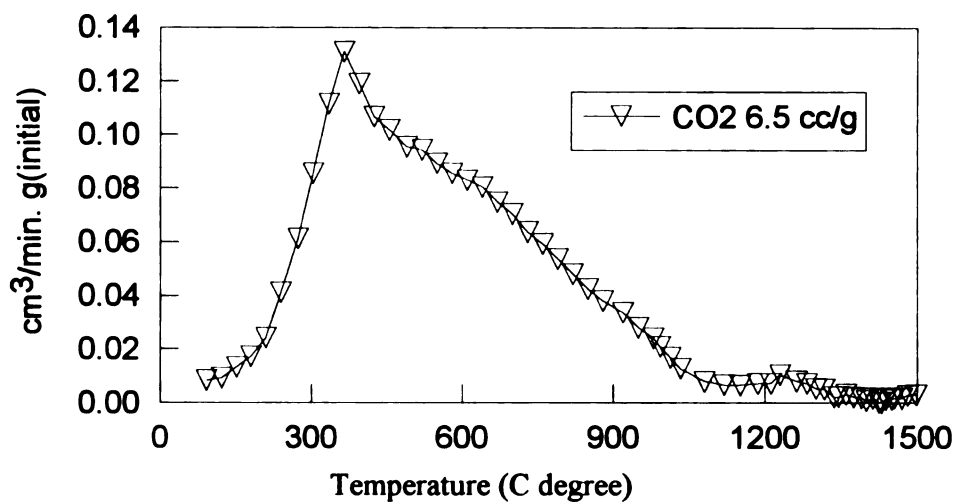


Figure 2-20 Outgas of as-prepared Saran char

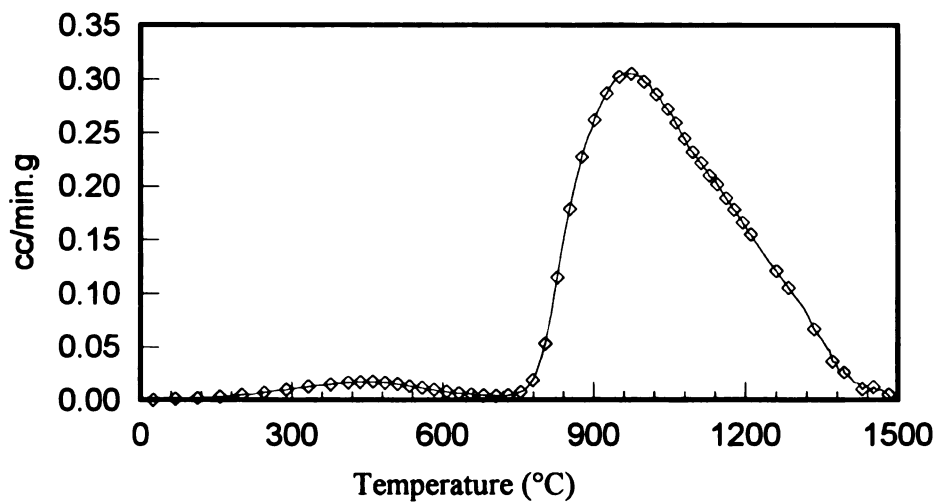


Figure2-21 Low rate TPD profile, heating rate $2^\circ\text{C}/\text{min}$
purge argon=60cc/Min , W=0.655g (Exp-015)

It should be noted that the baseline of M28 is not flat, probably because adsorbed N_2 from the reactor also contributes to the M28 signal. To get the real CO signal, we need to subtract the N_2 component using the M14 data.

B. Coal Char TPD Profiles

Coal char TPD profile (Figure 2-22) is different from Saran char. For CO, two clear peaks can be found. The amount desorbed is much greater than Saran char (10 times). This is an indication that coal char contains more oxygen than Saran char. The first peak position is at about the same position as Saran char. The second peak is situated at 1200~1400 °C, and seems like the caved-in oxygen proposed by Yang^[6].

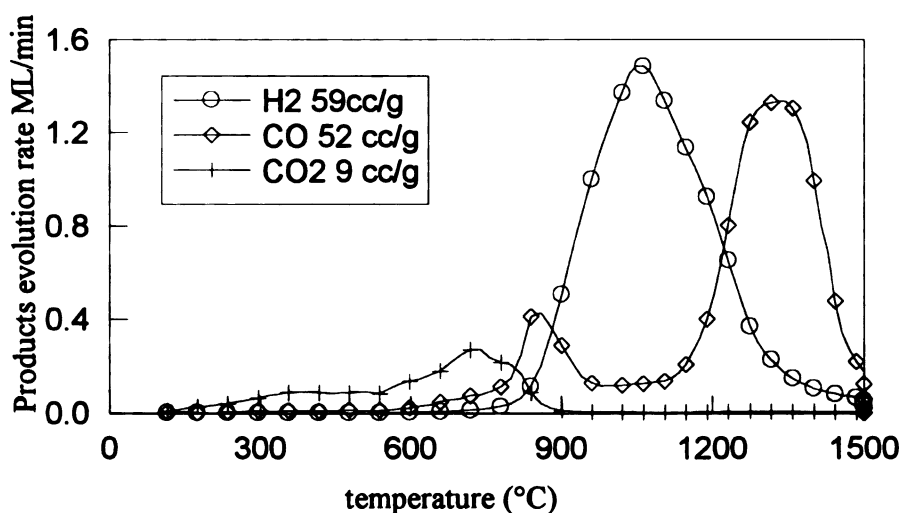


Figure 2-22. Coal char TPD profile, heating rate 10 °C /min

2-6-2. Saran Char Annealing

The pretreatment temperature of char has significant effects on gasification rate. Many previous researchers have done lots of work on this issue. However, very few researchers have used a temperature higher than 1200°C. Our purpose is to stabilize the char structure by using high temperature annealing (up to 1500°C and 10 hr.).

Saran char pretreatment experiments were done at the following conditions:

- ◆ Saran char 0.5-1 gram
- ◆ Argon gas flow rate 30-120 cc/min
- ◆ Temperature range 900-1500 °C
- ◆ Heating rate 3°C/min or 5°C/min

A. The Effects of Heating Rate and Annealing Temperature on BET

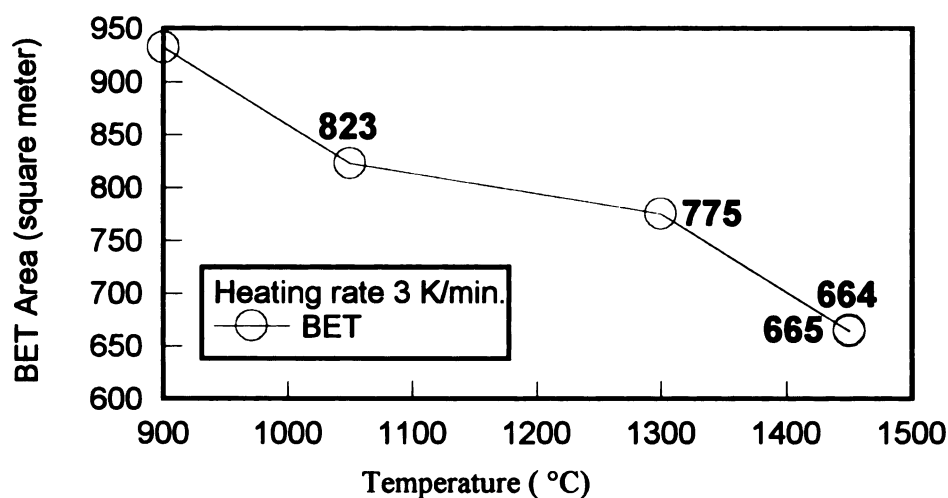


Figure 2-23 BET area changes with pretreatment temperature (heating rate 3°C/min)

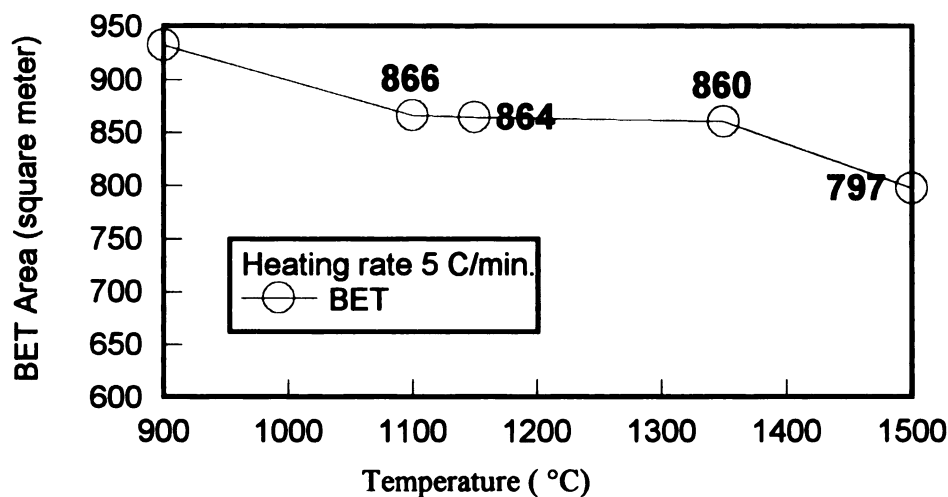


Figure 2-24 BET area changes with pretreatment temperature (5°C/min heating rate)

The pretreatment experiments are performed at several different temperatures and two heating rates ($3^{\circ}\text{C}/\text{min}$ and $5^{\circ}\text{C}/\text{min}$). At first, the purpose of changing the rate was to reduce experiment time; however, when comparing the experiment data we found the heating rate has some effect on the BET surface area. **Figures 2-23 and 2-24** give the BET area changing with pretreatment temperature at two heating rates. Although both figures have the same trend with pretreatment temperature, the change is not very significant. For $3^{\circ}\text{C}/\text{min}$ heating rate, BET area decreases 28% after a 1450°C heat treatment. For 5°C heating rate, the change is only 14% after 1500°C treatment. From the N_2 adsorption and desorption curves in BET measurements, we can see a trend that as pretreatment temperature increases, the adsorption process becomes slower. This suggests that the pore structure of Saran char must have changed. With the increase of pretreatment temperature, the changes become more and more significant. Unfortunately the structure of Saran char is too weak to stand the high pressure in mercury porosimetry measurements, so we cannot directly get the distribution of micro pore diameters to further verify the above deductions.

The BET surface area is shown as a function of annealing time in **Figure 2-25** for Saran char. With the increase in annealing time, the BET surface area decreases quickly, then stabilizes after 6 hours. In N₂ adsorption and desorption (**Figure 2-26** and **Figure 2-27**), we can see that the relative peak intensity and adsorption times before annealing and after annealing are significantly different. After annealing, the longer adsorption time and lower peak intensity suggests that the number of micro pores must have increased and the total surface area have decreased.

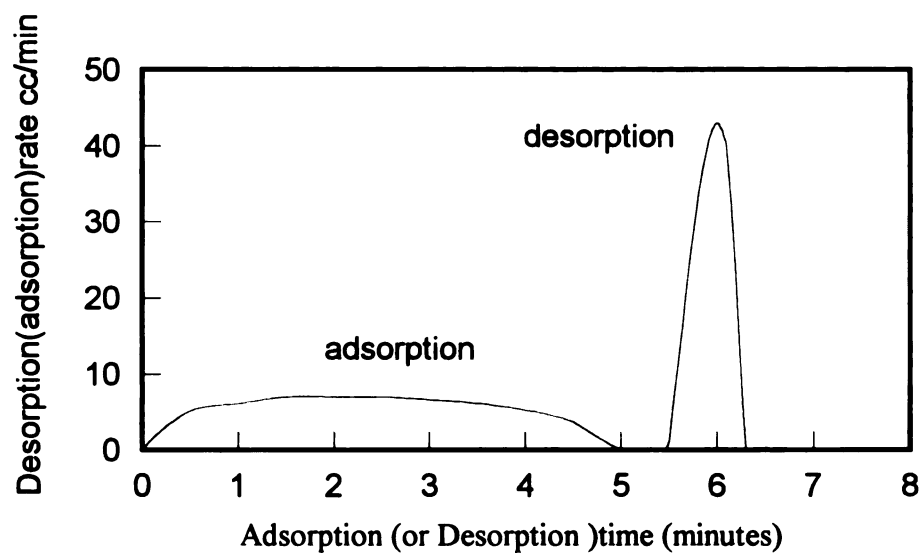


Figure 2-26 N_2 profile in BET for Saran char $P_{N_2}=0.05$ atm (sample weight=0.048g)

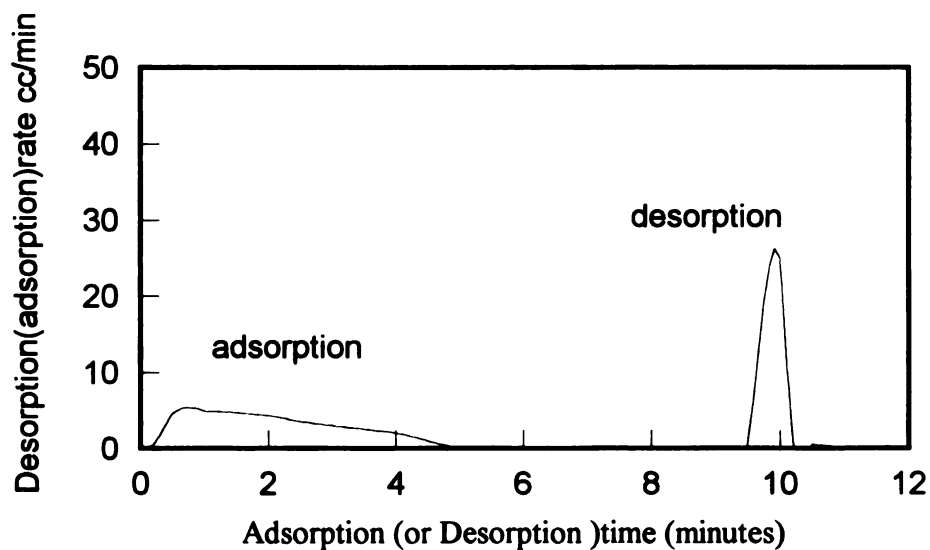


Figure 2-27 N_2 profile in BET for annealed Saran char $P_{N_2}=0.05$ atm ($W=0.048g$)

Annealing also changes the physical structure of Saran char. The difference is that when the annealing reaches a certain time (in this experiment it is about 6 hours), the BET surface area does not change further. From these phenomena, we can conclude that high temperature annealing makes the char reach a relatively stable structure. It is highly possible that annealing is a process of big pores collapsing and micro pores opening.

C. Conclusions

Both high temperature treating and annealing have effects on the Saran char's physical structure. With pretreatment temperature increasing, the BET area decreases. With the annealing time increase, the BET area decreases at first and then becomes stable (after 6 hours for Saran char). The annealing significantly changes Saran char BET area (~34%). High temperature treatment also is a process of further pyrolysis, which contributes to part of the surface change. We can speculate that big pores collapse and micro pores open during the annealing process.

After annealing, we can find that the Saran char near the frit (gas inlet) is a little darker than the normal one. It seems that the impurities in argon gas do react with the char sample. However, from simple estimation, the largest possible amount gasified with the active gas in argon is no more than 0.0013g (100cc/min, argon purity 99.999%, 20 hr.). Total weight loss is at least 0.1g in the high temperature pretreatment experiment, so, the weight loss is mainly due to pyrolysis.

2-6-3. Annealed Saran Char Exposure in Air

When outgassed Saran char is exposed in air, it will adsorb impurities from the air continuously. The amount of adsorbed impurities depends on exposure time. For

2-6-3. Annealed Saran Char Exposure in Air

When outgassed Saran char is exposed in air, it will adsorb impurities from the air continuously. The amount of adsorbed impurities depends on exposure time. For determining the extent of this effect, three experiments were designed and three different exposure times were used. Table 2-7, Table 2-8 and Figure 28~34 gives the experimental results.

Table 2-7 Impurities from Exposure

Species uptake	H ₂	CO(N ₂)	CO ₂
expose 2 min.	2.1 cc/g	17.3cc/g	4.1 cc/g
expose 0.5 hr.	4.3 cc/g	26.3 cc/g	7.2 cc/g
Expose 2 days	55.4 cc/g	83.3 cc/g	68.7 cc/g

Table 2-8 The Peak Position (°C) Changes with Exposure Time

Peak position	H ₂	CO(N ₂)	CO ₂	H ₂ O
Expose 2 min.	1280	660	970	No peak
Expose 0.5 hr.	1210	660	910	No peak
Expose 2 days	1300	800	210 & 720	210

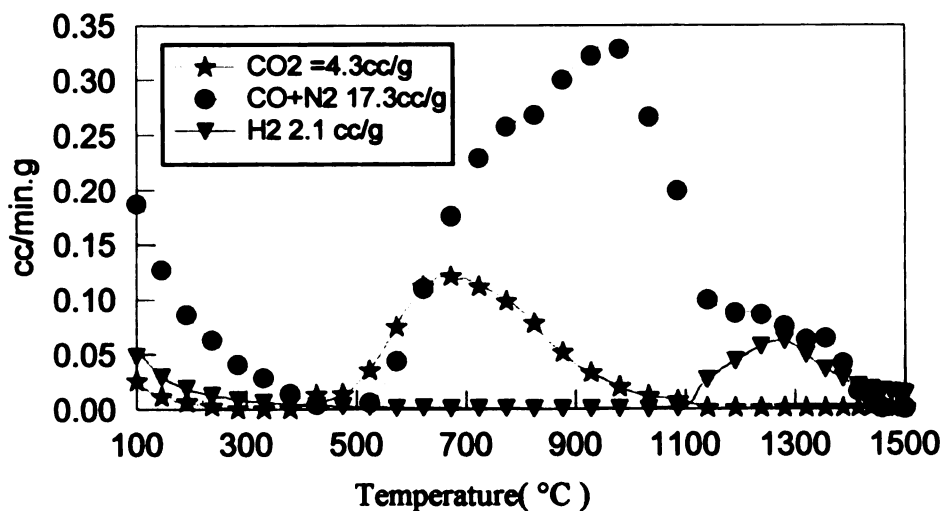


Figure 2-28 TPD profile of annealed Saran char following 2 min. hour exposure.

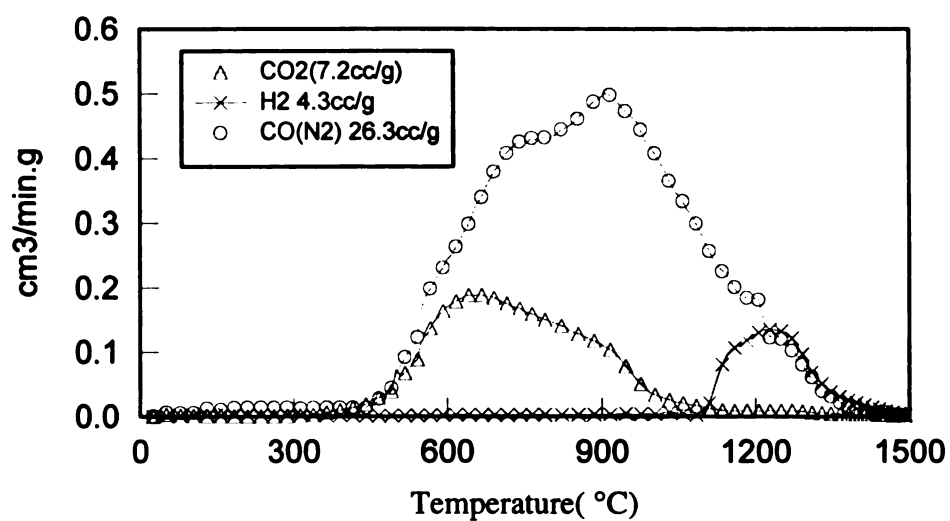


Figure 2-29 TPD profile of annealed Saran char following 0.5 hour exposure.

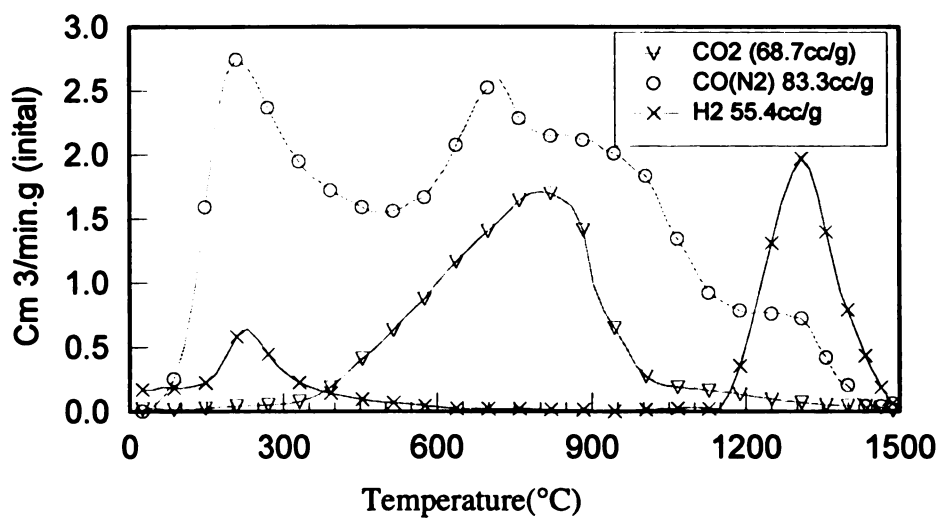


Figure 2-30 TPD profile of annealed Saran char following 2 days exposure.

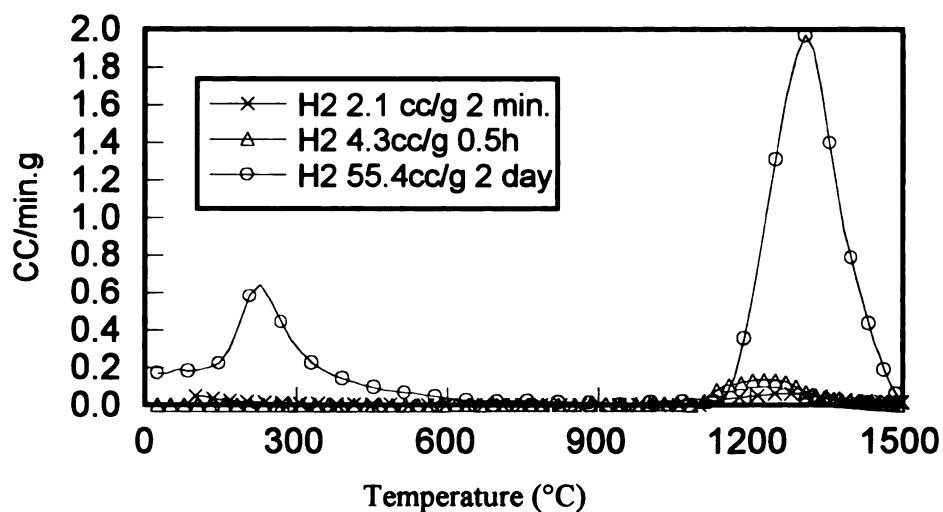


Figure 2-31 Uptakes of hydrogen changes with exposure time in air (annealed Saran char)

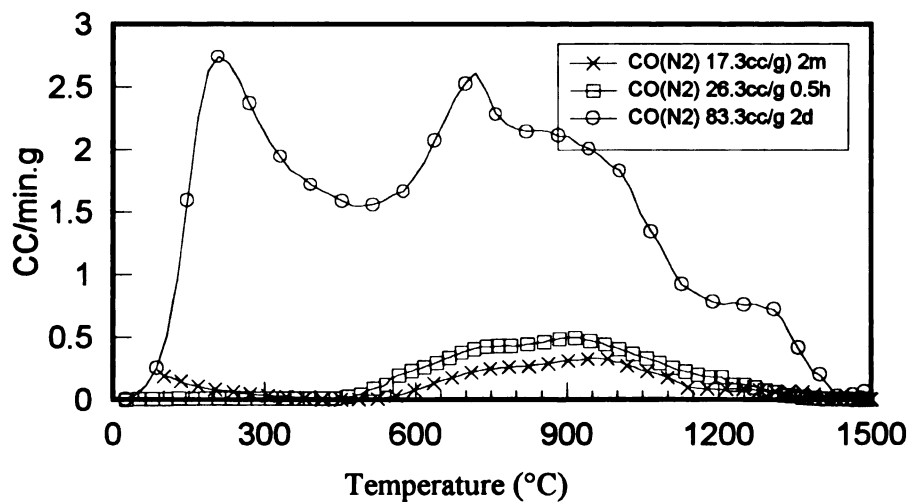


Figure 2-32 Uptakes of CO or N₂ change with exposure time char in air(annealed Saran)

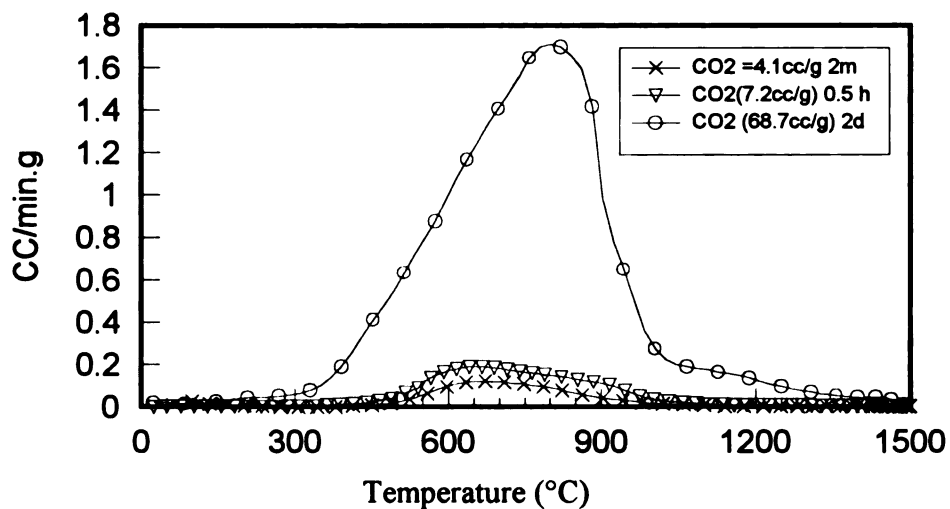


Figure 2-33 Uptakes of CO₂ changes with exposure time in air (annealed Saran char)

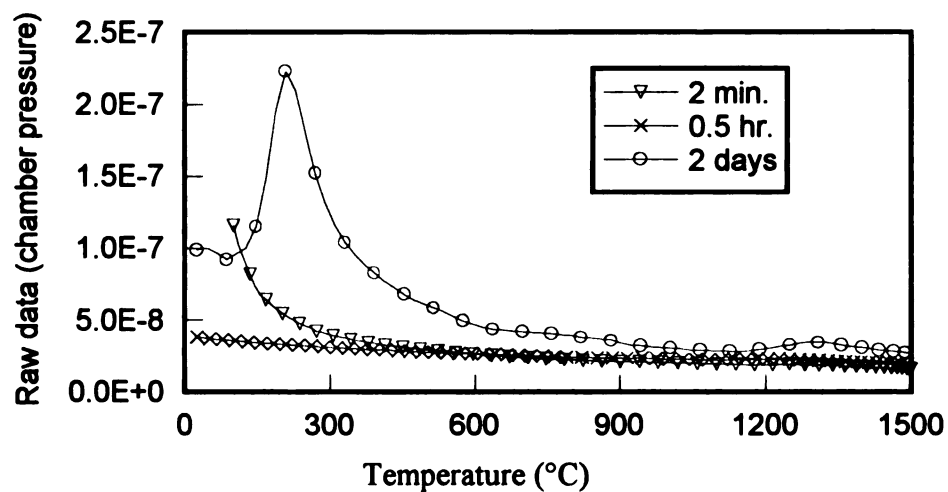


Figure 2-34 Uptakes of H₂O changes with exposure time of annealed Saran char in air

From the above experiments, it is clear that even very short exposure (of course, the air will enter the reactor when exposing the sample to air, and the sample could absorb impurities from this part of air), the changes in absorbed H_2 , CO and CO_2 are detectable. The follow conclusions could be made.

- Dissociatively adsorbed H_2 (emitted above 1000 °C) probably comes from decomposition of the water in air on the char surface. All exposures can increase the quantity desorbed, but the 2 minutes and 0.5 hr. exposure is tolerable, since the M2 signal only is about three time of the background.
- For M28, the 2 minutes and 0.5 hr. exposure are not much different from no exposure, but the two days exposure will produce several peaks. One is at 200 °C and the other are at about 1000 °C. After subtracting N_2 , the first peak almost disappears. So, the first M28 peak must come from adsorbed N_2 . The second peak is from oxygen adsorbed from air.
- For CO_2 (M44), no obvious peak can be found after a short time exposure (2 minutes and 0.5 hr.). But two days exposure does increase the M44 peak. The adsorbed CO_2 (or O_2) partially contributes to the M28 peak.
- For H_2O (M18), a short exposure to air will not induce an obvious peak at 200~250°C. The M18 peak (compared with no exposure experiment) is caused by air entering into the reactor when exposing the sample. But, for the two days exposure, the M18 (H_2O) peak is obvious.

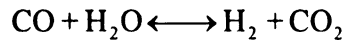
CHAPTER 3

THEORETICAL ALCULATIONS

3-1. Shift Reaction Equilibrium

The composition of gas produced from carbon gasification is affected by the CO+H₂O shift reaction. So, we need to investigate it first.

3-1-1. Equilibrium Constant Changes with Temperature



$$K_e = \frac{P_{\text{H}_2} P_{\text{CO}_2}}{P_{\text{H}_2\text{O}} P_{\text{CO}}} \quad \ln(K_e) = -\frac{\Delta G}{RT} \quad \text{E3-1}$$

According to Van't Hoff's equation:

$$\ln K_T = \ln K_{298.15} + \int_{298.15}^T \frac{\Delta H_{\text{rxn}}(T)}{RT^2} dT$$

$$\Delta H_{\text{rxn}}(T) = \Delta H_{\text{rxn}}(T_0) + \int_{298.15}^T C_p dT \quad (T_0=298.15\text{K}) \quad \text{E3-2}$$

At 298.15 °K the thermal data are

Table 3-1 Thermodynamic Data

	CO	H ₂ O	CO ₂	H ₂	CO+H ₂ O=CO ₂ +H ₂
ΔH (KJ/mol)	-110.53	-241.826	-393.51	0	-41.154
ΔG (KJ/mol)	-137.168	-228.582	-394.373	0	-28.623

From the data of **Table 3-1**, we can get $K_e(298.15) = 103469$ by using equation

E3-1. Heat capacity can be calculated by using $C_p = a + bT + cT^2$. The coefficients are listed in **Table 3-2**.

Table 3-2 Heat Capacity Coefficients

	a	b	c
CO	26.86	0.00697	-8.20E-07
CO ₂	26	0.0435	-1.48E-05
H ₂	29.07	-0.00084	2.01E-06
H ₂ O	30.36	0.00961	1.18E-06
Δ a, b, c	-2.15	0.026084	-1.32E-05

$$\Delta H_{rxn}(T) = \Delta H_{rxn}^0(T) + \Delta a(T - 298.15) + \frac{\Delta b(T^2 - 298.15^2)}{2} + \frac{\Delta c(T^3 - 298.15^3)}{3}$$

$$\begin{aligned} \ln Ke(T) = \ln Ke(T_0) + \frac{\Delta a}{R} \ln \frac{T}{T_0} + \frac{\Delta b}{2R} (T - T_0) + \frac{\Delta c}{6R} (T^3 - T_0^3) + \frac{1}{R} [-\Delta H_{rxn}^0(T) \\ + \Delta aT_0 + \Delta bT_0^2 + \Delta cT_0^3] * \left[\frac{1}{T} - \frac{1}{T_0} \right] \end{aligned}$$

E-3

This change in Ke with temperature is given in **Figure 3-1**.

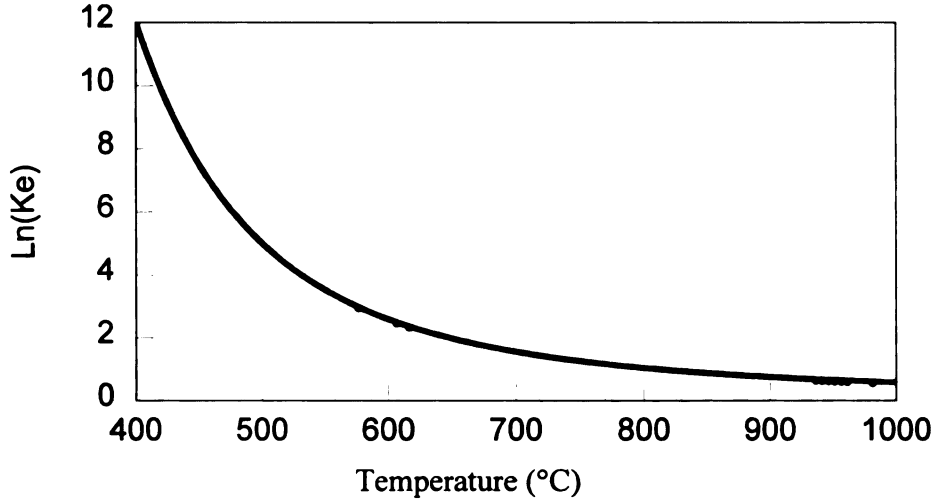


Figure 3-1 Equilibrium constant changes with temperature

3-1-2. Simulation of Steam Gasification (with Shift Reaction)

We assume that only CO comes from carbon surface reaction and that CO₂ only comes from the shift reaction, which is supported by other researchers (Hermann, 1986^[28]). The formation rate of CO is C₁, and Y is the conversion of steam (H₂O) from surface gasification reaction, X is the formation rate of CO₂, and W₀ is H₂O flow rate, and H₀ is hydrogen flow rate.

	C	+	H ₂ O	↔	CO	+	H ₂
Before gasification			W ₀				H ₀
After gasification			W ₀ (1-Y)		W ₀ Y		H ₀ +W ₀ Y
	CO	+	H ₂ O	↔	CO ₂	+	H ₂
After shift reaction	W ₀ Y -X		W ₀ (1-Y)-X		X		H ₀ +W ₀ Y+X

²⁸ Gunter **Hermann** and Klaus J. Huttering, carbon Vol. 24, No. 6. PP 705-713,1996

If we assume the shift reaction reaches equilibrium, then we can solve for the reactant gas composition.

$$K_e = \frac{P_{H_2} P_{CO_2}}{P_{H_2O} P_{CO}} = \frac{(H_0 + W_0 Y + X) \times X}{(W_0(1 - Y) - X) \times (W_0 Y - X)}$$

Solving this equation we get

$$X = \frac{H_0 + K_e W_0 + W_0 Y \pm \sqrt{(H_0 + K_e W_0 + W_0 Y)^2 - 4(K_e - 1)K_e W_0(1 - Y)Y}}{2(K_e - 1)} \quad \text{E3-4}$$

At 850 °C, $K_e=0.882$ and only one root is possible. At 725 °C, $K_e=1.40$ and there are two positive roots, but only one is meaningful. Total outlet mole flow (dry base, not including water) is:

$$T = 2W_0 Y + H_0 + X$$

The outlet hydrogen concentration is

$$H_2 \% = \frac{W_0 Y + H_0 + X}{T} \times 100\%$$

The CO concentration is

$$CO \% = \frac{W_0 Y - X}{T} \times 100\%$$

The CO₂ Concentration is $CO_2 \% = \frac{X}{T} \times 100\%$

We use the following parameters to simulate the process:

$W_0=120 \text{ cc/min.}=0.054 \text{ mol/min.}$

$H_0=0\sim 120 \text{ cc/min.}=0\sim 0.054 \text{ mol/min.}$

In a two hour steam gasification, the maximum carbon conversion is about 10% at our experimental conditions.

Therefore, the carbon consumption rate $= \frac{0.4 \times 10\%}{12.01 \times 120} = 2.78E - 05 \text{ mol / min}$

The corresponding to the steam conversion is $\frac{2.78E - 05}{40 / 22400} = 0.0155 = 1.56\%$

The corresponding to the steam conversion is $\frac{2.78E-05}{40/22400} = 0.0155 = 1.56\%$

So, in the following simulation we set the steam conversion $Y < 2\%$. For 850 °C gasification, the simulation results are given in **Figure 3-2~3-5**; For 725 °C gasification, the results are given in **Figure 3-5~ Figure 3-9**.

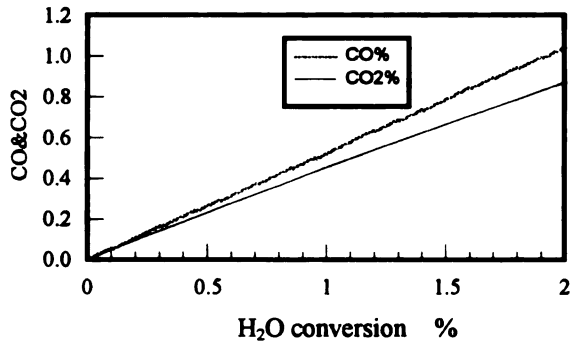


Figure 3-2 T=850°C, H₂=120, H₂O=120ml/min

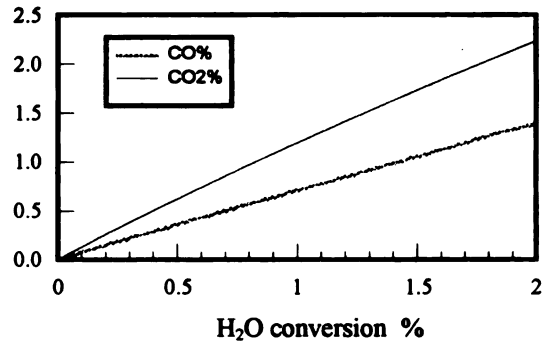


Figure 3-3 T=850°C, H₂=120, H₂O=120ml/min

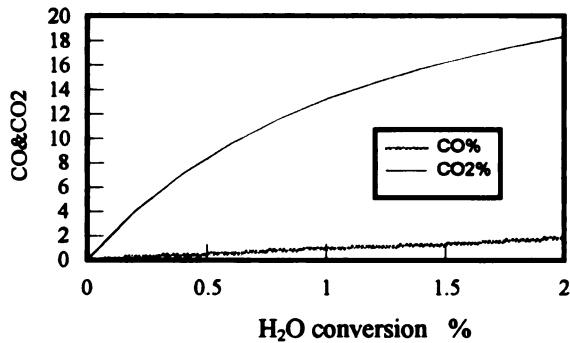


Figure 3-4 T=850°C, H₂=5, H₂O=120ml/min

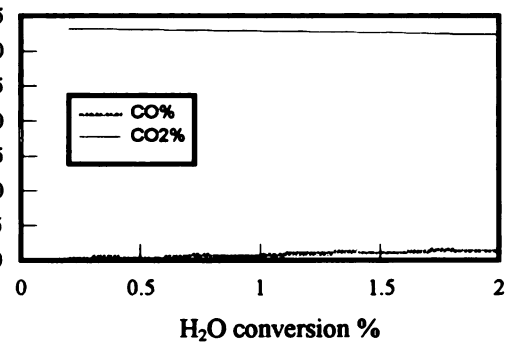


Figure 3-5 T=850°C, H₂=0, H₂O=120ml/min

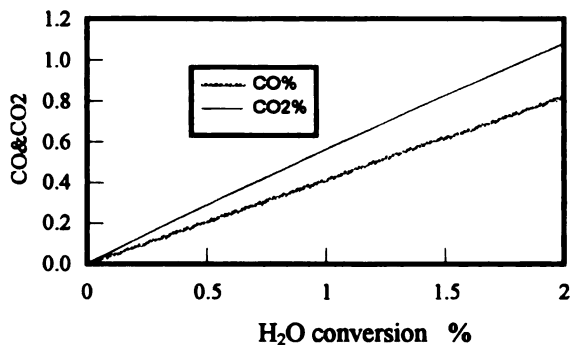


Figure 3-6 T=725°C, H₂=120, H₂O=120ml/min

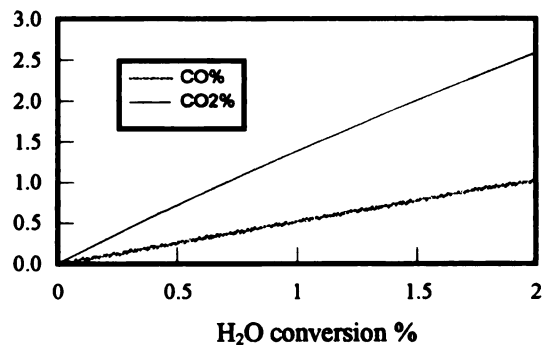


Figure 3-7 T=725°C, H₂=120, H₂O=120ml/min

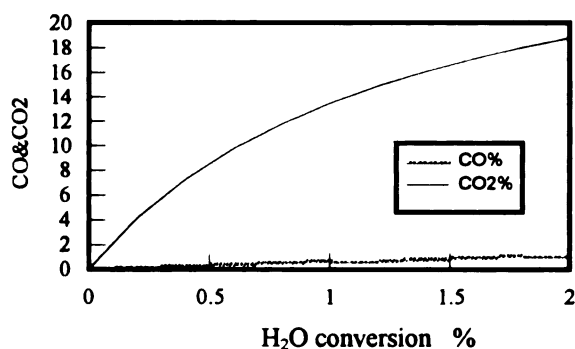


Figure 3-8 T=725 °C, H₂=5, H₂O=120ml/min

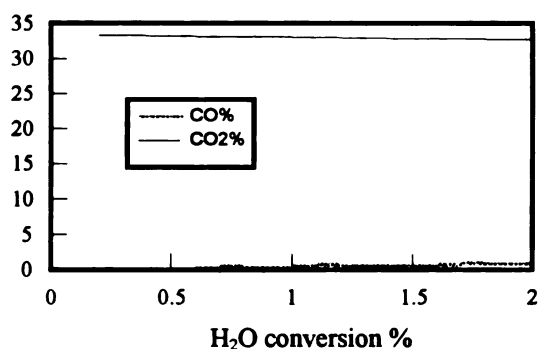


Figure 3-9 T=725 °C, H₂=0, H₂O=120ml/min

Apparently, if the reactant does not contain H₂ and the shift reaction reaches equilibrium, the main product should be CO₂.

3-1-3. Comparing with Experiment Data

We still assume only CO comes from carbon surface. Dividing the CO+CO₂ evolution rate by the total H₂O input, we can get the instantaneous conversion (Y) of steam. Therefore we can calculate the equilibrium CO&CO₂ composition using E3-4.

Figure 3-10 gives the comparison. We can see that the shift reaction is far from equilibrium in our Saran char steam gasification process.

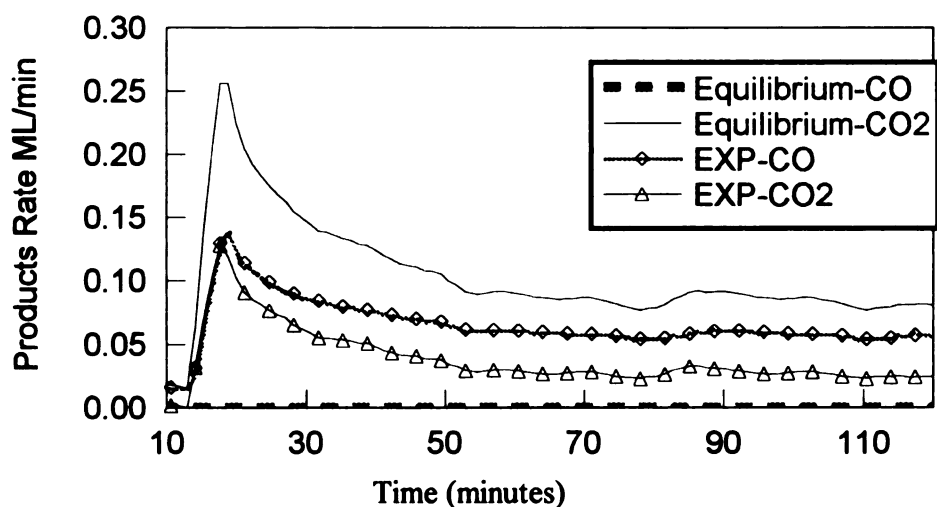


Figure 3-10 Comparison of experiment CO and CO₂ with the equilibrium CO & CO₂ (E9635 steam gasification)

3-2. Desorption Activation Energy of Hydrogen

3-2-1. Average Desorption Activation Energy

The rate of desorption from a uniform surface can be written as:

$$N(t) = -\frac{d\theta}{dt} = A_n \theta^n e^{-E/RT} \quad \text{E3-5}$$

Where A_n is the rate constant (frequency factor)

E is the activation energy of desorption

θ is the surface coverage (mole/m²)

$N(t)$ is desorption rate (mole/sec.m²)

n is the order of desorption reaction

The situation is simplified by experimentally imposing a uniform rate of heating on the sample. $T=T_0+\beta t$ and assume E is independent of surface coverage θ . For first order desorption $n=1$, after differentiating the above equation we can get:

$$\frac{dN(t)}{dt} = A_1 \frac{d\theta}{dt} e^{-E/RT} + (A\theta)e^{-E/RT} \left(-\frac{E}{R}\right) \left(-\frac{\beta}{T^2}\right) \quad \text{E3-6}$$

When the desorption rate reaches a maximum (peak position), we have:

$$\frac{dN(t)}{dt} = 0 \quad \text{E3-7}$$

Combining equation E3-5, E3-6, and E3-7 we can obtain an equation due to Redhead^[29]:

$$\frac{E}{RT_m^2} = \frac{A_1}{\beta} e^{-E/RT_m} \quad \text{E3-8}$$

Where T_m is the temperature at which the desorption rate reaches maximum, β is the heating rate, A_1 is rate constant of desorption, and E is the desorption activation energy for a uniform surface and uniform adsorbed species.

²⁹ P. A. Redhead , Vacuum, 12, 203 (1962)

This equation shows that T_m is independent of coverage for first order desorption with constant E . So, the desorption activation energy can be found directly from a measurement of T_m , provided a value of A_1 is assumed.

The relation between E and T_m is very nearly linear. In the range of $10^{13} > \frac{A_1}{\beta} > 10^8$,

E 3-8 can be approximated by following equation (Redhead^[29]):

$$\frac{E}{RT_m} = \ln \frac{A_1 T_m}{\beta} - 3.64 \quad \text{E3-9}$$

In the range of 500~1200 °C, the approximation can be made more accurate by using the following equation:

$$\frac{E}{RT_m} = \ln \frac{A_1 T_m}{\beta} - 3.1 \quad \text{E3-10}$$

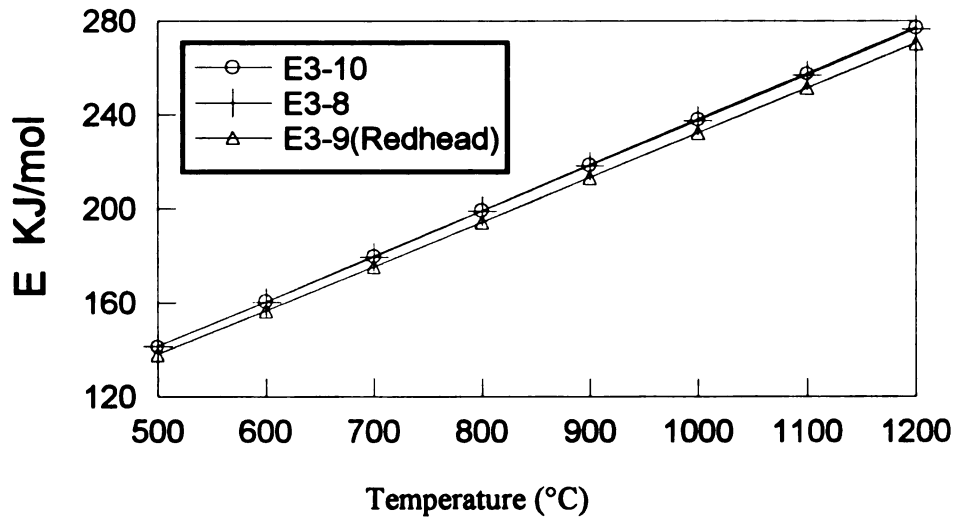


Figure 3-11 Desorption activation energies change with peak temperature

A comparison is given in **Figure 3-11**. It can be seen that the lines of **E3-8** and **E3-10** almost overlap. The activation energy can be determined without assuming a value of the rate constant A_1 by varying the heating rate β and plotting $\ln(T_m)$ against $\ln(\beta)$; E can then be obtained from the relation:

$$\frac{E}{RT_m} + 2 = \frac{d\ln\beta}{d\ln T_m} \quad \text{E3-11}$$

The rate constant A_1 can then be determined by substituting E into **E3-8**. If only two heating rates are used, E can be calculated by the following equation:

$$E = \frac{\ln\left(\frac{\beta_2}{\beta_1}\right) - 2 \ln\left(\frac{T_{p_2}}{T_{p_1}}\right)}{\left(\frac{1}{T_{p_1}} - \frac{1}{T_{p_2}}\right)} R \quad \text{E3-12}$$

Unfortunately, for reasonable accuracy, β must be varied by at least two orders of magnitude (Redhead^[29]). For our experimental conditions, this variation cannot be reached due to the limitations of the furnace. We thus can not use this method reliably to get the activation energy.

In the same way, we can get the similar equation for second order desorption

$$\frac{E}{RT_m^2} = \frac{2\theta_m A_2}{\beta} e^{-E/RT_m} = \frac{\theta_0 A_2}{\beta} e^{-E/RT_m} \quad \text{E3-13}$$

where θ_0 is the initial surface coverage, and θ_m is the surface coverage at T_m . In this case, T_m now depends on the surface coverage. θ_0 may be found from the area under the curve of the desorption rate as a function of time. For variable initial surface coverage

θ_0 , plotting $\ln(\theta_0 T_m^2)$ against $1/T_m$ gives a straight line of slope E/R . A_2 is then found by plugging E into the above equation (E3-13).

Thus, the order of desorption can be determined from the behavior of the maximum in desorption rate with coverage curves. A first order desorption with fixed activation energy gives rise to a peak in the desorption rate curve that does not change in temperature with coverage. If the temperature of the peak maximum decreases with coverage, the desorption reaction will be second order desorption or first order with an activation energy dependent on coverage. These two cases can be distinguished by the plot of $\ln(\theta_0 T_m^2)$ vs. $1/T_m$. A straight line means second order desorption.

3-2-2. Peak Shape Simulation

The shape of the experimental curve of desorption rate as function of sample temperature can be used to determine the order of desorption and whether the activation energy is constant or alternatively a function of surface coverage. In fact, the most accurate data we can get from desorption experiments is peak temperature T_m . For a linear temperature heating rate, we integrate E3-5 to obtain

$$\frac{A_n}{\beta} \int_{T_2}^{T_1} e^{-\frac{E}{RT}} dT = - \int_{\theta_1}^{\theta_2} \frac{d\theta}{\theta^n} = \begin{cases} = \ln \frac{\theta_1}{\theta_2} & \text{for } n = 1 \\ = \frac{1}{\theta_2} - \frac{1}{\theta_1} & \text{for } n = 2 \end{cases} \quad (\text{using } dT = \beta dt) \quad \text{E3-14}$$

The integral may be evaluated by using the substitution $u = -\frac{E}{RT}$, integrating by parts, and using the identity

$$\int \frac{e^u}{u} du = \frac{e^u}{u} \times H(u) \quad \text{for } |u| \gg 1$$

$$\text{where } H(u) = 1 + \frac{1!}{u} + \frac{2!}{u^2} + \dots$$

Because $u = \frac{E}{RT} \gg 1$ (this is true for most case, for example, when $E=200$ KJ/mol

and $T=1000$ K, $u=24$), using only the first two terms in the $H(u)$ expansion is enough for reasonable accuracy. We can get

$$\frac{A_n}{\beta} \int_{T_1}^{T_2} e^{-\frac{E}{RT}} dt = \frac{A_n R}{\beta E} \left\{ T_2^2 e^{-\frac{E}{RT_2}} - T_1^2 e^{-\frac{E}{RT_1}} \right\} \quad \text{E3-15}$$

By combining E3-14, E3-15 and E3-5, we can obtain an equation to describe the shape of the desorption rate curve. For first order desorption:

$$-\ln\left(\frac{N}{N_m}\right) = \frac{E}{R} \left(\frac{1}{T} - \frac{1}{T_m} \right) + \left(\frac{T}{T_m} \right)^2 e^{-\frac{E}{R} \left(\frac{1}{T} - \frac{1}{T_m} \right)} - 1 \quad \text{E3-16}$$

where N_m is desorption rate at T_m .

It can be seen that the desorption rate curve (**Figure 3-12**) is asymmetric about the maximum at T_m .

In the same way, for second order desorption, we have:

$$\frac{N}{N_m} = 4 \left\{ e^{-\frac{E}{2R} \left(\frac{1}{T_m} - \frac{1}{T} \right)} + \left(\frac{T}{T_m} \right)^2 e^{-\frac{E}{2R} \left(\frac{1}{T} - \frac{1}{T_m} \right)} - 1 \right\}^{-2} \quad \text{E3-17}$$

When $\left(\frac{T}{T_m} \right)^2 \rightarrow 1$, which is true around T_m , this equation can be simplified as

$$\frac{N}{N_m} \approx \cosh^{-2} \left\{ -\frac{E}{2R} \left(\frac{1}{T} - \frac{1}{T_m} \right) \right\} \quad \text{E3-8}$$

Thus, the desorption curve is symmetric about the maximum at T_m when $|T - T_m|$ is small. **Figure 3-12** shows the theoretical desorption rate curve for first order and second order.

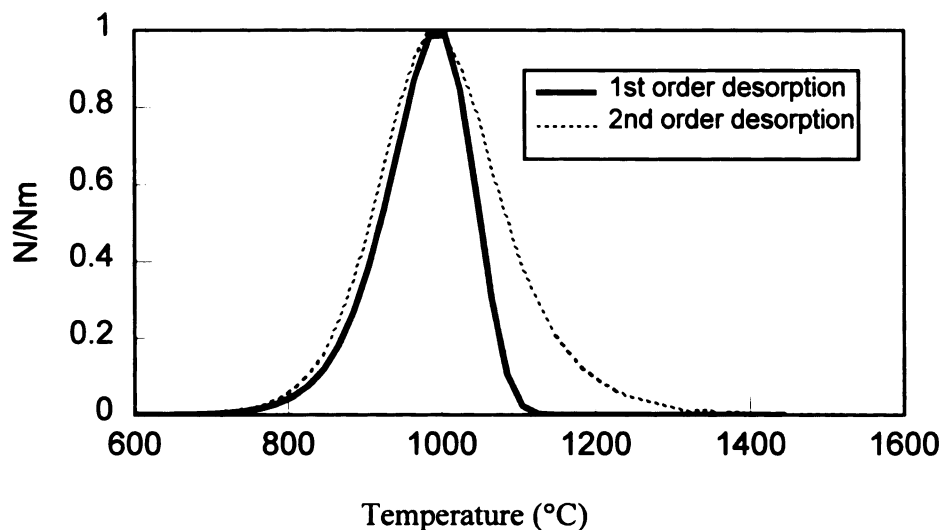


Figure 3-12 Simulation of desorption ($T_m = 1000$ °C and $E = 237.8$ KJ/mol)

3-2-3. Estimating the Desorption Activation Energy

The desorption energy E may be calculated from T_m with the usual assumption that $A = 10^9 \text{ sec}^{-1}$ (Redhead^[29]). **Figure 3-13** is the energy change with peak position T_m for first order desorption. The asymmetric shapes in most of our H_2 TPD curves (see Section 2-6 and Chapter 4) suggest that the hydrogen desorption from Saran char is more like a first order reaction if E does not change with coverage. For a peak position located at 1100 °C, the average desorption activation energy is about 250 KJ/mol (60 Kcal/mol), a quite strong chemisorption. The C-H bond energy (Pan and Yang) is 376 KJ/mol for zigzag face and 354 KJ/mol for armchair face. It seems that the estimated desorption energy here is smaller. The Error probably come from the A value assignment.

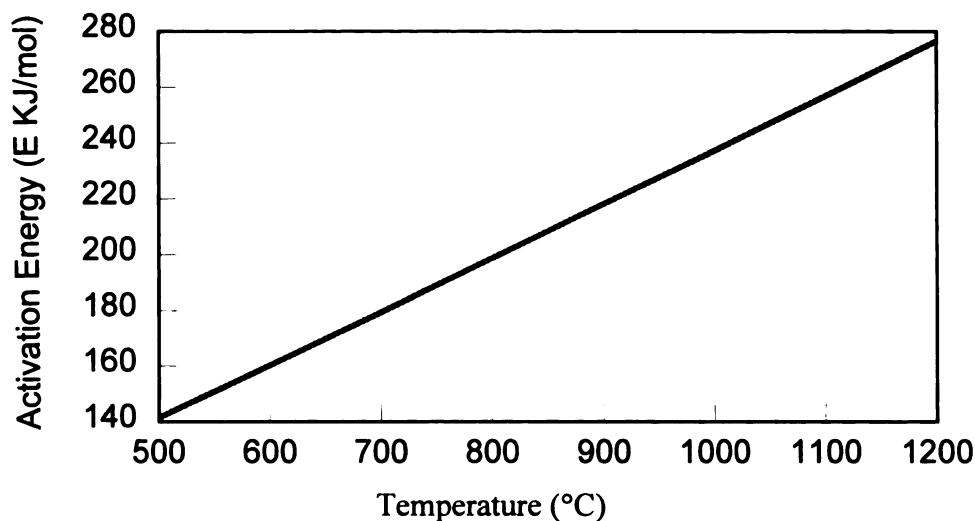


Figure 3-13 Activation energy dependence on peak temperature T_m

3-2-4. Distribution of Desorption Activation Energies

The difference between the experimental TPD profile and the simulated TPD profile shows that either E changes with coverage or that the surface is not uniform. The observation that the population of hydrogen does not decrease evenly over the entire TPD spectrum also suggests that the char surface exhibits a distribution of desorption activation energies. Du et al. ^[30] has developed distributed activation energy models for CO. Similarly, these models can be used to calculate the adsorbed hydrogen activation energy distribution.

According to Du, the relationship between instantaneous H_2 desorption rate and the distribution of desorption activation energies can be expressed as:

$$\frac{d[H]}{dt} = [H]_0 S(E) \frac{dE}{dt} \quad \text{E3-19}$$

where E is the local desorption activation energy, as approximated by an instantaneous step at energy E . $S(E)$ is the desorption activation energy probability density function.

³⁰ Du, Z., A.F Sarofim, and J. P. Longwell, Energy & fuels 4,296 (1990.).

$d[H]/dt$ is the desorption rate of H_2 , and $[H_0]$ is the total initial amount of H_2 on surface.

The parameters are related by:

$$\frac{E}{RT} = \ln \frac{A_1 T}{\beta} - 3.1 \quad \text{E3-10}$$

Since the TPD data give the instantaneous rate directly, dE/dt can be obtained from the above equation:

$$\frac{dE}{dt} = R\beta \left(\ln \frac{A}{\beta} - 2.1 + \ln T \right) \quad \text{E3-20}$$

In the original equation **E3-10**, T is peak temperature. Here, it is desorption temperature. That is because local activation energy is approximated by an instantaneous step. We think there is a continuous energy distribution, so every local activation energy corresponds to a desorption temperature T . If we use a linear heating ramp $T=T_0+\beta t$, $S(E)$ can be calculated using the following equation (combining E3-19, E3-20 and using $d[H]=0.5d[H_2]$):

$$S(E) = \frac{0.5dH_2 / dt}{[H_0]R\beta \left(\ln \frac{A}{\beta} - 2.1 + \ln T \right)} \quad \text{E3-21}$$

For simplification, we also use $A=10^9$ as in above section, which is also used by most researcher. **Figure 3-14** presents the D_2 desorption activation energies for the following TPD of a Saran char deuterium gasification. **Figure 3-15** is the H_2 desorption energy distribution.

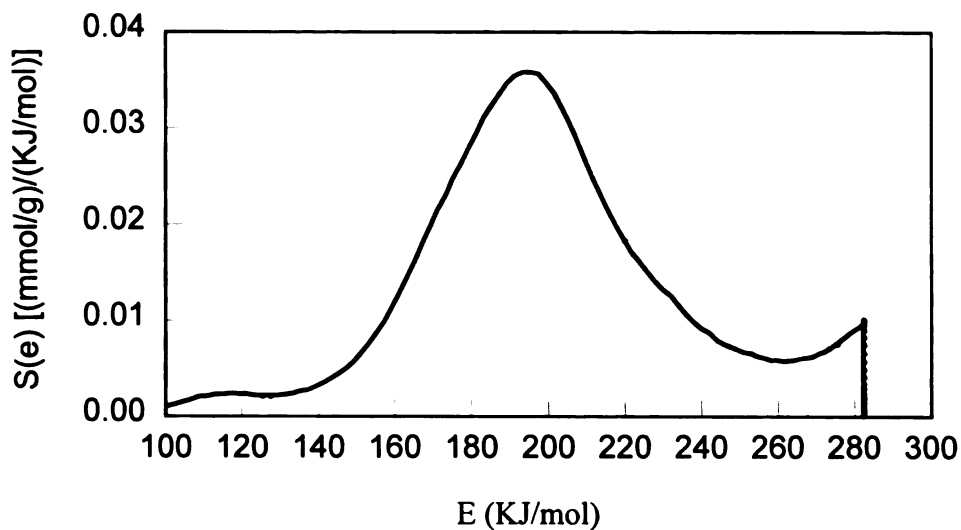


Figure 3-14 Distribution of desorption activation energies for D₂ TPD spectra Following 6 hours D₂ gasification (E9619)

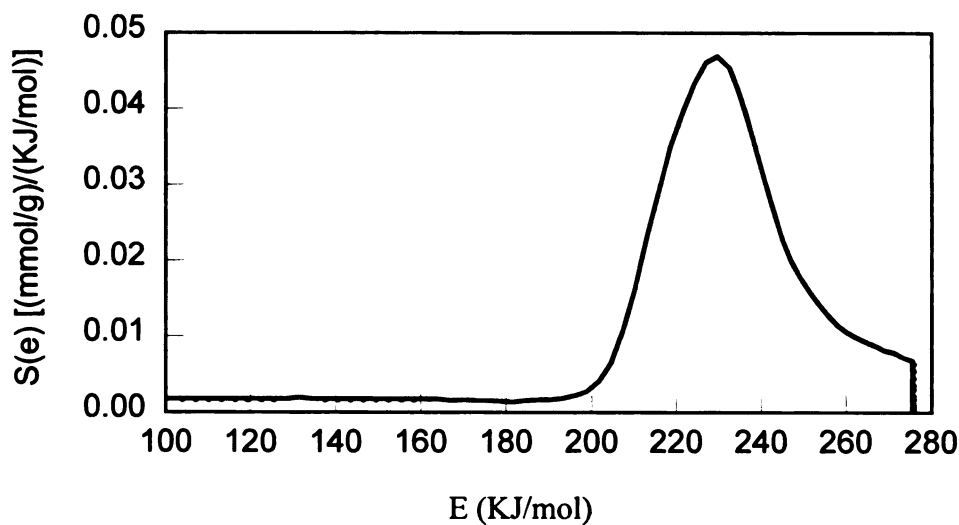


Figure 3-15 Distribution of desorption activation energies for H₂ TPD spectra following 4 hours H₂ gasification of annealed Saran char (E9624)

3-3. Active Site Density Estimation

3-3-1. BET Surface Area and Adsorbed H₂

Figure 3-16 is the adsorbed hydrogen concentration on annealed Saran char following $\text{H}_2\text{O}/\text{H}_2$ gasification (at 850 °C reactant gas composition: argon 0~60%, H_2O 0~40%, H_2 0~100%).

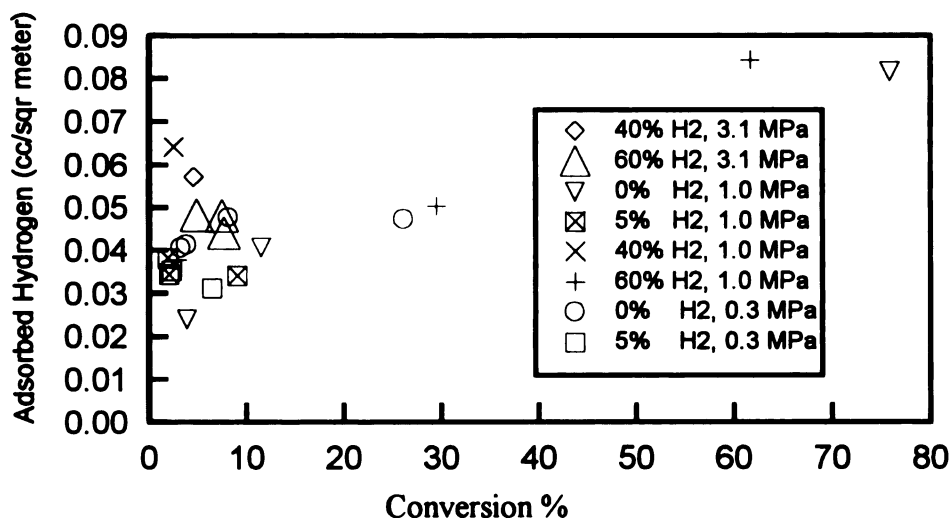


Figure 3-16 Adsorbed hydrogen vs. conversion

In the above figure, although there is some scattering, we find that the quantity of H_2 per unit BET area is almost constant and does not change with carbon conversion. For Saran char, this value is about $0.05 \text{ cm}^3(\text{STP})/\text{m}^2$. Thus, we can estimate the active site density at about $2.2 \times 10^{-8} \text{ mol} / \text{m}^2$, which corresponding to 37.2 \AA^2 per hydrogen atom. That means on average, for every 37.2 \AA^2 BET area there is an active site.

Table 3-3 gives the calculation of the fraction of active sites occupied by oxygen (C-O complex) in steam gasification (with or without H_2).

Table 3-3 Active Sites Occupied by Oxygen

"O" cc/g	site (mol O)/g	BET (from conversion)*	site (mol)/ m ²	% of total site #	Exp. #
5.5	2.46E-04	1133	2.17E-07	9.7	9635 (H ₂ O)
1.1	4.91E-05	1025	4.79E-08	2.1	9636(H ₂ O+H ₂)

Table 3-4 Active Sites Occupied by Hydrogen

"H ₂ " cc/g	site (mol 2)/g	BET (from conversion)	(mol H ₂)/ m ²	% of total site #	Exp. #
52.08	2.33E-03	1133	2.05E-06	90.3	9635 (H ₂ O)
39.31	1.75E-03	1025	1.71E-06	97.9	9636(H ₂ O+H ₂)

3-3-2. Comparing with Hermann (1996)'s Data^[28]

The value 2.2×10^{-6} mol (H₂)/ m² is much smaller when compared to Hermann's^[28] data [1.2×10^{-4} (mol 2CO+H₂)/m²]. The reason probably is the carbon material used is much different. Hermann used more active coke (600°C from PVC) with a BET area of only 1 m²/g. (For our char, the BET area is over 800 times larger than Hermann's char).

* From regression H₂ BET data. In low conversion (<40%), BET=810+18.26*conversion%

3-4. Reaction Activation Energy

According to the Arrhenus law:

$$K = K_0 e^{\frac{-E}{RT}} \quad \text{E3-22}$$

K is reaction rate constant, E is reaction activation energy.

$$R = K_0 e^{\frac{-E}{RT}} f(c_i) \quad \text{E3-23}$$

R is reaction rate and $f(c_i)$ is a function of reactant concentration.

If we know the reaction rates (R) at different temperature, we can calculate the reaction activation energy use equation **E3-22**

$$E = \frac{R \ln \frac{R_1}{R_2}}{\left(\frac{1}{T_2} - \frac{1}{T_1}\right)} \quad \text{E3-24}$$

Table 3-5 Experimental data

	reactants	Temperature	Rate (cc/min.g)			
			CO	CO2	CH4	SUM rate
9635	H2O+Ar	725	0.0610	0.0290	0.0074	0.0974
9637	H2O+Ar	850	0.1900	0.7700	0.5000	1.4600
9636	H2O+H2+Ar	725	0.0570	0.0240	0.0200	0.1010
9638	H2O+H2+Ar	850	0.1200	0.0500	0.0970	0.2670

Table 3-6 Apparent Active Energy for H₂O+Ar Gasification

H ₂ O+Ar gasification T ₁ =725 °C T ₂ =850°C					
	CO	CO ₂	CH ₄	use total rate	CO+CO2
	R850/R725	R850/R725	R850/R725	R850/R725	R850/R725
	3.1148	26.5517	67.5676	14.9897	10.6667
(1/T ₂ -/T ₁)	-1.12E-04	-1.12E-04	-1.12E-04	-1.12E-04	-1.12E-04
LN(R850/R725)	1.1362	3.2791	4.2131	2.7074	2.3671
Ea cal/mol	20247	58435	75080	48247	42183
or Kcal/mol	20.2	58.4	75.1	48.2	42.2

Table 3-7 Apparent Active Energy H₂O+H₂+Ar Gasification

H ₂ O+H ₂ +Ar gasification		T ₁ =725°C, T ₂ =850°C			
	CO	CO ₂	CH ₄	use total rate	CO+CO ₂
	R850/R725	R850/R725	R850/R725	R850/R725	R850/R725
	2.1053	2.0833	4.8500	2.6436	2.0988
(1/T ₂ -1/T ₁)	-1.12E-04	-1.12E-04	-1.12E-04	-1.12E-04	-1.12E-04
LN(R850/R725)	0.7444	0.7340	1.5790	0.9721	0.7413
Ea cal/mol	13266	13080	28138	17324	13211
or Kcal/mol	13.3	13.1	28.1	17.3	13.2

The calculated results are given in **Table 3-5~3-7**. Comparing **Table 3-6** and **Table 3-7**, The activation energy for steam gasification is larger than the steam/H₂ gasification.

CHAPTER 4

CHAR GASIFICATION

4-1. Saran Char Gasification

4-1-1. As-prepared Saran Char Steam and Steam/H₂ Gasification

For steam/argon gasification (**Figure 4-1**), the initial gasification rate is relatively high. After about 2 % carbon conversion, the rate curve tends to level out, although a slight decline still can be seen. Compared to CO+CO₂ formation, the CH₄ evolution rate is very limited.

The steam/H₂ gasification is given in **Figure 4-2**. Methane is the dominant product. The rate curve tends to decrease quickly out to 14 % carbon conversion. The hydrogen inhibition of CO formation is obvious; at 10% carbon conversion, the total gasification rate is only about one third of the gasification rate of steam/argon. The CO₂ evolution rate is lower than steam gasification and also very limited compared to CO and CH₄, since H₂ in the gas phase has shifted CO₂ to CO, or the adsorbed hydrogen inhibits the formation of CO₂.

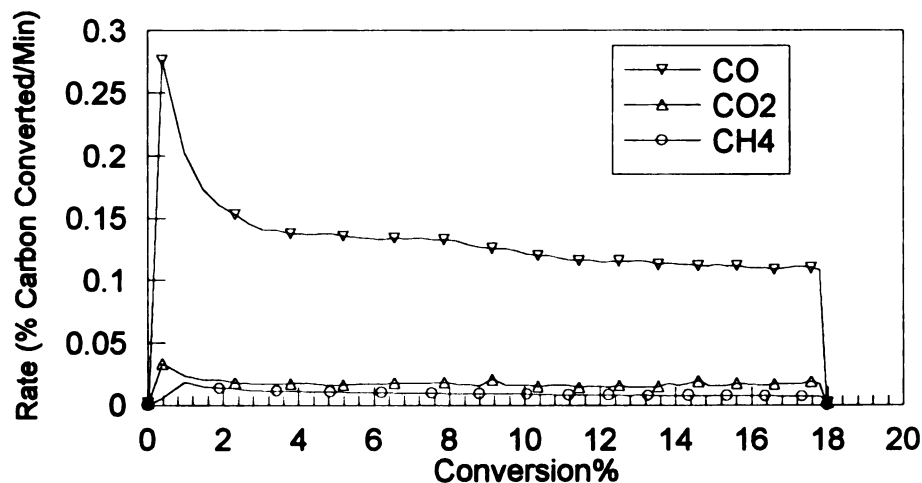


Figure 4-1 Gasification of Saran char in 3.1 MPa
H₂O(40%)/Ar (60%) at 725°C (EXP-X-6)

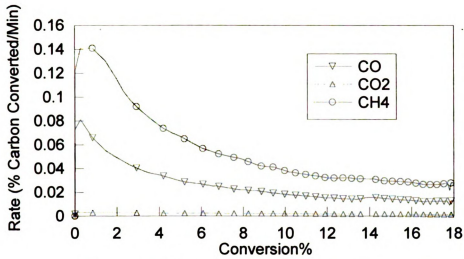


Figure 4-2 Saran char gasification in 3.1 MPa $\text{H}_2\text{O}(40\%)/\text{H}_2(60\%)$ at 725°C (EXP-X-8).

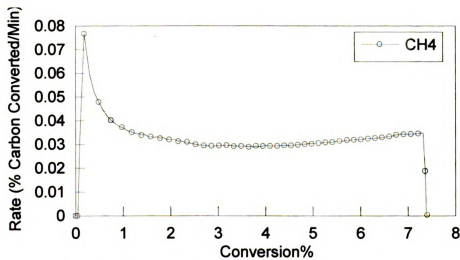


Figure 4-3 4 hr. Annealed Saran char H_2 gasification at 850°C and 3.1 MPa. (E7062)

4-1-2. Annealed Saran Char H_2 /Steam Gasification

The only product in pure hydrogen gasification (**Figure 4-3**) of annealed Saran char is CH_4 . The initial rate is about twice the gasification rate at higher conversion. Although a very slight increase above 4% conversion can be seen, the methane formation rate tends to stabilize after 1% carbon conversion. After 4% conversion, a slight upward trend can be seen in the rate curve. We could say that the gasification process reaches such a state that the surface reaction reaches steady state and the surface area increases slowly with carbon burn off.

For annealed Saran char steam/ H_2 gasification (**Figure 4-4**), the total gasification rate is lower than that of as-prepared Saran char at the initial stage. But, after 2% carbon conversion, the rate is about same as that of as-prepared Saran char. Methane formation rate is very low compared to CO and CO_2 formation. A slight increase can be seen in rate with conversion.

The inhibition of hydrogen on steam gasification rate of annealed Saran char is clearly seen in **Figure 4-5**. The steam/ H_2 gasification product distribution is similar to that of as-prepared Saran char, and $CO+CO_2$ formation rate is about one-fourth the rate in steam/argon gasification of annealed Saran char. Methane formation in H_2O/H_2 gasification is much higher than H_2O/Ar gasification, but the rate is still lower than in pure H_2 gasification. This phenomenon is contrary to Huttinger's^[5] conclusion, as they thought H_2O could enhance methane formation rate.

⁵ **Huttinger**, K.J. and Merdes, W.F., Carbon 30(6), 883 (1992).

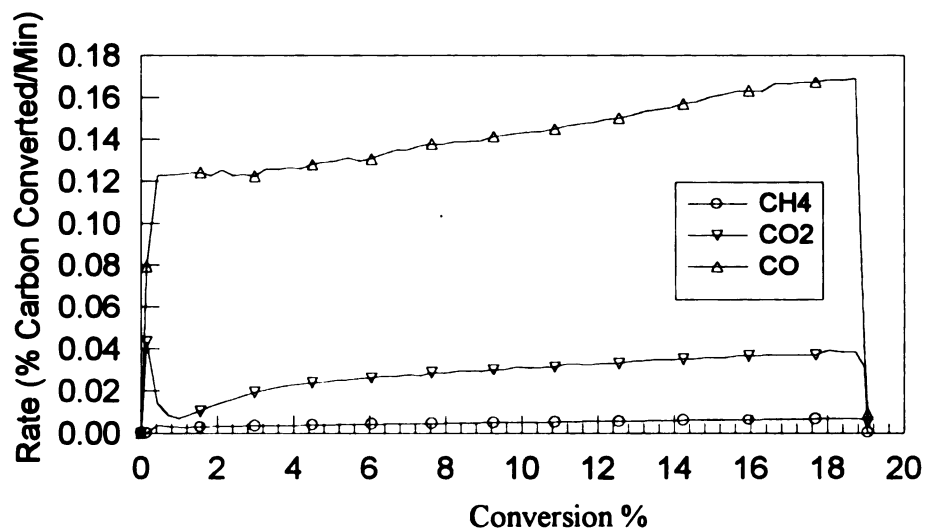


Figure 4-4 Annealed Saran char gasification of 40% H_2O /60%Ar at 850 °C and 3.1 MPa. [2 hour] (E7030)

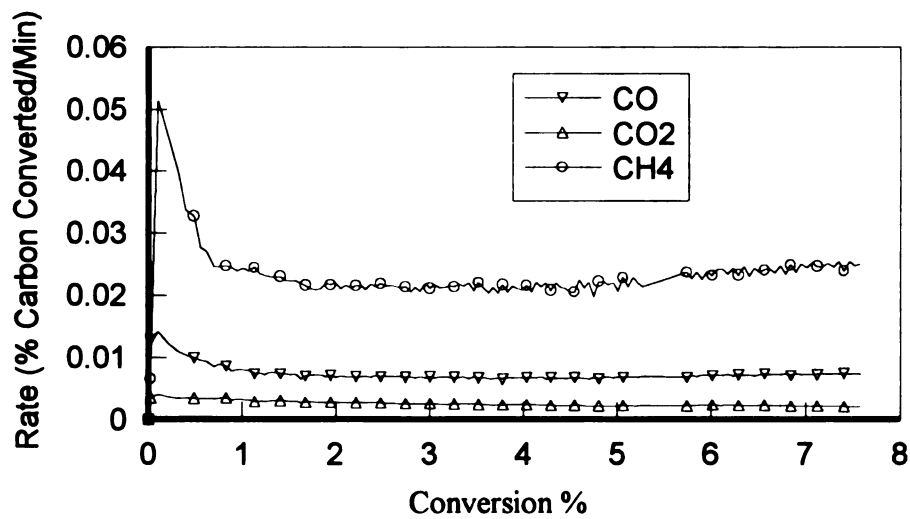


Figure 4-5 Annealed Saran char 40% H_2O /60% H_2 gasification at 850 °C and 3.1 MPa. [4 hour]. (7058).

4-1-3. Hydrogen TPD Profiles of Annealed Saran Char Following Gasification

A. H_2 gasification

Figure 4-6 is a typical hydrogen temperature programmed desorption (TPD) profile following gasification in pure H_2 for 6 hours. It shows a maximum peak at about 1200 °C, with H_2 evolution starting about 900 °C and continuing up to 1500 °C; this is clear evidence that hydrogen is dissociatively chemisorbed on the char surface. The hydrogen peak is broad and asymmetric, indicating a distribution of hydrogen adsorption energies on the char surface, or that desorption is a first order reaction (see Chapter 3).

The H_2 desorption peak shape and location in TPD changes with conversion following pure hydrogen gasification as given in **Figure 4-7**. We can see the basic shape is very similar, but the quantity of adsorbed hydrogen increases and the peak maximum shift to higher temperature with increasing conversion.

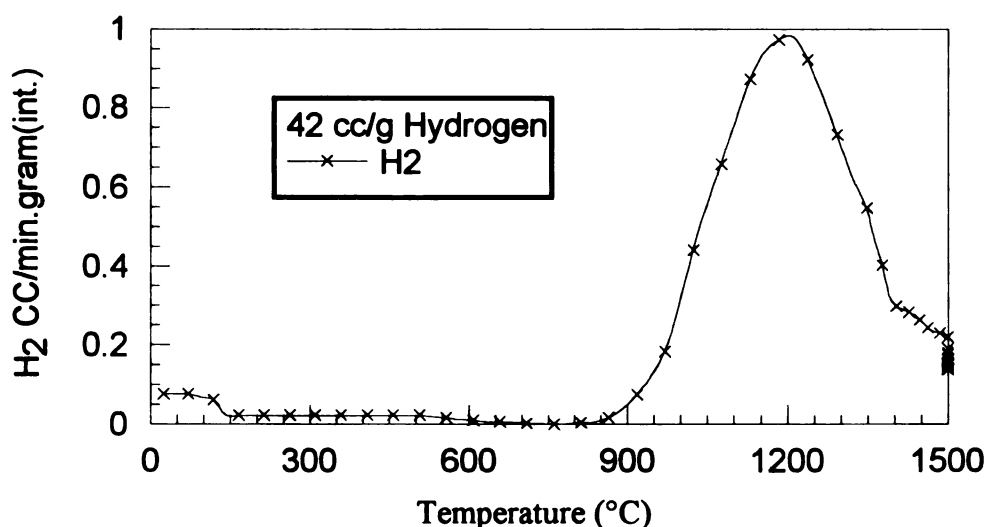


Figure 4-6 H_2 TPD profile following 6 hr pure H_2 gasification of Saran char at 850 °C and 3.1 MPa.(7063)

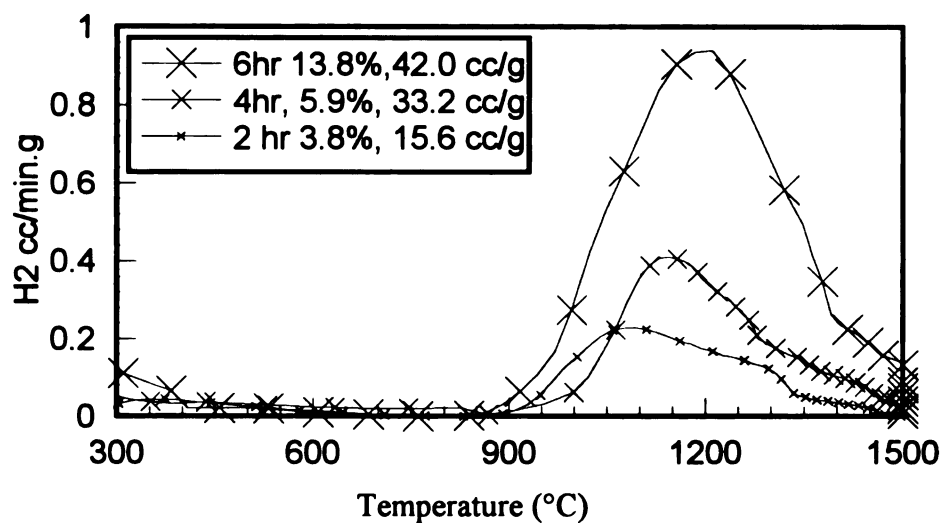


Figure 4-7 Comparison of H_2 TPD profile following pure H_2 gasification of annealed Saran char at 850 $^{\circ}C$ and 3.1 MPa(E 7064,E7062 and 7063)

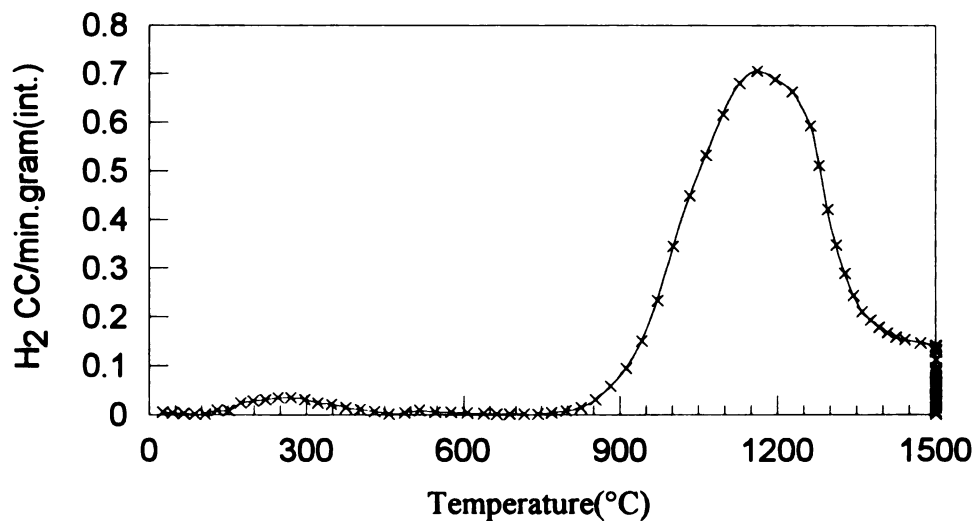


Figure 4-8 H_2 TPD profile following 6 hr 60% H_2 /40%Ar gasification of Saran char(E7065)

1

f

g

C

sl

D.

Fig

char

reac

hydr

B. H_2 /Ar Gasification

After the addition of 40% argon to hydrogen during gasification, the TPD profile following reaction (**Figure 4-8**) is very similar to that following pure hydrogen gasification. The peak maximum position is at a little lower temperature.

C. Steam Gasification

For steam gasification (**Figure 4-9**), the TPD profiles are different in that their shapes are more symmetric.

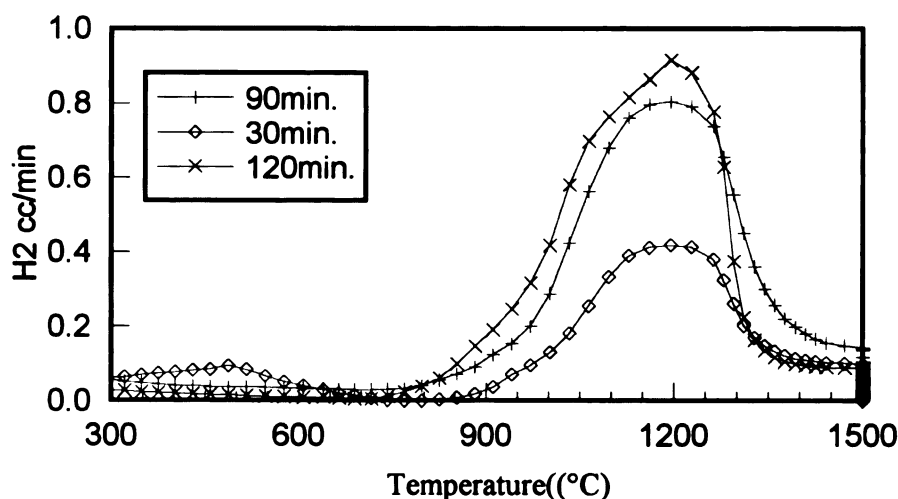


Figure 4-9 H_2 TPD profile following steam 40%/Ar gasification of annealed Saran char at 850 °C and 1.0 MPa. (E7038,7039,7040)

D. Adsorbed Hydrogen (Deuterium) Change with Conversion

The quantity of hydrogen adsorbed as a function of carbon conversion is given in **Figure 3-10**. For a wide variety of gasification conditions, hydrogen adsorption on Saran char during gasification is characterized by very rapid uptake upon initial exposure to reactant gas up to 0.5% conversion. At high conversions, the absolute amount of hydrogen adsorbed increase steadily out to 70% char conversion, where the value of

nearly $100 \text{ cm}^3(\text{STP})/\text{g}$ corresponds to H/C ratio in the char of 1:10. The quantity adsorbed depends solely on the char conversion and is independent of reactant gas composition.

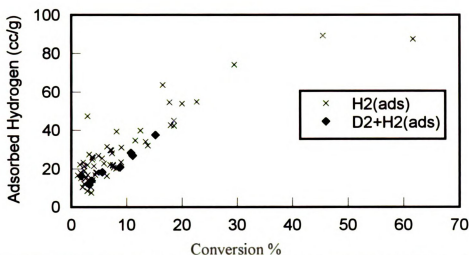


Figure 4-10 Adsorbed hydrogen change with conversion

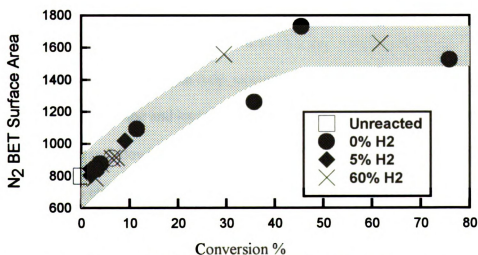


Figure 4-11 BET area changes with conversion

E. BET Area Changes with Conversion

The surface area (BET) change with conversion is given in **Figure 4-11**. At conversion less than 30%, the increase is near linear. After that, the trend tends to be flat. The maximum possible BET area is 1600 m²/g.

4-1-4. The Desorption Profiles of CO and CO₂ after Gasification

The quantity of CO and CO₂ desorbed from annealed Saran char during TPD following gasification was monitored in several experiments. When hydrogen was present in the reactant gas during the gasification at 850 °C, only very small quantities of CO (less than 0.04 mmol/g) and no CO₂ was observed. When reaction gas contained only steam/argon, slightly greater quantities of CO (up to 0.07 mmol/g) were observed in TPD (**Figure 4-12**). For all reactant gases, the CO desorption peak is symmetric with a peak maximum at 1000 °C. The CO desorbed represents “stable” surface oxides on the char at gasification conditions.

The low temperature gasification is a little different. When hydrogen is present in the reactant gas, less than 0.04 mmol CO/g and no CO₂ was observed during TPD. Following gasification in steam/argon only, in contrast, 0.21 mmol CO/g was observed to desorb during TPD. The shape and location of the CO TPD peak following gasification at 725 °C was the same as following gasification at 850 °C, signifying that the nature of the surface oxides on the char is the same at the two temperatures (**Figure 4-12**).

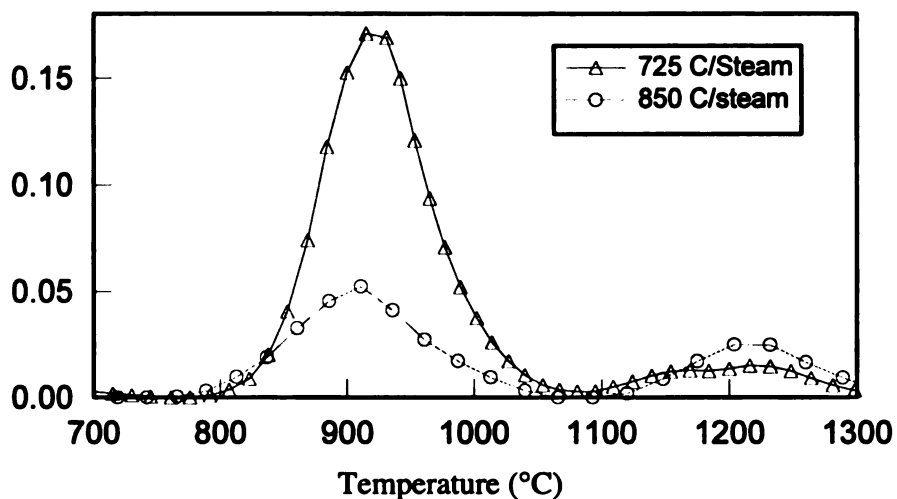


Figure 4-12 CO TPD profiles following 40% steam/60% argon gasification at 725 °C and 850 °C (E9635 and E9637)

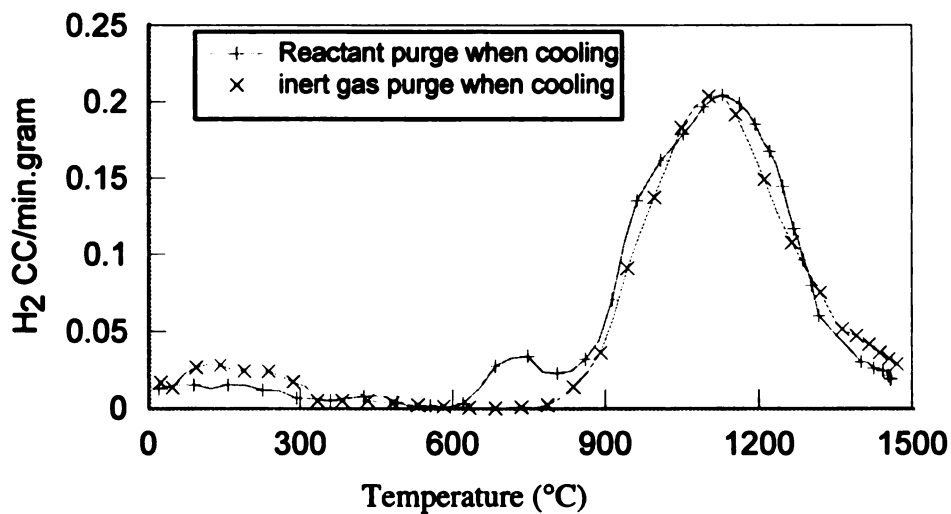


Figure 4-13 H₂ TPD profiles of annealed Saran char after gasification T=850 °C, P=1 MPa, cooling in argon and cooling in hydrogen (E7069 and E9603).

4-1-5. Weakly Bound Hydrogen Detection

The so-call weakly bound hydrogen (associative hydrogen) can not be seen in our regular TPD. The reason is the temperature we used for gasification is over 700 °C, and from the literature, weakly-bound hydrogen only exists below 650 °C. To verify this phenomena, a special experiment was designed in which we cooled the gasified sample in hydrogen instead of argon. **Figure 4-13** is the result of this experiment. It is clear that there is a small peak starting at 650 °C that is identifiable as weakly adsorbed H₂; we cannot find this peak in any TPD with inert gas purging.

4-1-6. Discussion on Saran Char Gasification

During gasification, carbon surface area tends to increase with conversion due to the carbon burning off and pore opening, and the active sites will decrease with reaction. These two factors contribute to the rate curve shape (apparent rate). The surface area increase is a slow process. For as-prepared Saran char, the surface active sites are abundant. During gasification, the active sites decrease in number faster than the surface area increases, so the rate curve has a decreasing trend.

For gasification of annealed Saran char, the rate increases with carbon conversion. After annealing, the microstructure of Saran char must be stabilized. The process of losing active sites is slower than the surface increase, and we always see an increasing trend in the annealed Saran char gasification rate.

From Saran char gasification, we found that the quantity of hydrogen adsorbed on annealed Saran char is independent of reactant gas composition and, on a unit surface area (BET) basis, is a single, constant value (2×10^{-3} mmol H₂/m²) at conversions above 0.5%. Gasification rate, on the other hand, is strongly dependent on the reactant

composition. It is thus clear that the large quantities of hydrogen adsorbed can not be responsible for observed difference in gasification rate at different composition.

As evidenced by the high temperature TPD peak, dissociative chemisorption clearly takes place on the annealed char surface during gasification. The presence of strongly bound hydrogen certainly affects gasification rate by blocking potentially reactive sites for steam gasification, but because this hydrogen saturates the surface at all conditions, it exerts a constant inhibition.

The weakly bound hydrogen, proposed to be associatively adsorbed as surface methylene groups is present in a concentration of 0.025 mmol H₂/g, about 1% of total quantity of hydrogen adsorbed on the char. Because it is stable only at low temperature, the associatively adsorbed hydrogen could not inhibit gasification by blocking active sites.

Hydrogen occupies the vast majority (over 95%) of adsorption sites on the char surface, as evidenced by comparing the quantities of CO and H₂ released during TPD. Computational molecular modeling showed the hydrogen preferably adsorbs on both zigzag and armchair sites on graphite surface; these ordered edges are thus the location of the large quantities of hydrogen. The constant value of surface hydrogen concentration per unit area ($\sim 2 \times 10^{-3}$ mmol H₂/m²) indicates that the quantity of edge sites per unit area remains constant over the course of conversion.

At conversion large than 1%, the char surface consists of ordered edges saturated with hydrogen (3-5 mmol/g), as well as less ordered structure(defects and amorphous material)^[27]. So, we could say that hydrogen gasification at edge sites makes the primary contribution to methane formation. Steam gasification is proposed to take place primarily

on less-ordered structure, where surface oxides can steadily adsorb (0.2 mmol/g) and adsorbed hydrogen does not block C(O) formation. Steam gasification likely does not occur to a significant extent at edge sites.

The fact that both quantities of hydrogen adsorbed and char reactivity per unit area is unchanging over conversion from 5~40% is interesting. It seems that the relative concentrations of ordered (edge) and amorphous sites on the char surface are constant over this conversion range or physical changes in char morphology with conversion coincidentally result in constant rate.

²⁷ **Michael G. Lussier**, Ph.D. dissertation Michigan State University (1997)

4-2. Coal Char Gasification

Limited numbers of coal char gasification experiments were done for the purpose of verifying the rate trends.

4-2-1. As-received Coal Char Steam/H₂ Gasification

Steam/Ar gasification of Coal char is different with Saran char (**Figure 4-14**) in that the dominant product is CO₂. The ash in coal char catalyzes the shift reaction. The composition of reactor effluent almost reaches the equilibrium composition of the shift reaction (see Chapter 3.1).

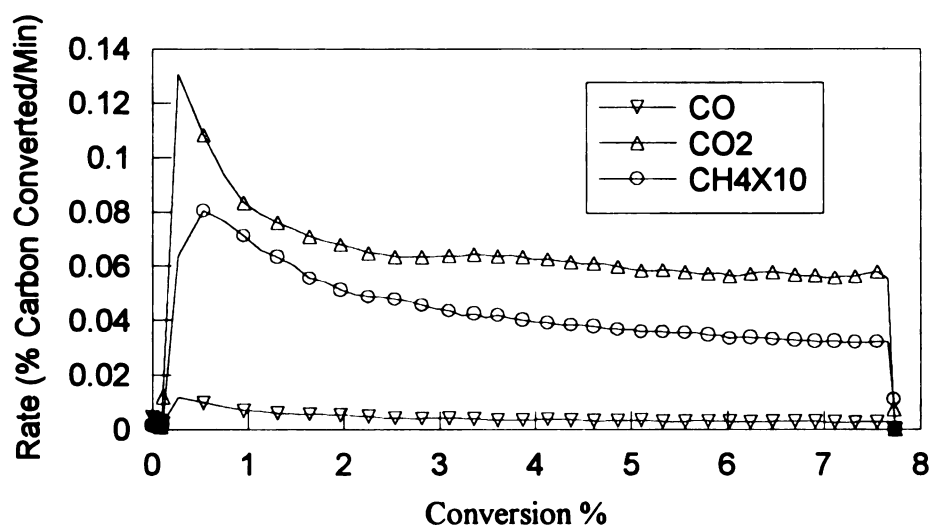


Figure 4-14 Coal char gasification in 1.0 MPa 40% H₂O/60% Ar at 725 °C[2 hours] (EXP-X-9).

After addition of H₂ to steam gasification (**Figure 4-15**), the rate profile is much different from steam/argon gasification. The CO evolution rate is higher than CO₂. This further verifies the shift reaction is rapid in this system. Below 4% conversion, the rate decreases quickly, and then the curve levels out above 4% conversion.

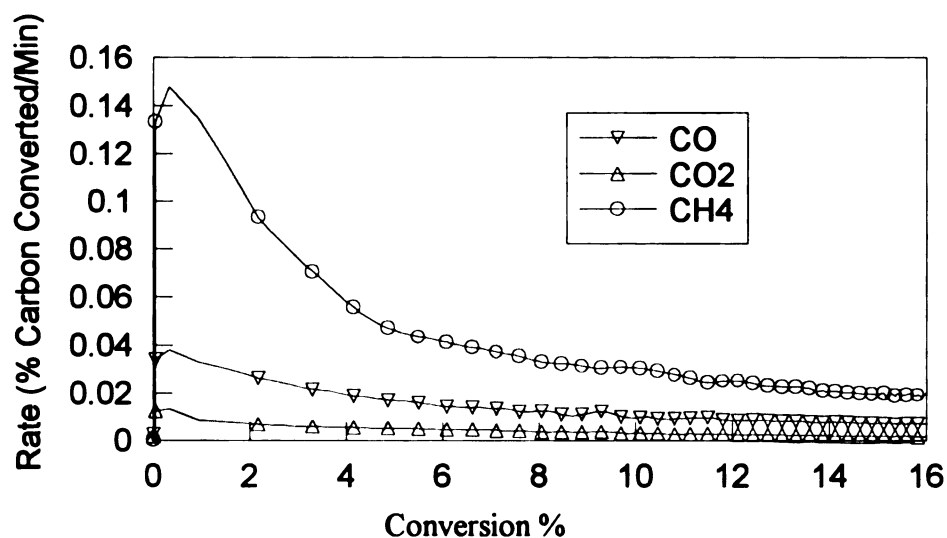


Figure 4-15 Coal char gasification in 1.0 MPa H₂O(40%)/H₂ at 725 °C. 6 hours reaction time, Conversion 16.3% (X-7).

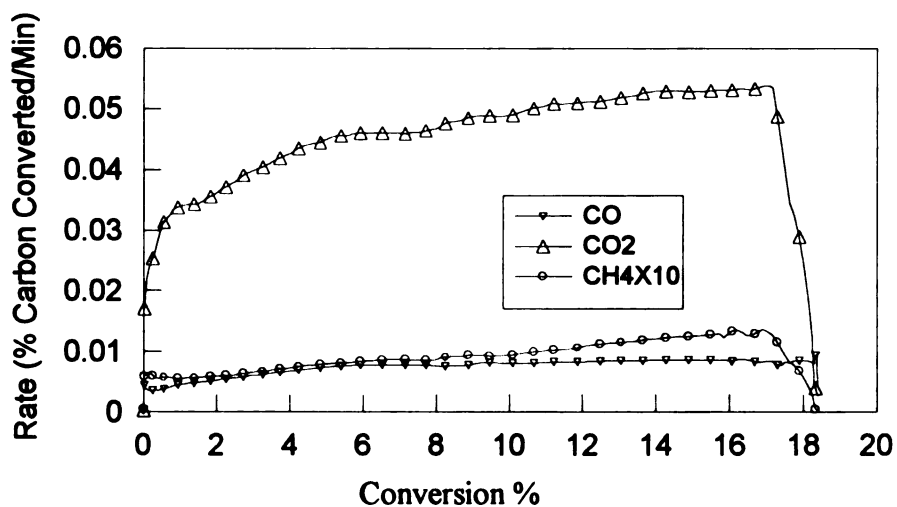


Figure 4-16 Annealed coal char gasification in 1.0 MPa H₂O(40%)/Ar at 850 °C, 6 hours reaction and 19% conversion (E9601).

4-2-2. Annealed Coal Char Steam Gasification

Using different gasification times, three steam/argon gasifications were done on the annealed coal char (PSOC 1493). The rate curve of gasification for 6 hours is given in **Figure. 4-16**. The dominant product is CO_2 , again different from annealed Saran char for which the major product is CO.

After gasification, the N_2 BET surface area was measured and is given in **Figure 4-17**. Compared to Saran char, the BET area is much lower. The BET areas increase rapidly with conversion (up to 10%) and then levels out, similar to Saran char. The low initial area is attributed to pore blockage during charring; carbon sample surface area rapidly increases as the pore structure is opened by the carbon burn-off.

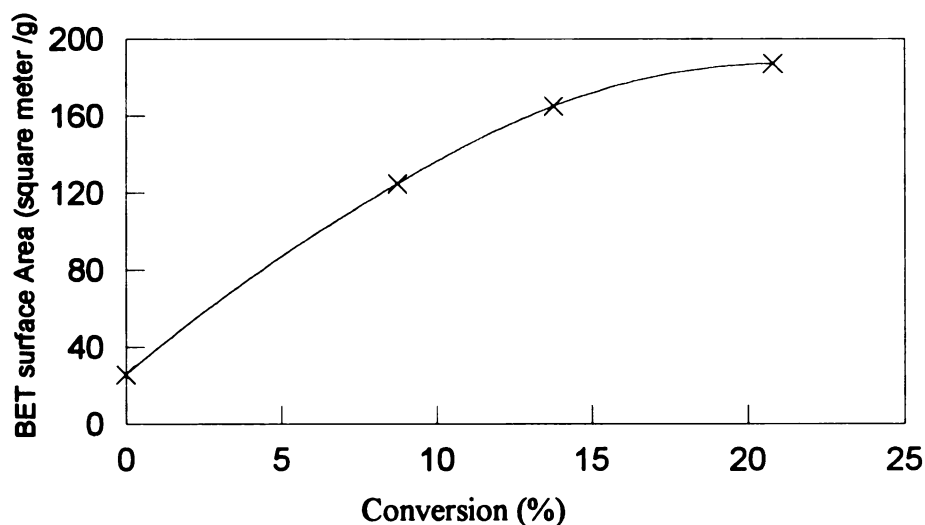


Figure 4-17 N_2 BET surface area with conversion after gasification at $T=850\text{ }^\circ\text{C}$, and 1 MPa (40% H_2O +60%Ar)

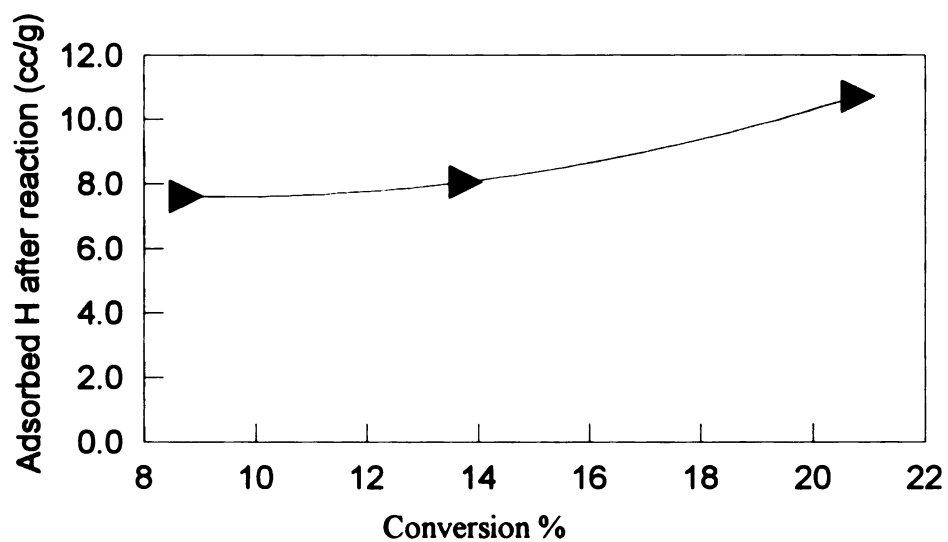


Figure 4-18 40% H₂O + 60% Ar gasification at T=850 °C, P=1 MPa

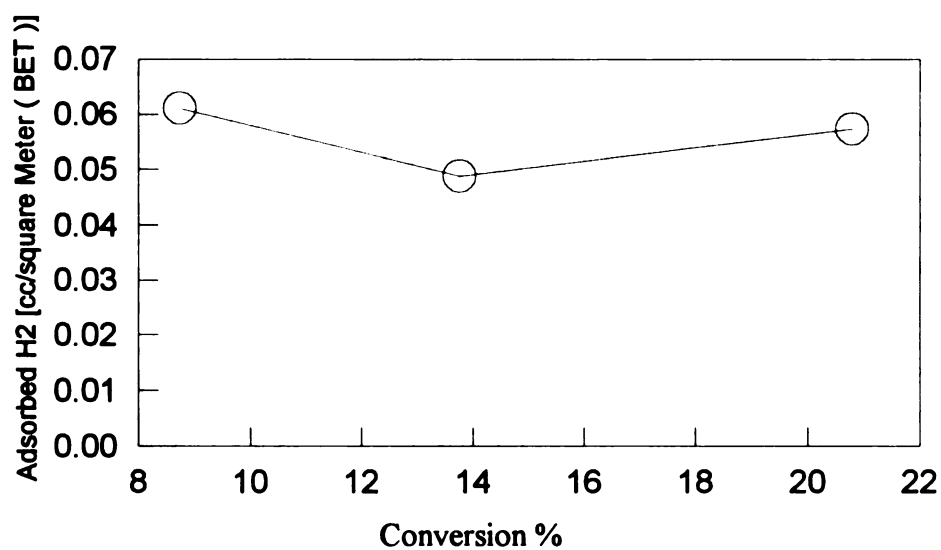


Figure 4-19 40% H₂O + 60% Ar gasification at T=850 °C, P=1 MPa

Figure 4-18 gives the quantity of adsorbed hydrogen from TPD analysis as a function of conversion. Because of the lower surface area, less hydrogen is adsorbed on coal than on Saran char (at the same conversion). Similar to Saran char, the quantity of H_2 adsorbed per unit area (**Figure 4-19**) is essentially unchanged with conversion. The quantity of hydrogen adsorbed per unit area, however, is approximately 1.5~2 times that on Saran char; perhaps because of the presence of ash or hetero-atoms that may enhance adsorption. If we assume each H is adsorbed on one active site, the site density is about $5 \times 10^{-3} \text{ mmol/m}^2$.

4-2-3. Hydrogen TPD Profiles of Annealed Coal Char Following Gasification

Figure 4-20 is H_2 profile following steam gasification of coal char. The peak position is a little lower temperature than that for the Saran char (1150 °C). The peak position does not change with conversion. The shape tends to be a symmetric curve.

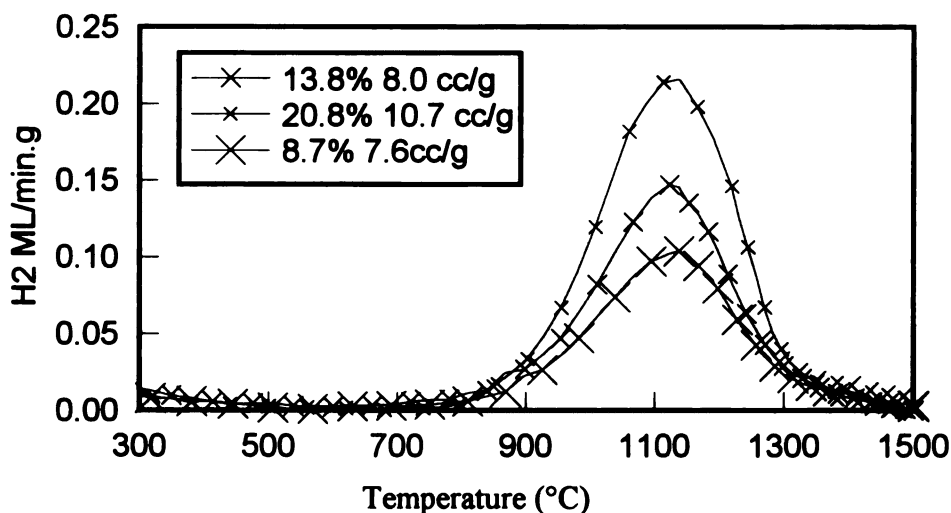


Figure 4-20 H_2 TPD profiles of steam gasification of annealed coal char at 850 °C and 1 MPa. Desorbed H_2 changes with conversion (E9601, 9602, 9603)

4-2-4. The TPD Profiles of CO and CO₂ after Coal Gasification

The TPD profiles of annealed coal char are totally different than those for annealed Saran char. No CO₂ peaks are observed in the TPD after steam gasification, but complex large CO peaks are obvious. Figure 4-21 gives the CO TPD profiles for three different steam gasification times. The complex profiles suggest that there are many different types of oxygen groups on the Saran char after gasification.

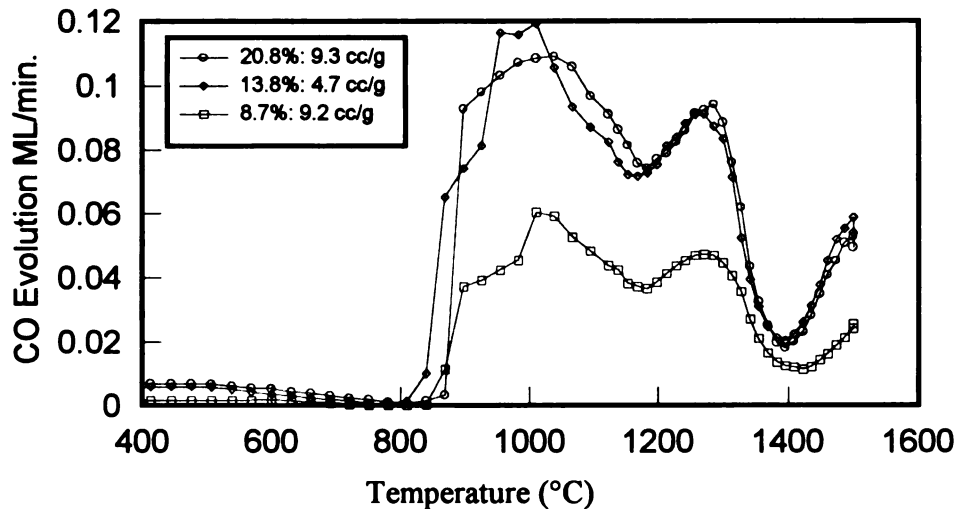


Figure 4-21 CO TPD profiles following Steam gasification of annealed coal char at 850 °C and 3.1 MPa for three conversion.

4-2-5. Discussion of Coal Gasification

From the limited number of coal char gasification experiments, we found the same trends in gasification rate profiles. But the ash in coal char accelerates the shift reaction, and is also responsible for the large amount of oxygen groups on the coal char surface during gasification.

In summary, coal char gasification is more complicated than Saran char due to impurities present. Although we found some trends that are very similar to Saran char, the steam/H₂ gasification mechanism may not be exactly the same.

4-3. Isotopic Effects

4-3-1. Annealed Saran Char Gasification by D₂

Compared to H₂ gasification, gasification rate in D₂ is much lower as seen in **Figure 4-22**. Comparing with **Figure 4-3**, we can find the trend is also different. The D₂ from the following TPD is also smaller than the hydrogen gasification (**Figure 4-23**).

Gasification of annealed Saran char in 3.1 MPa D₂ at 850 °C for 6 hours led the deposition of about 13.7 cc (STP)/g D₂ onto the char surface (**Figure-23**), and about four percent carbon conversion. This quantity of D₂ is substantially less than the corresponding quantity of H₂ adsorbed in hydrogen; four hour gasification in 3.1 MPa H₂ results in about 32 cc(STP)/g adsorbed. A duplicate run (**Figure-23**) confirms the reliability of the quantity of D₂ adsorbed.

The reasons for low gasification rate and low quantity of adsorbed D₂ still are not fully understood. From the adsorbed H₂(D₂) with conversion plot (**Figure 4-10**), it seems the low D₂ is still in the same range as H₂. The difference in the diffusive coefficient between H and D could cause the difference of reactivity and accessibility to micro pore structure. Then the lower carbon conversion causes the smaller amount of D₂ deposition

Also, the upturn in D₂ TPD near 1500 °C may suggest that not all D is desorbed before 1500 °C; e.g., some remains on surface. (No similar upturn in H₂ TPD). We tried to use D-NMR experiments to measure adsorbed D on the char surface. But the amount of D is too small and beyond the NMR detection limit. So, we cannot get any significant D peaks for the gasified char sample or the residual char sample (After TPD).

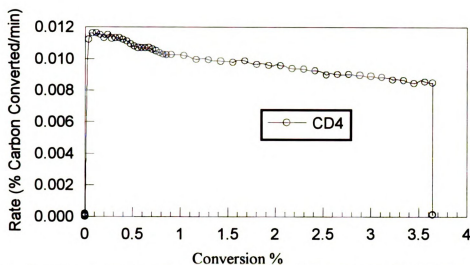


Figure 4-22 Annealed Saran char $D_2(60\%)/Ar$ gasification at 850 °C and 3.1 MPa, time: 6 hr. (E9620)

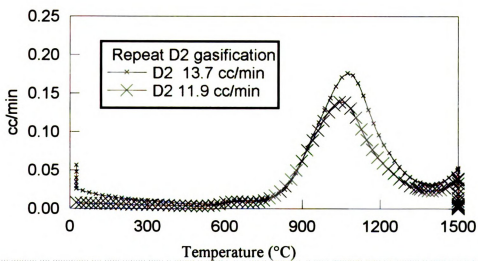


Figure 4-23 The deposited D after D_2 gasification on the char is less than that of H_2 gasification(two TPD after 6 hr. D_2 gasification)

4-3-2. Annealed Saran Char Gasification by D₂O

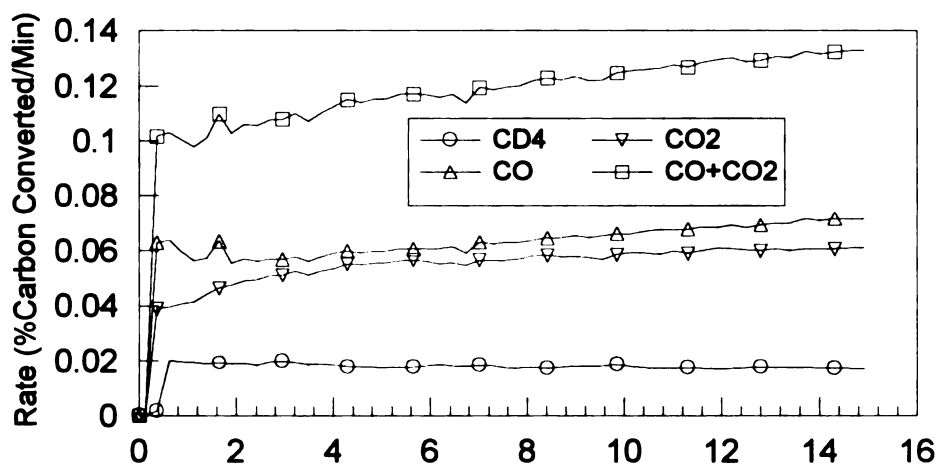


Figure 4-24. D₂O gasification of annealed Saran char at 3.1 MPa and 850 °C, time = 2 hours.

Gasification rate of annealed Saran char in D₂O is given in **Figure 4-24**. Compared to H₂O gasification, the total gasification rate in D₂O is about 3/4 that of steam gasification (**Figure 4-4**). This also showed that the D isotope slows the carbon gasification rate.

The molecular weight of D₂O is about 10% higher than H₂O, which causes 25% lower gasification rate. If the gasification rate is limited by oxygen exchange, then the isotope will not affect the steam gasification at all. So, the isotopic effect must come from the equilibrium of steam decomposition reaction ($C + D_2O \rightleftharpoons D_2 + C(O)$).

Basically, the experimental results of isotopes are reasonable, because the heavy molecule will lower the diffusion and adsorption ability and slow reaction rate. But from our limited number of experiments, we cannot get further details about this issue.

4-4. Mechanism Derivation and Identification

4-4-1. Mechanism

A. Reverse Oxygen Exchange Inhibition

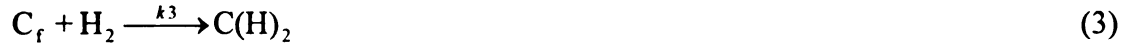
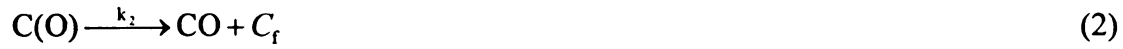


$$C_t = C_f + C_{C(O)} \quad (\text{site balance}) \quad (4)$$

Assume surface concentration of C(O) sites remains constant, so that amount produced equals the amount consumed. The formation rate of CO is:

$$r = k_2 C_{C(O)} = \frac{C_f P_w k_1 k_2}{k_2 + k_{-1} P_H + k_1 P_w} = \frac{C_f P_w k_1}{1 + \frac{k_{-1}}{k_2} P_H + \frac{k_1}{k_2} P_w} \quad (A)$$

B. Hydrogen Inhibition by Formation of a C(H)₂ Complex



$$C_t = C_f + C_{C(H)_2} + C_{C(O)} \quad (\text{site balance}) \quad (4)$$

The C(O) balance (formation rate equal consumption rate) is from (1) and (2). Assume that reaction (3) reaches equilibrium. In the same way, we get:

$$r = k_2 C_{C(O)} = \frac{C_f P_w k_1}{1 + \frac{k_3}{k_{-3}} P_H + \frac{k_1}{k_2} P_w} \quad (B)$$

C. Hydrogen Inhibition by Formation of a C(H) Complex



$$C_t = C_f + C_{C(H)} \quad (\text{site balance})(5)$$

Neglect $C(H)_2$, assume equation (3) is reversible and reach equilibrium easily. At steady state, $C(O)$ formation (1) rate equals consumption (2) rate. The CO formation rate is

$$r = k_2 C_{C(O)} = \frac{C_f P_w k_1}{1 + \frac{k_4}{k_{-4}} P_H^{0.5} + \frac{k_1}{k_2} P_w} \quad (C)$$

The generalized rate expression is thus

$$r = k_2 C_{C(O)} = \frac{k_f P_w}{1 + K_1 P_w + K_2 P_H^n} \quad (D)$$

For oxygen exchange $K_2 = k_{-1}/k_2$

For hydrogen inhibition by formation of a $C(H)_2$ complex: $K_2 = k_3/k_{-3}$

For hydrogen inhibition by formation of a $C(H)$ complex $K_2 = k_4/k_{-4}$

4-4-2. Kinetic Model

Results of all gasification experiments in steam/ H_2 mixture were fit to Equation (D) to determine which mode of hydrogen inhibition best fits the data and to calculate rate constant for elementary reaction steps in the model. Gasification rate (CH_4 can be neglected compared to CO and CO_2) for each experiment was calculated on a per unit BET surface area basis. The regression coefficient (r^2) for dissociative hydrogen adsorption ($n=0.5$) was 0.67 and for reverse oxygen exchange or weak hydrogen adsorption ($n=1$) was 0.957, clearly showing that dissociative hydrogen adsorption is not responsible for inhibiting gasification rate at our experimental conditions. Here we already rule out the weak hydrogen adsorption from the weakly adsorbed hydrogen detection. This result is supported by the fact that rate depends on hydrogen partial

pressure while quantity of hydrogen dissociatively adsorbed does not. (The regression work of this section was done by Michael^[27])

The rate constants and elementary rate constants are shown in **Table 4-1**. For reverse oxygen exchange, the equilibrium constant (k_1/k_{-1}) is 0.028, signifying that oxygen fractional coverage on active sites ($C(O)/C_f$) is relatively low when gas phase hydrogen is present. The equilibrium constant for associative hydrogen adsorption is large ($k_3/k_{-3} = K_2 = 420 \text{ MPa}^{-1}$), indicating that if “associative” adsorption is the primary mode of hydrogen inhibition, then hydrogen fractional coverage on the char surface would have to be very high compared to oxygen.

Table 4-1 Rate Constants from experimental Data at 850 °C

Rate constants for Equation D with n=1		
k_f	$5.3 \times 10^{-5} \text{ mmol C m}^{-2} \text{ sec}^{-1} \text{ MPa}^{-1}$	$= C_t k_1$
K_1	12 MPa^{-1}	
K_2	420 MPa^{-1}	
Elementary constants for Steam Gasification		
$k_1 C_t = k_f$	$5.3 \times 10^{-5} \text{ mmol C m}^{-2} \text{ sec}^{-1} \text{ MPa}^{-1}$	
$k_3 C_t = k_f / K_1$	$4.5 \times 10^{-6} \text{ mmol m}^{-2} \text{ sec}^{-1}$	
Elementary constants for Reverse Oxygen Exchange Steam Gasification		
$k_{-1} C_t = k_f K_2 / K_1$	$1.9 \times 10^{-3} \text{ mmol C m}^{-2} \text{ sec}^{-1} \text{ MPa}^{-1}$	
Equilibrium Constant for “Associative” Hydrogen Adsorption		
K_2	420 MPa^{-1}	

²⁷ **Michael G. Lussier**, Ph.D. dissertation Michigan State University (1997)

4-5. Conclusions

Hydrogen inhibits the steam gasification of carbons via different mechanisms at different extents of conversion. At very low conversion, or in environments where the quantity of hydrogen is limited, dissociative adsorption is observed to inhibit steam gasification at ordered edge sites on the char. At higher hydrogen pressures, the effect of adsorbed hydrogen is still present but can not be observed because it saturates the edge sites on the char surface. At these higher pressures, steam gasification rate is observed to be inhibited by reverse oxygen exchange which is dependent on hydrogen partial pressure in the reactant gas. “Associative” hydrogen adsorption is rule out as an inhibition pathway in high temperature gasification (850 °C). The results obtained here help to unify the findings of prior researchers who have conducted experiments at widely varying conditions and attributed hydrogen inhibition to different mechanism.

CHAPTER 5

HYDROGEN STABILITY ON CARBON SURFACES

5-1. Stability of Adsorbed Hydrogen to Oxidation by O₂

To examine the stability of adsorbed D or H to molecular oxygen, a series of experiments (gasification then oxidation) were conducted (**Table 1**). First, annealed Saran char was gasified in 3.1 MPa H₂ or D₂ at 850 °C for 4~6 hours to ensure the surface was saturated with H or D. Then the reactor was cooled down to oxidation temperature (450~480 °C) with argon purging, and oxidation was conducted in 5 or 10 mol % O₂ in argon for 1~3 hours. This temperature range of oxidation was chosen from the char oxidation experiment (see Chapter 2). Such a temperature was used to ensure that the oxidation was conducted in excess oxygen at low reaction rates and not all carbon was oxidized when exposed to O₂. At this temperature, the carbon burn-off (by molecular oxygen) rate continuously decreased with time, and a lot of molecular oxygen existed in the effluent gases (see **Figure 5-1**).

Table 5-1 Experimental Data Summary

EXP. No	9621	9622	9623	9624	7062	9620
Gasification agent	40% D ₂ +Ar	40% D ₂ +Ar	H ₂	H ₂	H ₂	40% D ₂ +Ar
Gasification time (hour)	6	6	4	4	4	6
Apparent weight Loss ^[1]	4.7%	5.3%	9.7%	8.3%	6.0%	4.0%
Oxidation time	1 hour	1.9 hour	2.5 hr	1.7 hr		
Oxidation Temperature	455 °C	445°C	455 °C	476°C	NA	NA
CO produced during Oxidation cc/g ^[1]	1.3	1.1	2.6	1.8		
CO ₂ Produced during Oxidation cc/g ^[2]	15.5	23.2	33.2	46.0		
% of initial carbon converted	2.1%	3.0%	4.9%	6.2%		
CO from TPD cc/g ^[3]	6.9	8.2	1.1	17.3		
CO ₂ from TPD cc/g ^[3]	1.63	1.04	0.50	1.14		
O ₂ uptake(of int. weight)% ^[4]	1.7	1.7	0.4	3.4		

¹ From the residual sample weighting

² From the analysis of effluent gas composition during oxidation

³ From the analysis of effluent gas composition during TPD

⁴ From the amount of CO and CO₂ during the TPD

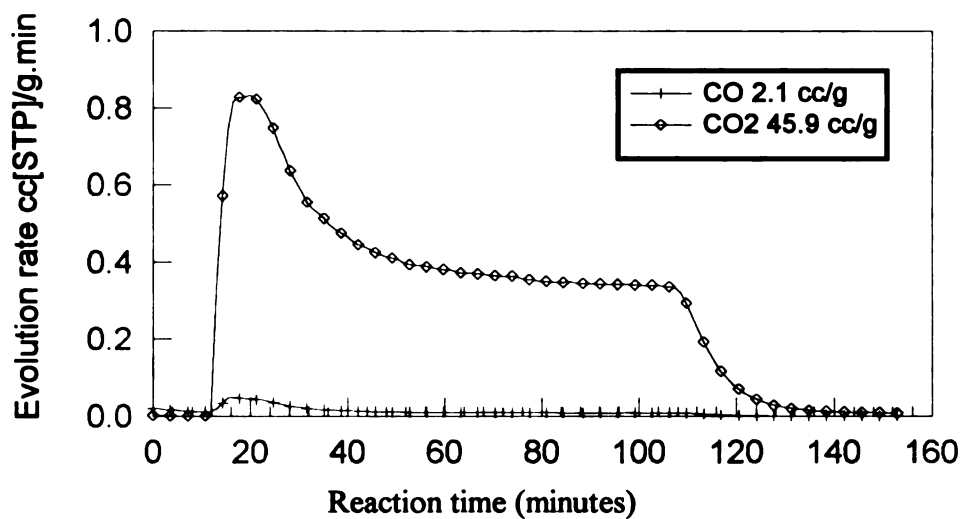


Figure 5-1 CO and CO₂ profiles during oxidation (T=476 °C, P_{O₂}=0.05 atm)(9624)

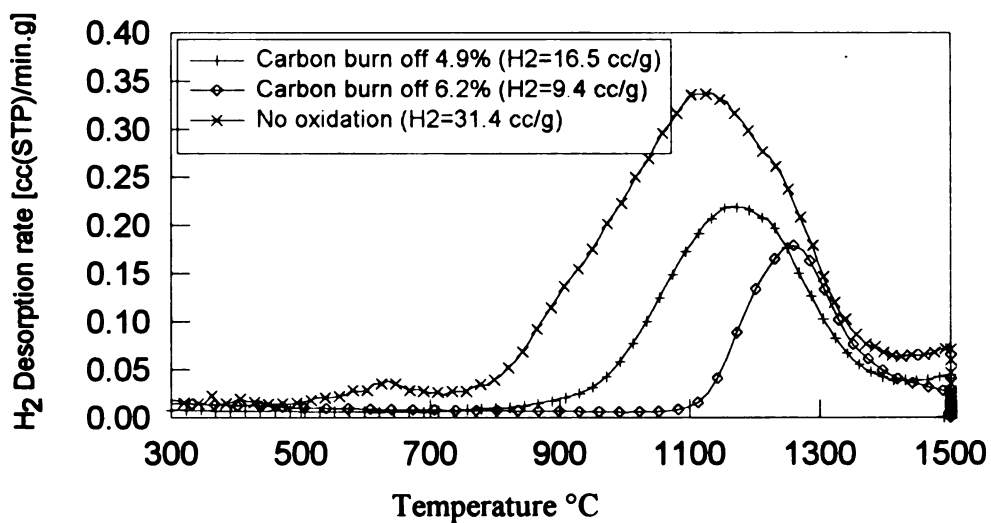


Figure 5-2 H₂ TPD profile at different oxidation severity following H₂ gasification and oxidation (9623,9624,7062)

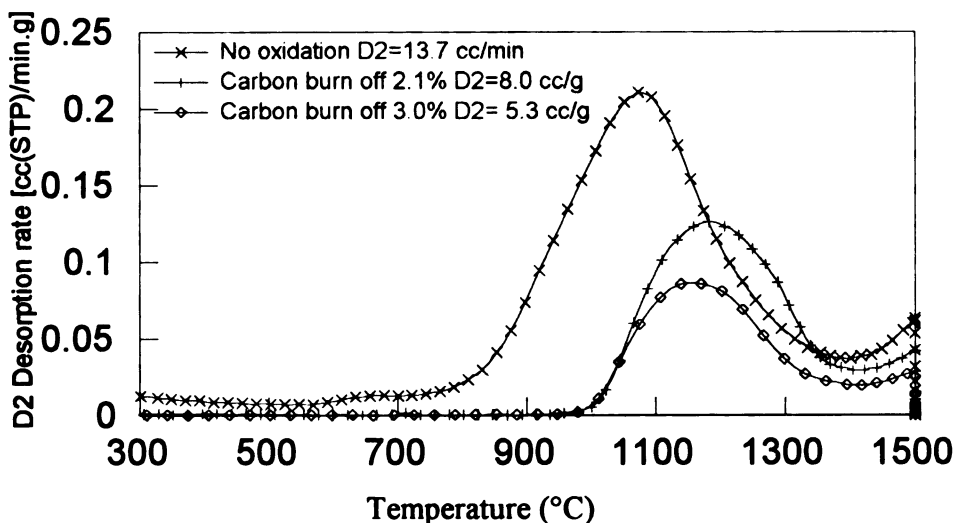


Figure 5-3 D₂ TPD profile at different oxidation severity following 6 hours D₂ gasification at 850 °C and 3.1 MPa (9620,9621,9622)

The effect of oxidation by O₂ on adsorbed hydrogen is seen in **Figure 5-2**, and the corresponding effect on adsorbed deuterium is given in **Figure 5-3**. Clearly, oxidation is able to remove adsorbed H or D at least to some degree from the char surface, as the amount of hydrogen (deuterium) remaining declines as the severity of oxidation increases. Second, more weakly bound hydrogen (or deuterium) is clearly removed first, as the temperature of the peak maximum desorption rate of the residual hydrogen increases with the severity of oxidation.

Table 5-2 Material Balance

EXP. No	9621	9622	9623	9624
Weight loss in gasification from product gas analysis	4.0%	4.0%	6.0%	6.0%
Weight loss in oxidation from product gas analysis	2.1%	3.0%	4.9%	6.2%
O uptake from TPD analysis	1.7%	1.7%	0.4%	3.4%
Actual recorded sample weight loss	4.7%	5.2%	9.7%	8.3%
Difference	0.3%	0.1%	0.7%	0.5%

Table 5-3 Oxidation Effects

	H ₂ gasification		D ₂ gasification	
EXP. No	9623	9624	9621	9622
Before Oxidation(H ₂)	31.4 cc/g	31.4 cc/g	13.7 cc/g	13.7 cc/g
Associated Carbon with H ₂ adsorbed	3.4%	3.4%	1.5%	1.5%
Oxide Carbon	4.9%	6.2%	2.1%	3.0 %
H ₂ left after oxidation	16.5 cc/g	9.4 cc/g	8.0 cc/g	5.3 cc/g
Associated Carbon with H ₂ adsorbed	1.8%	1.0%	0.86%	0.57%

From all H₂ (and D₂) TPD profiles, only one major peak is found, so it is reasonable to assume all H is bound to carbon by single bonds. After 4 hour hydrogen gasification, 31.4 cc/g H₂ is adsorbed on the carbon sample, which will associate with 0.034g/g carbon (3.4% of the initial char sample). The formation of oxygen groups on the char surface will offset the weight loss from carbon burn off (see **Table 5-2**)

Table 5-3 summarizes the oxidation effect. In all cases, we can see that the amount of oxide carbon [carbon bound as C(O)] is greater than the amount of carbon that is bound to H (or D) before oxidation, but quite a large amount of H (or D) still exists on the carbon sample.

If we assume that oxidation only starts from the outer surface of carbon particles, we can deduce that adsorbed hydrogen not only exists on the outer surface, it also exists inside the pore structure. From D₂O (or H₂O) profiles of oxidation following D₂ (or H₂) gasification (**Figure 5-4** and **Figure 5-5**), we can see that the H(or D) evolution (in the form of H₂O or D₂O) is fast at the beginning of oxidation and continuously decreases during the oxidation process. That means the H (or D) on the outer surface can be easily removed upon exposure to the molecular oxygen, but the H (or D) in the pore structure is not that easily accessed. It is necessary to burn all surrounded carbon before removing

them. From all these, we would say only the hydrogen (or deuterium) that is accessible to molecular oxygen can be removed.

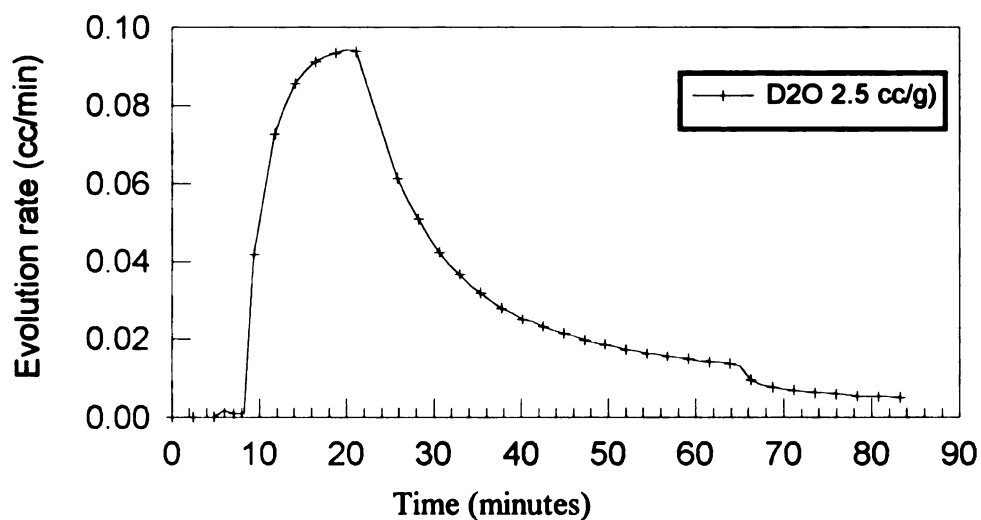


Figure 5-4 D₂O profile during oxidation (T=455°C, P_{O₂}=0.05 atm) (9621)

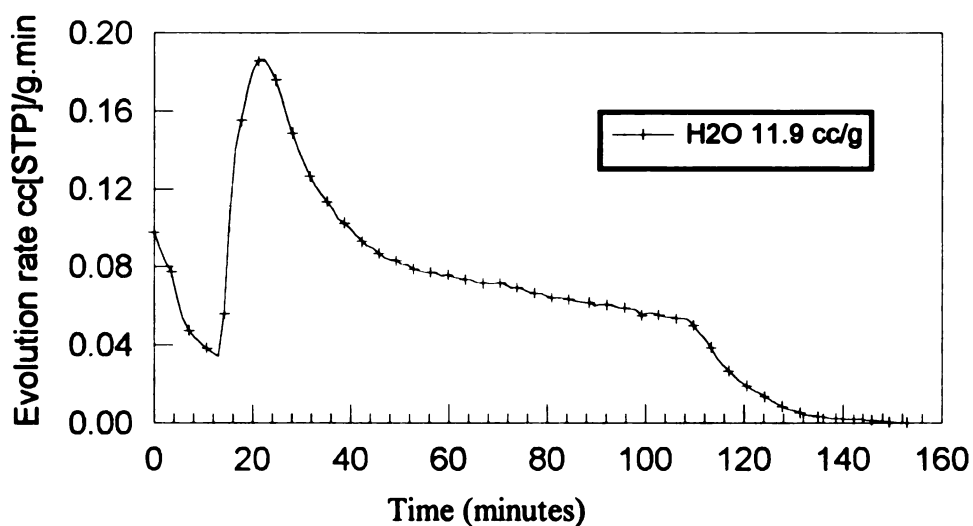


Figure 5-5 H₂O profile during oxidation (T=476 °C, P_{O₂}=0.1 atm)(9624)

5-2. D-H Exchange During Gasification

To further explore the stability of surface H, we designed D-H exchange gasification experiments to study the exchange of adsorbed deuterium. After a long gasification (6 hours) in 3.1 MPa D_2 at 850 °C, it is assumed that only D_2 is present on the carbon surface. Following gasification, we switched the reactant gas to H_2 and continued the gasification an additional length of time. After gasification, we conducted TPD to measure adsorbed D and H. Before H_2 gasification, the quantity of D_2 on carbon is 13.7 cc/g. After 0.8 hour H_2 gasification, 9.5 cc/g D_2 exists on carbon sample from TPD (Figure 5-6). So, a 0.8 hour gasification in H_2 is not enough to exchange all D off the char surface. The identical peak position of D_2 HD and H_2 in TPD profiles is a evidence that the exchange has no preference for different adsorption energy distribution if it does exist.

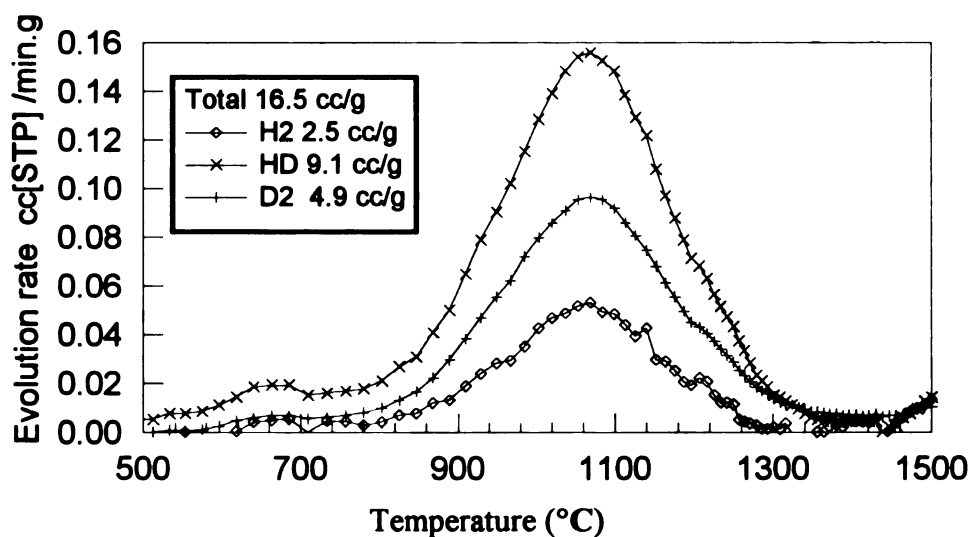


Figure 5-6 TPD of sample from 6 hours D_2 +Ar and 0.8 hr H_2 +Ar gasification at P=3.1 MPa and T=850 °C, annealed Saran char (9608)

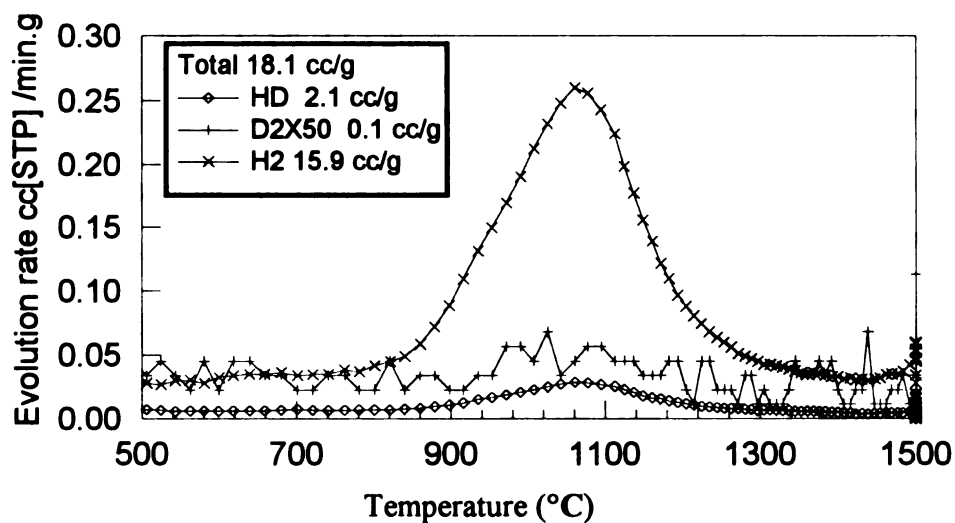


Figure 5-7 TPD of sample from 6 hr. D_2 +Ar and 2.5 hours H_2 +Ar gasification at 3.1 MPa, $T=850\text{ }^\circ\text{C}$, annealed Saran char (9610)

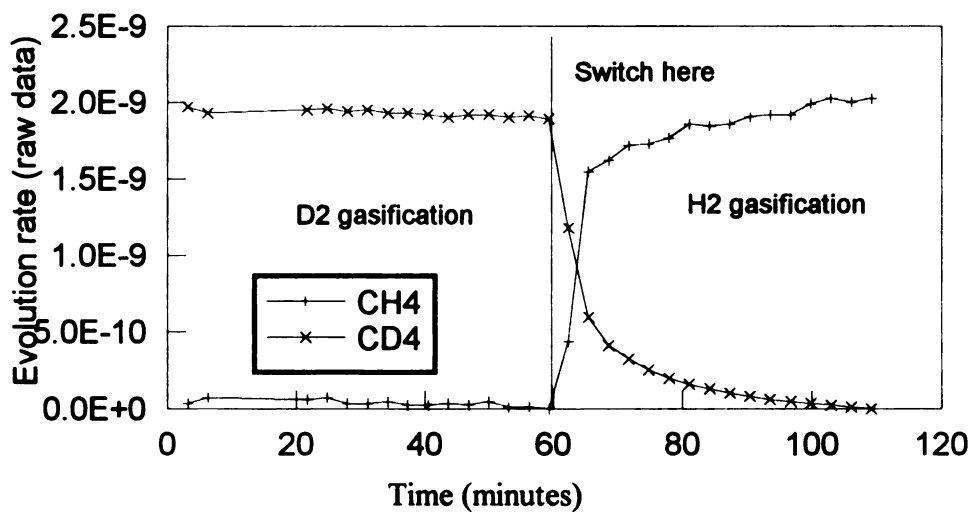


Figure 5-8 CD_4 and CH_4 evolution during switch (6 hr. D_2 +Ar and 0.8 hour H_2 +Ar gasification $P=3.1\text{ MPa}$, $T=850\text{ }^\circ\text{C}$, annealed Saran char(9608)

Figure 5-7 gives the quantity of H_2 , HD, and D_2 present on the char after six hours D_2 gasification followed by 2.5 hr H_2 gasification. Clearly, most adsorbed deuterium has been replaced by H on the char sample. The quantity of H_2 adsorbed (15.6 cc/g) is very close to the quantity of D_2 desorbed following D_2 gasification only (13 cc/g). It is reasonable to conclude that sites on which D is adsorbed following D_2 gasification are the only ones available for H adsorption during H_2 gasification.

From the transient profile of CD_4 (**Figure 5-8**), we can see the evolution is fast after switch, so the outer surface D-H exchange is fast. But the D trapped in the pore structure is much more difficult to exchange and even 2.5 hr H_2 gasification can not replace all deuterium.

The simple calculation is given in **Table 5-4**. When the amount of carbon gasified by H_2 approaches the amount of carbon that is bound to D, there is more than half the residual D on the char sample (E9608). Even for 2.5 hours H_2 gasification, where the 3.8% carbon converted is over twice the amount of carbon bound to D, 1.1 cc/g D_2 still stays on the char. This suggests that H_2 gasification does not necessarily occur on the sites which deuterium adsorbed on. It is well known that after adsorbing hydrogen, the armchair carbon sites tend to be gasified firstly. So, the deuterium adsorbed on armchair sites will be peeled off readily. On another hand, the deuterium adsorbed on zigzag carbon can not be replaced until the surrounding carbon is burnt off(see Chapter 6).

Table 5-4 D-H Exchange Effects

Exp. No	9620	9608	9610
H ₂ gasification time	0 hr	0.8 hr	2.5 hr
Before switch cc D ₂ /g	13.7	13.7	13.7
D ₂ left cc/g	13.7	9.5	1.1
Associated carbon %	1.5	1.0	0.1
Gasified carbon by H ₂ %	0	1.2	3.8

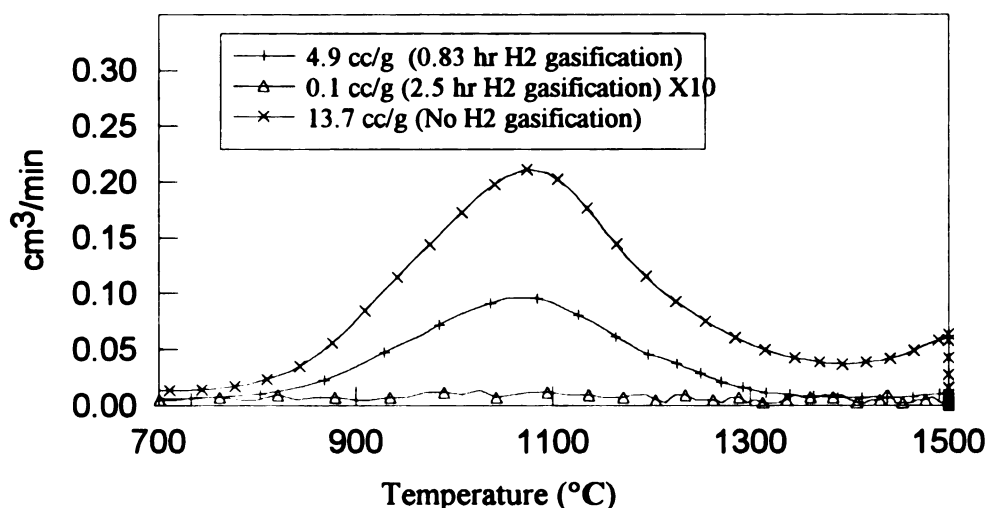


Figure 5-9 D₂ TPD profiles change with H₂ gasification time following 6 hr D₂ gasification at 850 °C (9608,9610,9620)

Figure 5-9 is the summary data of the D-H exchange experiments. The amount of residual D decreases with H₂ gasification time following the 6 hours D₂ gasification. The most significant phenomena are the peak position and shape. The amount of residual D changes with time of following H₂ gasification, but the peak position and peak shape are unchanged. That means that D-H exchange is different from molecular oxidation in that this process does not take place with more weakly-bound hydrogen preferentially.

5-3. H-D Exchange During Gasification

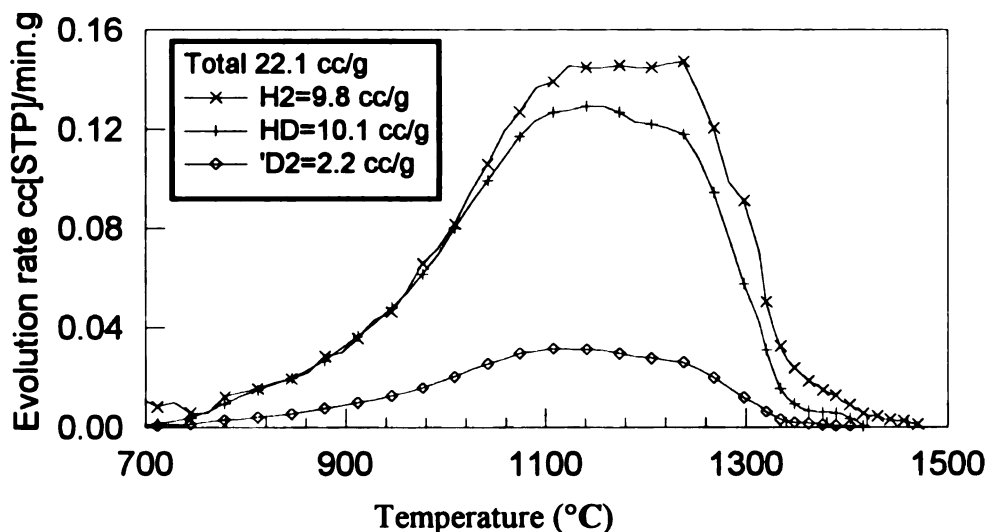


Figure 5-10 TPD of sample from 4 hours H₂+Ar and 0.7 hr. D₂+Ar. gasification at P=3.1 MPa, T=850 °C, annealed Saran char (9630)

To further understand the mechanism of surface H exchange, we also designed H-D exchange gasification experiments to study the exchange of adsorbed hydrogen. After a long gasification (4 hour) in H₂, 32 cc/g H₂ is present on the carbon sample. We then switched reactant gas to D₂ and continued the gasification an additional length of time. After gasification, we conducted TPD to measure adsorbed D and H. We can see that a 0.7 hour gasification in H₂ can exchange half the adsorbed H₂ (**Figure 5-10**). This is faster than D-H exchange (comparing to **Figure 5-6**).

From **Figure 5-11** and **Figure 5-12**, we can further identify that the fast exchange of hydrogen by deuterium only occurs at the beginning. But after 2.5 hr. D₂ gasification, fair amounts of hydrogen (5.9 cc/g) still exist on the carbon sample. This is another significant different from D-H exchange. It seems that adsorbed hydrogen could migrate into the pore structure of the carbon sample and make it difficult to access for the following D₂ gasification. It is also possible the faster H-D exchange rate comes from the high hydrogen gasification rate (The adsorbed H is active than D).

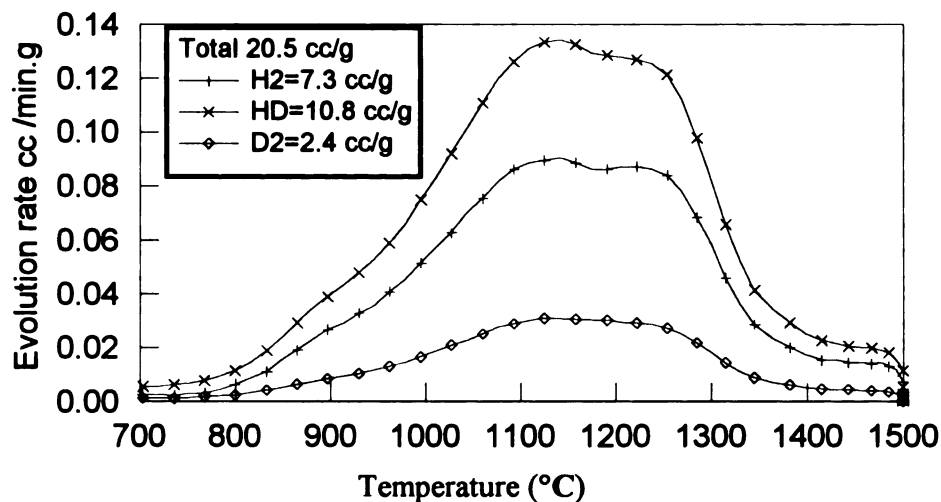


Figure 5-11 TPD of sample from 4 hours H₂+Ar and 1.3 hr. D₂+Ar gasification at P=3.1 MPa, T=850 °C, annealed Saran char (9631)

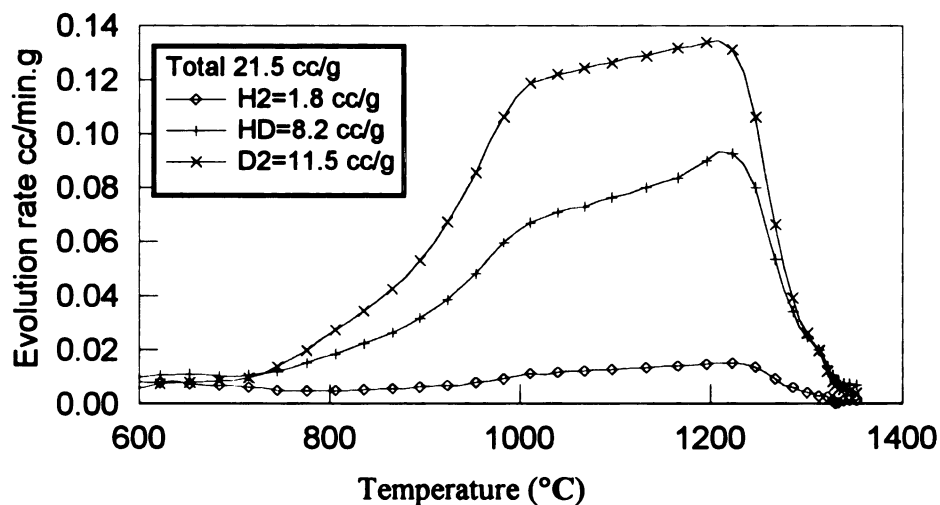


Figure 5-12 TPD of sample from 4 hours H₂+Ar and 2.5 hr. D₂+Ar gasification at P=3.1 MPa, T=850 °C, annealed Saran char(9632)

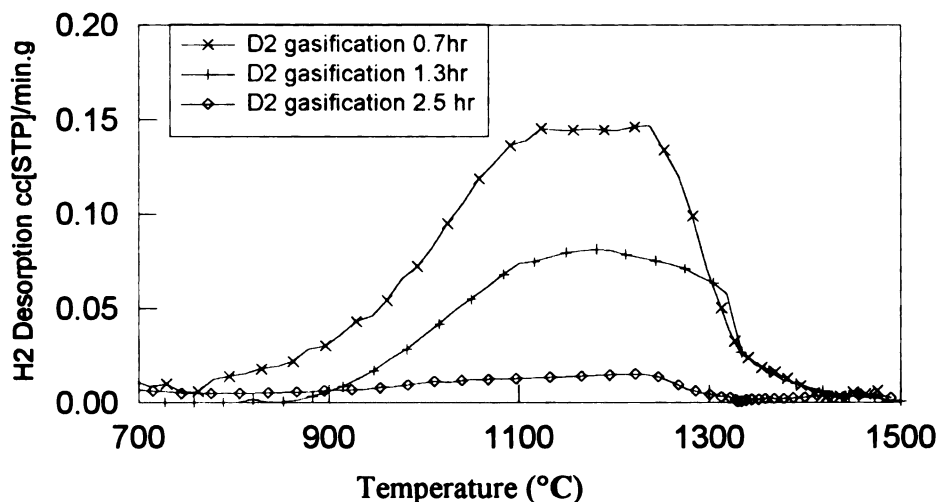


Figure 5-13 H₂ TPD profiles change with D₂ gasification times following 4 hr H₂ gasification at 850 °C, 3.1 MPa (9630,9631,9632)

Table 5-5 H-D Exchange Effects

D ₂ gasification time	0 hr	0.7 hr	1.3 hr	2.5 hr
Before switch cc H ₂ /g	31.4	31.4	31.4	31.4
H ₂ left cc/g	31.4	14.9	12.7	5.9
Associated carbon %	3.4	1.6	1.4	0.74
Gasified carbon by D ₂ %	0	0.50	0.87	1.7

From the summary experimental data (Table 5-5), we can clearly see the H-D exchange is much faster than corresponding D-H exchange. For 0.7 hour D₂ gasification, only 0.5% carbon conversion results in exchange of half of the adsorbed hydrogen (which bonds to 1.7% carbon). That means that the adsorbed H does exchange with D₂ in gas phase. clearly does happen in this case. The fast exchange also indicates that the bond energy of C-D is larger than C-H. So, adsorbed H is easily replaced by D₂ from gas phase, but H-D exchange is not such easy.

5-4. Conclusions

In conclusion, the adsorbed hydrogen (or Deuterium) is quite stable. The molecular oxygen can remove the adsorbed hydrogen when the associated carbon is burnt off. Carbon atoms and adsorbed hydrogen atoms have same opportunities to be oxidized. No preference is found in the oxidation process; weakly bound hydrogen (probably most on outer surface) is removed first. “Trapped” H (or D) is very difficult to be removed unless the surrounding carbon atoms are burnt off.

Adsorbed D(H) can be exchanged during the following H_2 (D_2) gasification. The exchange process has no preference for different bind energy of adsorbed D if it does exist. H-D exchange is faster than D-H exchange and the exchange really take place, as opposed to simple gasification of carbon with adsorbed species (H or D) present. We also found that some H could be trapped in the inner structure, and could not be exchanged (or removed) until the surrounding carbon was gasified.

CHAPTER 6

RATE ENHANCEMENT USING MOLECULAR OXIDATION

Introduction

From Chapter 4, we know that adsorbed hydrogen strongly inhibits steam/ H_2 gasification. It is therefore reasonable to think about removing adsorbed hydrogen during gasification to recover and retain activity of the carbon. Reaction rates decrease rapidly during the initial steam/ H_2 gasification, due to rapid uptake of hydrogen. Probably, this would occur following H_2 removal during gasification, so we would not expect the rate recovery following H_2 removal could last very long, unless hydrogen is continuously removed from the surfaces.

The experimental scheme to investigate hydrogen removal during gasification is given in **Figure 6-1**. First, Saran char is gasified in H_2 /steam for 4 to 6 hours, and then switched to purge argon. When the reactor temperature drops to 450~480 °C, the char sample was oxidized in 10% (or 5%) O_2 in argon for a certain time. After finishing the oxidation, reactant gas is switched back to purge argon and the reactor as heated up again. Once the reactor reached gasification temperature, gases were switched to H_2 /steam to conduct the gasification again for 1~3 hours.

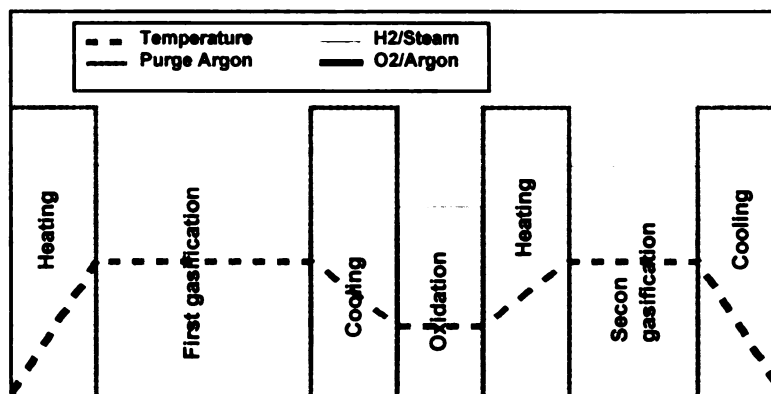


Figure 6-1 Experimental scheme

6-1. Oxidation Effects

Oxidation following gasification will remove adsorbed hydrogen to some degree, as seen in Chapter 5. After gasification and oxidation, the following CO and CO₂ TPD profiles were taken (**Figure 6-2** and **6-3**). The shape of the profiles depends strongly on oxidation conditions. For H₂ gasification and then oxidation, the CO peak is located at 900~950°C and the CO₂ peak sits at about 700 °C (**Figure 6-2**); for D₂ gasification and oxidation, the CO peak is located at 900°C and the CO₂ peak at 600 °C (**Figure 6-3**).

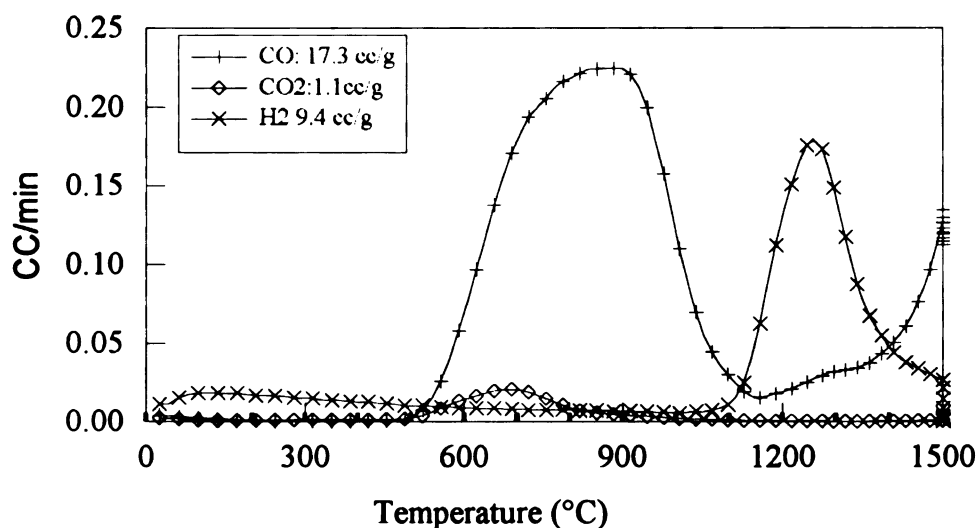


Figure 6-2 CO and CO₂ desorption profiles from annealed Saran char following gasification in H₂ for 4 hr at 850 °C and then oxidation in 10% O₂ in Ar at 476 °C for 1.7 hour(E9624)

Table 6-1 Estimation of The Surface Site Density

EXP. No	CO	CO ₂	H ₂ (Or D ₂)	Sum of sites	Before oxidation
E9624	17.3	1.1	9.4	28.9	~34
E9621	6.9	1.6	8.0	18.1	~13

From the two experimental results (**Figure 6-2** and **Figure 6-1**), we can see that most adsorbed oxygen is given off during the TPD in the form of CO. **Table 6-1** gives the simple estimation of the surface site density by adding CO, CO₂ and H₂ or D₂. From these,

we find the adsorbed oxygen is using the same sites as adsorbed hydrogen. The CO peak after 1300 °C is most likely from the ceramic TPD reactor, as it is seen during the blank run.

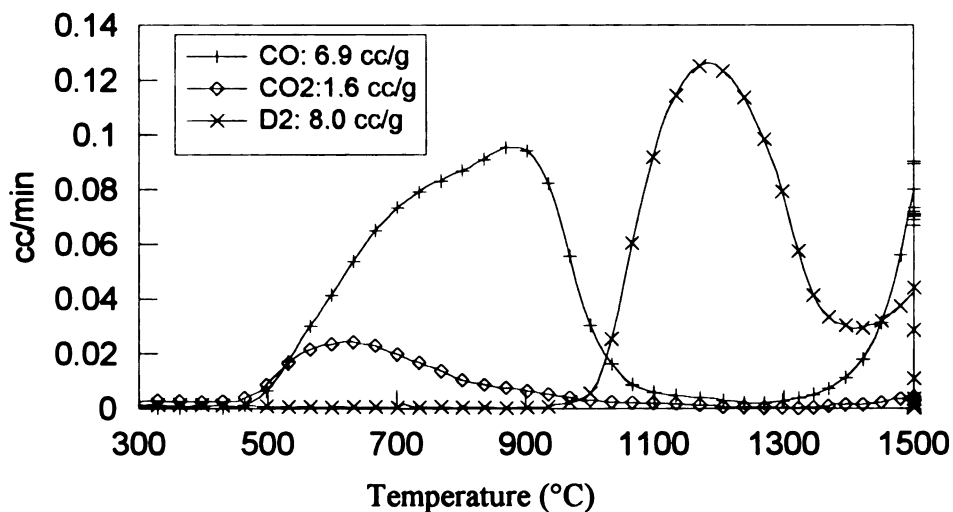


Figure 6-3 TPD profiles of annealed Saran after 6 hours D₂ gasification and 1 hour oxidation (5% O₂ in argon and 60 cc/min) at 455 °C (E9621)

6-2. H₂ Gasification Rate Enhancements

Results of H₂ gasification rate enhancement experiment is given in **Figure 6-4**.

We can see that the enhanced methane formation rate is almost twice as high as before oxidation. The rate enhancements apparently can continue a long time. This phenomenon is unexpected, since we only expect rate enhancement at initial stages of reaction. To explain this, we need to look into the detailed structure of the carbon sample.

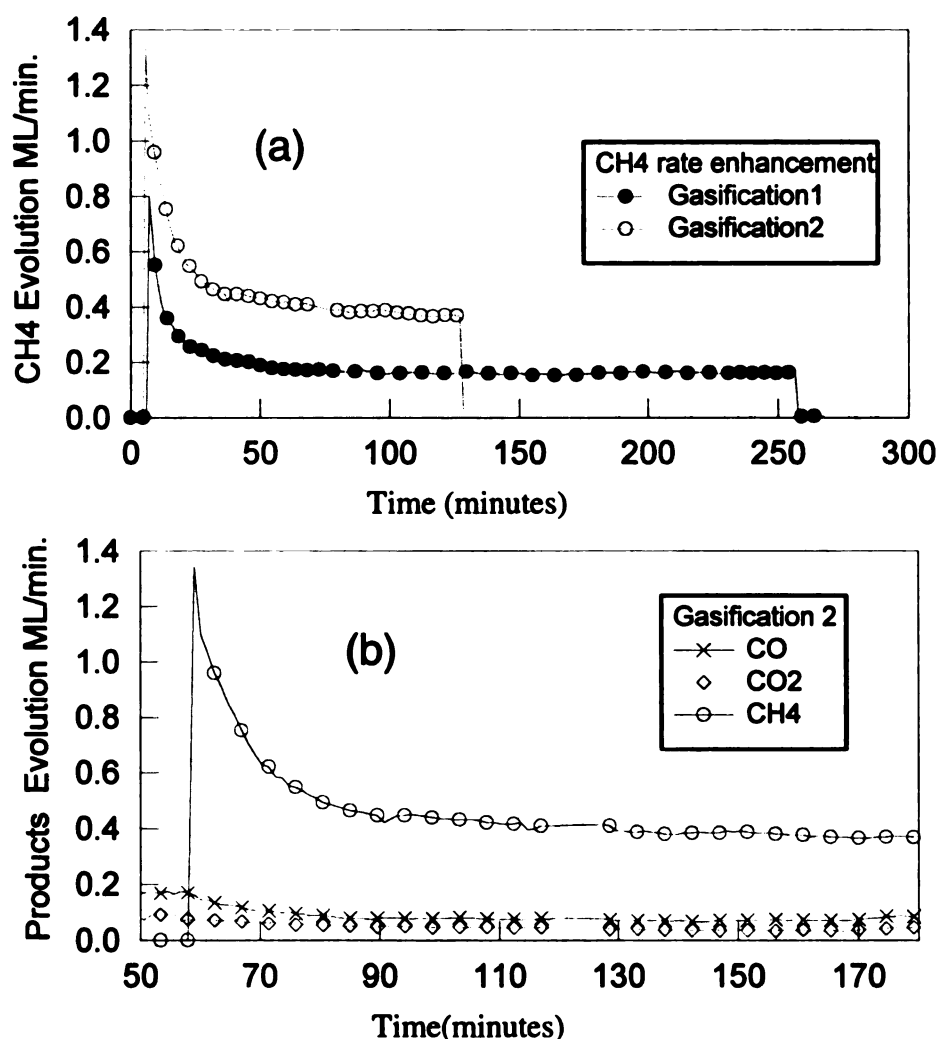


Figure 6-4 Annealed Saran char gasified in 3.1 MPa H₂ at 850°C to 5.9% conversion (Gasification 1), then oxidized at 450 °C with P_{O₂}=0.1 atm for 1 hour, then gasified again in 3.1 MPa H₂ (Gasification 2). (a) Rate curves for H₂ gasification showing rate enhancement; (b) Product profiles during gasification 2. (E9633)

First, the surface area of carbon samples increases with gasification. Also, according to many researchers, the zigzag carbon configuration becomes more and more dominant on the carbon surface as gasification progress. Apparently, these two factors work together to give the apparent constant methane (CH_4) formation rate after the initial stage of reaction. Our experiments (Chapter 4) showed that the increase in surface area is very slow. To maintain relative constant gasification rate during the hydrogen gasification, the rate of increase of the zigzag carbon configuration must also be very slow. Therefore, we can say that the changes in configuration of atoms on the carbon surface is a very slow process. In most case, after one layer gasification, the armchair configuration is more likely to be maintained than the zigzag configuration(**Figure 6-5**).

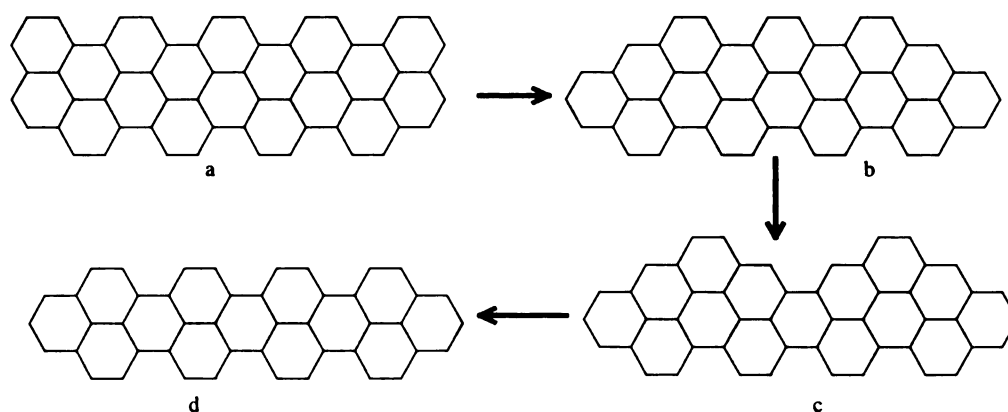


Figure 6-5 Armchair carbon maintain its structure during gasification

In this first step, the most active dangling edge carbon atoms are burnt off. Next, the carbon atoms at the middle of the armchair positions are burnt off. Now, most of the surface carbon is in the zigzag configuration. Apparently, the top two carbon rings are still more active than the others. The further burn-off of the four top carbon atoms will recover the full armchair configuration. Of course, this is only one possible explanation, Lussier^[27] provide more detail in his dissertation. That is why the gasification rate can be

maintained for a long time. That does not mean that the armchair configuration will be maintained forever. During the gasification process, the zigzag configuration always tends to replace armchair configuration.

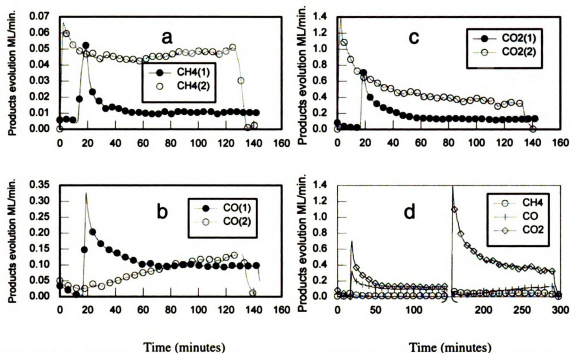
Although this process is slow, the zigzag configuration will dominate the carbon surface after a long enough time. According to Yang^[6]'s work, oxidation processes have no preference for armchair or zigzag sites. After oxidation, the fraction of armchair sites should increase and the ratio of zigzag sites should decrease.

The dimensions of ordered structure in Saran char is very small and small ordered elements may be burnt off with gasification(or oxidation) progress. This process will open enclosed pore structure and increase the surface area. In the above experiments, the BET surface area increases about 20% due to oxidation. After gasification 1 the BET is 900 m²/g, and after oxidation the BET area is 1100 m²/g. Steam and H₂ gasification prefer to occur on the armchair carbon, and hydrogen prefers to adsorb on zigzag carbon. The increase of surface area and armchair ratio work together to make the apparent rate enhancement possible. All these contribute to the long time constant methane formation rate.

Yang's theory may explain the initial high rate due to the formation of new armchair carbon. But their results come from graphite, and cannot explain why the enhancement can continue for a long time in our experiment.

⁶ Yang, R.T. and Duan, R.Z., Carbon 23(3), 325 (1985).

6-3. Steam Gasification Rate Enhancements



Time (minutes)

Time (minutes)

Figure 6-6 Rate enhancement by oxidation.

Conversion: 5.0% (gasification 1), 2%(oxidation), 10.7%(gasification 2) [H₂O gasification of annealed Saran char at 725 °C and 3.1 MPa; oxidation at 425 °C and 3.1 MPa for 1 hr]

a) CH₄ formation; b) CO₂ formation; C) CO formation; d) overall reaction

Steam gasification is more complicated than pure hydrogen gasification. The gasification temperature also affects the rate enhancement results.

For the 725 °C, rate enhancement experiment is given in **Figure 6-6**. Methane formation rate is almost four times higher as after than before oxidation, although the rate is very low compared to the CO and CO₂ formation rate. This methane rate enhancement is much larger than in H₂ gasification. Practically, this enhancement is meaningless, since the enhanced methane rate still is too low to have any value, but it useful for understanding the methane formation mechanism. In this experiment, very low oxidation temperature (425 °C) was used to burn off about 2% of initial carbon. Thus,

we cannot believe that the surface area has changed significantly. The methane rate enhancement only can come from the uptake of oxygen groups on the carbon surface. The adsorbed oxygen substitutes the adsorbed hydrogen, so the extension of hydrogen inhibition decreases. According to Huttinger's^[5] methane formation mechanism, the oxygen group is necessary for methane formation and oxygen groups can exist on the carbon surface at low gasification temperatures.

Although many researchers thought that CO₂ only comes from the shift reaction, we do not agree. From the CO and CO₂ evolution rate profiles, we can clearly see that some CO₂ does come from carbon surface reaction. Theoretically, at the same reaction conditions, the extent of the shift reaction should not change. At the beginning of the second gasification, the formation rate of CO and CO₂ changes with time (**Figure 6-6 b,c**). We can only conclude that CO₂ not only comes from the shift reaction, but also from the surface carbon gasification at 725 °C. After oxidation, a fair amount of oxygen groups exist on the carbon surface. So, the dominant product is CO₂, and the CO rate is very low at the beginning of the gasification. With reaction progress, the surface oxygen groups are consumed, the CO₂ formation rate decreases and the CO rate increases. Even after 2.5 hours, the CO₂ formation rate continues to decrease. At the same time, the CO formation rate increases to the value before oxidation and is still increasing. Nevertheless the decreasing CO₂ formation rate is still much higher than the value before oxidation. The surface area increase also contributes to the apparent rate enhancement. After the total (17.7%) carbon conversion during gasification and oxidation, the BET area increases about 50% (from 800 to 1200 m²/g).

⁵ **Huttinger, K.J. and Merdes, W.F., Carbon 30(6), 883 (1992).**

total (17.7%) carbon conversion during gasification and oxidation, the BET area increases about 50% (from 800 to 1200 m²/g).

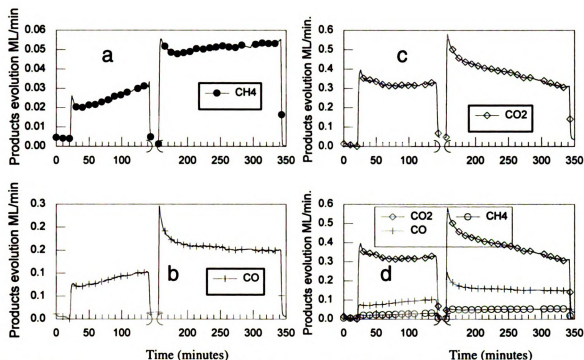


Figure 6-7. Rate enhancement by oxidation.

Conversion: 7.0% (gasification 1), 14.4% oxidation) and 18.6% (gasification 2).
gasification in 3.1 MPa steam at 850 °C; oxidation at 450 °C for 70 min[9637]

a) CH₄ formation; b) CO₂ formation; c) CO formation; d) overall reaction

Results of the 850 °C steam gasification rate enhancement experiment (**Figure**

6-7) is much different from the results of 725 °C gasification. The formation rate of CO after oxidation is higher than before oxidation, and the rate seems quite stable. The CO₂ formation rate is slightly enhanced, but returns to the value before oxidation after a while. From **Figure 6-2** and **Figure 6-3**, we know that most adsorbed surface oxygen groups can not survive at the temperatures higher than 850 °C. The high reaction temperature will lead to very little oxygen groups deposition on the carbon surface during oxidation. So, enhanced methane rate and CO formation rate are limited at high temperature

surface area about 42% (from 950 to 1350m²/g), which roughly agrees with the apparent rate enhancement of methane and CO.

The initial higher CO₂ formation rate probably comes from the limited adsorbed oxygen and the active carbon atoms, which are formed during the oxidation. We can see that the rate quickly decreases back to the value before oxidation. It seems that the surface area increase did not affect the CO₂ formation! It is highly possible that this amount of CO₂ is only from the shift reaction. Unfortunately, the surface reaction combined with the shift reaction make this phenomenon more complicated. From these limited experiments, we can not figure out the real reason.

6-4. H₂/Steam Gasification Rate Enhancements

The steam/H₂ gasification at 725 °C is more interesting (Figure 6-8). The CO rate change is similar to steam gasification at 725 °C. The CO rate is very low at the beginning of the second gasification, then increases. The enhanced CO₂ rate continues for a limited time and then returns to the level before oxidation. This is further evidence of hydrogen and oxygen in a competitive adsorption. Hydrogen is more easily adsorbed on the carbon surface. Because H₂ exists in the gas phase, the surface oxygen groups are quickly replaced by adsorbing hydrogen. The methane rate enhancement looks more like pure H₂ gasification, as the rate is about twice as before oxidation.

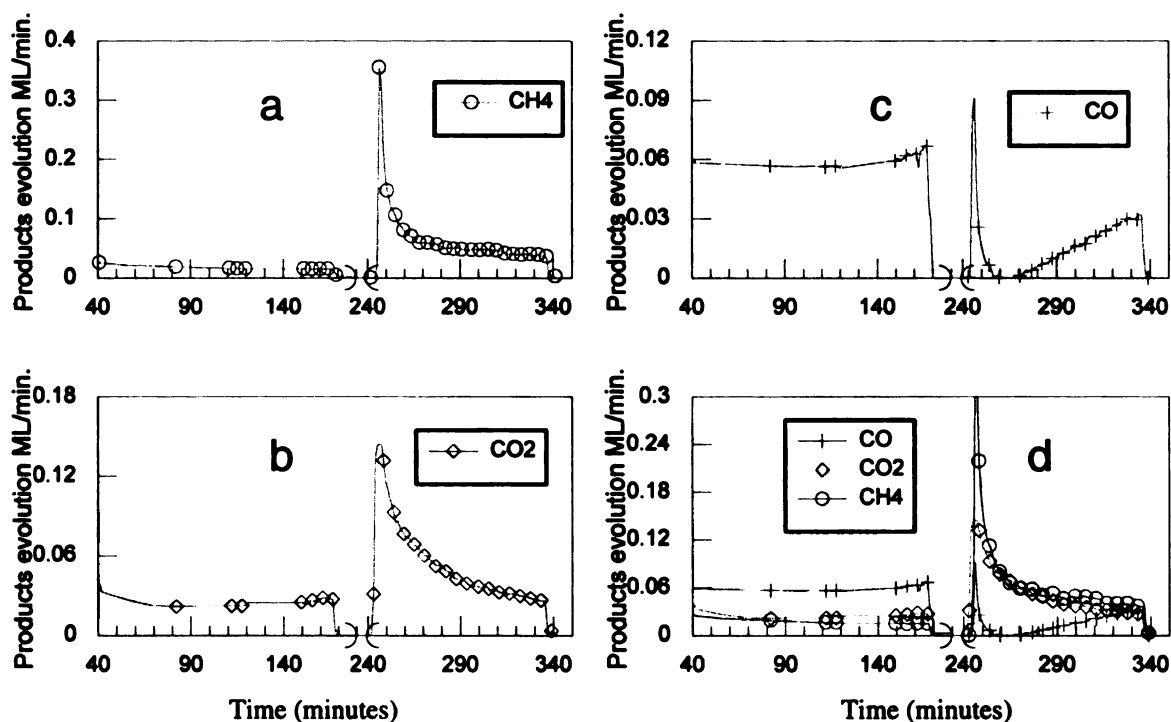


Figure 6-8. Rate enhancement by oxidation.

Conversion: 2.1% (gasification1), 1.6% (oxidation) and 8.1% (gasification2). Gasification of annealed Saran char in 3.1 MPa H₂/H₂O at 725 °C; oxidation at 450 °C for 60 min

a) CH₄ formation; b) CO₂ formation; c) CO formation; d) overall reaction

6-5. Conclusions

Rate enhancement by molecular oxygen itself is meaningless, since the main products are CO_2 . But the limited number of rate enhancement experiments do give us some detail information about the Saran char gasification.

- ◆ The 725 °C and 850 °C steam/ H_2 gasification is much different. At the low temperature steam gasification, surface oxygen groups are very important for gasification. So, the history of the char (which will decide the surface oxygen) will strongly affect the gasification rate. But at high temperature, the oxygen groups can not survive. The oxidation process has very limited affect on the subsequent following gasification.
- ◆ Comparing **Figure 6-6** and **Figure 6-7**, we know that the enhanced gasification rate at low temperature (725°C) can match the rate of high temperature gasification (850°C). The methane formation rate also has same trend.
- ◆ Oxidation by molecular O_2 will not only react with surface hydrogen, it also will react with surface carbon. This will change the surface structure. The formation of new arm-chair edges, the increased surface area, and the uptake oxygen groups all will contribute to the enhancement of the H_2 /steam gasification rate. By these limited experiments, it is impossible to give a universal mechanism.

CHAPTER 7

CONCLUSIONS AND RECOMMENDATIONS

The results of these studies lead to some important conclusions about the hydrogen deposited during carbon gasification. However, there are still many unanswered questions, and some recommendations are thus made within the framework of the present study to resolve some of the relevant questions.

7-1.Conclusions

7-1-1.Hydrogen Stability after Char Gasification

The adsorbed hydrogen (or Deuterium) is quite stable on the char surface. Molecular oxygen can remove adsorbed hydrogen with carbon burnt off. Carbon atoms and adsorbed hydrogen atoms have the same chance to be oxidized, and no preference is found in the oxidation process. Weakly bound hydrogen tends to be removed first. Some hydrogen may migrate into the pore structure, where even severe oxidation condition can not remove it.

Adsorbed D (H) can be exchanged during the following $H_2(D_2)$ gasification. The exchange process has no preference for adsorbed D(H) with different binding energies. From H-D exchange, we have confirmed that the adsorbed hydrogen is in a dynamic state during gasification and continuously exchanges with hydrogen in the gas phase.

7-1-2.Gasification and Hydrogen Inhibition

Hydrogen inhibits the steam gasification of carbons via different mechanisms at different extents of conversion. At very low conversion, or in environments where the quantity of hydrogen is limited, dissociative adsorption is observed to inhibit steam gasification at ordered edge sites on the char. At higher hydrogen partial pressures, the effect of adsorbed hydrogen is still present but can not be observed because it saturates the edge sites on the char surface; steam gasification rate is observed to be inhibited by

reverse oxygen exchange which is dependent on hydrogen partial pressure in the reactant gas. Because of the unstability of “associative” adsorbed hydrogen, it is ruled out as an inhibition pathway in high temperature gasification (850 °C).

7-1-3. Rate Enhancement by Molecular Oxygen Oxidation

At the low temperature steam gasification, surface oxygen groups are important for gasification. So, adding oxygen groups by oxidation to the char surface will significantly enhance the subsequent gasification rate. But at high temperature, the oxygen groups can not survive, so the oxidation process has a very limited effect on subsequent gasification.

Oxidation by molecular O_2 will not only react with surface hydrogen, it also will react with surface carbon. This will change the surface structure. The formation of new arm-chair edges, the increased surface area, and the uptake of oxygen groups all will contribute to the enhancement of H_2 /steam gasification rate.

7-1-4. Isotopic Effect

The isotopic effect have been seen on the D-H and H-D exchange, D_2 gasification and the D_2O gasification. H-D exchange is much faster than D-H exchange. At the same reaction conditions, deuterium gasification rate is about one fourth of H_2 gasification rate; the gasification rate of D_2O is about three fourth of the steam gasification rate.

7-2.Recommendations

There are still some speculations involved in the interpretation of the stability of adsorbed H(D). Experiments have shown that H is easily exchanged by D, but D is exchanged by H only with difficulty. We know that the mass difference will affect adsorption and diffusion ability, but the detail is unclear yet. For further work, molecular orbit theory is needed to simulation the adsorption on carbon surface.

The rate enhancement is very meaningful to industrial application. We got some preliminary results, but the real mechanism is unclear yet. For the three possible source of enhancement: removing of adsorbed hydrogen, surface area change and change the carbon surface structure, we do not know which is the dominant factor. Further investigation is advisable by other surface analysis technique.

Hydrogen desorption energies distribution is another speculation. Armchair and Zigzag are two possible sites for the adsorption of hydrogen, so at most two adsorption energy exist. Because the TPD process is a combination of surface desorption reaction and the hydrogen migration from bulk carbon to the surface, it is difficult to determine the energy distribution from the TPD profile. For further identifying, details of mechanism of desorption and adsorption of hydrogen on carbon, probably graphite (with real surface adsorption) is need to measure the desorption of hydrogen from the carbon, One can then use desorption theory to get the real desorption energy.

LIST OF REFERENCE

- 1 Steinberg, M., 1987 Int. Conf. on Coal Sci. 11, J. A. Moulijn, ed., 953 (1987).
- 2 Redmond, J. P. and Walker, P. L. Jr., J. Phys. Chem. 64, 1093 (1960).
- 3 Biederman, D.L. et al., Carbon 14, 351 (1976).
- 4 Yang, R.T. and Yang, K.L., Carbon 23(5), 537 (1985).
- 5 Huttinger, K.J. and Merdes, W.F., Carbon 30(6), 883 (1992).
- 6 Yang, R.T. and Duan, R.Z., Carbon 23(3), 325 (1985).
- 7 E,J Hippo, N murdie and A. Hyjiazie, Carbon 27, 689 (1989)
- 8 Treptau, M.H. and Miller, D.J., Carbon 29, 531 (1991).
- 9 Blackwood, J.D. Aust. J. Chem. 12, 14 (1959).
- 10 Cao, J.R., and Back M.H., Carbon 23, 141 (1985).
- 11 Walker, Carbon, Vol. 29, P41,1991
- 12 Pan, Z.,J and Yang, R. T. Ind. Eng. Chem. Res. 1992,31,2675
- 13 Chen and Yang, Ind. Eng. Chem. Res.,32,2835, 1993
- 14 Zielke, C.W. and Gorin, E., Ind. and Enq. Chem. 47(4), 820 (1955).
- 15 Ergun, S and Mentser, M In Chemistry and Physics of Carbon (by P.L.Walker. Jr) Vol. 2 P203. 1966
- 16 Long, F.J., and Sykes, K.W., Proc. Royal Soc. London A193, 377 (1948).
- 17 Gadsby, J., Hinshelwood, C.N., and Sykes, K.W., Proc. Royal Soc. London A187, 129 (1946).
- 18 Huttinger, K.J., ACS Div. Fuel Chem. Prepr. 34(1), 56 (1989).
- 19 Blackwood, D.J. and McGrory, F., Aust. J. Chem. 11, 16 (1958).
- 20 Montet, G.L., and Myers, G.E., Carbon 9, 673 (1971).
- 21 Yates, J.T.Jr. and McKee, D.W., J. Chem. Phys. 75, 2211, (1981).
- 22 Mims, C.A. and Pabst, J.K., ACS Div. Fuel Chem. Prepr. 25(3), 263 (1980).
- 23 Gulbransen, E.A., Nature 212, 1420 (1966).
- 24 Ishikawa, Y. et al., Chem. and Phys. of Carbon 12, Walker, P.L.Jr. and Thrower, P.A., ed., 40 (1975).
- 25 Ozaki, A., Isotopic Studies of Heterogeneous Catalysis, New York, Academic Press, Inc. (1977
- 26 Michael G. Lussier etc. Carbon Vol. 32 No8, Pp1493-1598,1994
- 27 Michael G. Lussier, Ph.D. dissertation Michigan State University (1997)
- 28 Gunter Hermann and Klaus J. Huttinger, carbon Vol. 24, No. 6. PP 705-713,1996
- 29 P. A. Redhead ,vacuum, 12, 203 (1962)
- 30 Du, Z., A.F Sarofim, and J. P. Longwell, Energy & fuels 4,296 (1990).)
- 31 Blackman, Modern Aspects of graphite Technology, p6,(1970).

MICHIGAN STATE UNIV. LIBRARIES



31293017126560